Technische Universität München
TUM School of Life Sciences

From SNP to function: a framework to decode pleiotropy in complex traits

Isabel Sofia de Deus e Sousa

Vollständiger Abdruck der von der TUM School of Life Sciences der Technischen Universität München zur Erlangung einer

Doktorin der Naturwissenschaften (Dr. rer. nat.)

genehmigten Dissertation.

Vorsitz: Prof. Dr. Martin Klingenspor

Prüfer*innen der Dissertation:

1. Prof. Dr. Johann J. Hauner
2. Prof. Dr. Heiko Witt

Die Dissertation wurde am 10.02.2023 bei der Technischen Universität München eingereicht und durch die TUM School of Life Sciences am 03.08.2023 angenommen.

Acknowledgements

First of all I would like to thank Prof. Dr. med. Hans Hauner for the opportunity to work in his group and for his support, discussions and advice during this process.

I would like to thank Dr. Melina Claussnitzer for the opportunity to work on this interesting project, for the supervision and guidance through the experimental work and for her comments on this work.

I would also like to thank all the members of AG Hauner in Freising for welcoming me in the group and supporting my work: Sylvi for taking care of everyone; Manu for the invaluable support in the lab; Teresa, Britta, Julius, Simone, Laura, Julia and Julie for the good work environment, mutual encouragement and support; Viki and Lizzy for the initial guidance into the project; Bea and Dr. Skurk for the support with the human study.

A special thanks to Bahareh for the constant support and encouragement inside and outside the lab - your friendship was very important during this time and will continue to be going forward.

I would also like to thank Dr. Bader, Dr. Laumen, Dr. Seeliger and Prof. Dr. Zehn for sharing their knowledge and resources to support my project.

To the “flag gang”, thank you for the friendship, support and making my time in Munich very enjoyable, for all the trips, brunches, coffees and barbecues at the Isar in the summer - you were an indispensable support during this time.

To all my tango friends in Munich, thank you for the beautiful tandas, for the support and growth as a person and as a dancer alongside my doctoral work.

Last but not least, a great thank you to my family and specially my parents for supporting my international endeavors, for their unconditional love and support, and for always being there for me.

Abstract

Since the human genome was first sequenced, millions of single nucleotide polymorphisms (SNP) have been identified. For the past 15 years, genome wide association studies (GWAS) compared SNPs in large cohorts of individuals to identify genomic regions and variants associated with complex human traits and diseases. However, the interpretation of the data is challenging due to the fact that complex traits are influenced by more than one variant, with the same locus often affecting more than one phenotypic trait (pleiotropy). The abundance of pleiotropy across the human genome creates a challenge for functional studies attempting to identify the causal variants and biological mechanisms underlying complex traits and diseases.

This study presented a framework for dissecting the function of non-coding pleiotropic loci, facilitating the understanding of the biological mechanisms connecting causal SNPs to complex human traits and diseases. This framework was tested in two examples of pleiotropy: bone mineral density (BMD) and metabolic traits; Alzheimer's disease (AD) and type 2 diabetes (T2D).

Using GWAS summary statistics, the adenylate cyclase 5 (ADCY5) locus was found to be associated with femoral neck bone mineral density (FNBMD) and fasting glucose levels. The variant rs56371916 was shown to play a causal role in biological mechanisms related to these phenotypes by affecting the binding affinity of the transcription factor sterol regulatory-element-binding protein 1 (SREBP1) in mesenchymal cells, leading to altered *ADCY5* gene expression and differentiation capacity in both adipocytes and osteoblasts.
The second part of this study identified the Mitogen-Activated Protein Kinase 5 (MAP2K5) locus as being associated with T2D and AD. Knock down of MAP2K5 in human $CD4^+$ T cells impaired Treg development and promoted Th17 cell differentiation, leading to an imbalance of the Th17/Treg ratio and depletion of the naive T cell pool. Co-culture of T cells with differentiated adipocytes and SH-SY5Y neuronal cells reduced their viability and expression of differentiation markers while upregulating inflammation markers. Overall, these results indicate that causal variants affecting MAP2K5 expression promote Th17 cell differentiation and a pro-inflammatory environment favoring the development of T2D and AD.

This work, by enabling the systematic dissection of pleiotropic GWAS loci, presents a framework for unraveling the biological mechanisms underlying pleiotropic traits and diseases, in particular noncoding variants. This will ultimately facilitate translational advances for more effective prevention and treatment of human diseases.

Zusammenfassung

Seit der ersten Sequenzierung des menschlichen Genoms wurden Millionen von Einzelnukleotidpolymorphismen (SNP) identifiziert. In den letzten 15 Jahren wurden in genomweiten Assoziationsstudien (GWAS) SNPs in großen Kohorten von Individuen verglichen, um genomische Regionen und Varianten zu identifizieren, die mit komplexen menschlichen Merkmalen und Krankheiten assoziiert sind. Die Interpretation der Daten ist jedoch schwierig, da komplexe Merkmale von mehr als einer Variante beeinflusst werden, wobei derselbe Ort häufig mehr als ein phänotypisches Merkmal (Pleiotropie) beeinflusst. Die Fülle der Pleiotropie im gesamten menschlichen Genom stellt eine Herausforderung für funktionelle Studien dar, die versuchen, die kausalen Varianten und biologischen Mechanismen zu identifizieren, die komplexen Merkmalen und Krankheiten zugrunde liegen.

Diese Studie bildet einen Rahmen für die Analyse der Funktion nicht-kodierender, pleiotroper Loci, der das Verständnis der biologischen Mechanismen erleichtert, die kausale SNPs mit komplexen menschlichen Merkmalen und Krankheiten verbinden. Dieser Rahmen wurde in zwei Beispielen von Pleiotropy getestet: Knochenmineraldichte (BMD) und Stoffwechselmerkmale; Alzheimer-Krankheit (AD) und Typ-2-Diabetes (T2D).

Unter Verwendung der GWAS-Zusammenfassungsstatistik wurde festgestellt, dass der ADCY5-Locus mit FNBMD- und Nüchternglucosespiegeln assoziiert ist. Es wurde gezeigt, dass die Variante rs56371916 eine kausale Rolle bei biologischen Mechanismen spielt, die mit diesen Phänotypen zusammenhängen, indem sie die Bindungsaffinität des Transkriptionsfaktors SREBP1 in mesenchymalen Zellen beeinflusst, was zu einer veränderten ADCY5-Genexpression und Differenzierungskapazität sowohl in Adipozyten als auch in Osteoblasten führt.

Der zweite Teil dieser Studie identifizierte den MAP2K5-Locus als mit T2D und AD assoziiert. Der Abbau von MAP2K5 in menschlichen $CD4^+$ T-Zellen beeinträchtigte die Treg-Entwicklung und förderte die Th17-Zelldifferenzierung, was zu einem Ungleichgewicht des Th17/Treg-Verhältnisses und einer Erschöpfung des naiven T-Zell-Pools führte. Die Co-Kultur von T-Zellen mit differenzierten Adipozyten und neuronalen SH-SY5Y-Zellen verringerte ihre Lebensfähigkeit und Expression von Differenzierungsmarkern, während Entzündungsmarker hochreguliert wurden. Insgesamt zeigen diese Ergebnisse, dass kausale Varianten, die die MAP2K5-Expression beeinflussen, die Th17-Zelldifferenzierung und eine entzündungsfördernde Umgebung fördern, die die Entwicklung von T2D und AD begünstigt.

Diese Arbeit ermöglicht die systematische Dissektion von pleiotropen GWAS-Loci und bietet einen Rahmen für die Aufklärung der biologischen Mechanismen, die pleiotropen Merkmalen und Krankheiten, insbesondere nicht-kodierenden Varianten, zugrunde liegen. Dies wird letztendlich die Fortschritte bei der Translation für eine wirksamere Prävention und Behandlung menschlicher Krankheiten erleichtern.

Index

Abbreviations

AC	Adipocytes
Acaca	Acetyl-coa Carboxylase Alpha
ACC1	Acetyl coenzyme A carboxylase 1
ACD	Average cell diameter
ACV	Average cell volume
AD	Alzheimer's disease
ADCY5	Adenylate cyclase 5
AMPK	AMP-activated protein kinase
APOE4	Apolipoprotein E4
APP	Amyloid precursor protein
APP2	Aminopeptidase P2
ATGL	Adipose triglyceride lipase
B/P	Biotin-pantothenate
BCIP/NBT	5-bromo-4-chloro-3-indolyl phosphate/nitro blue tetrazolium
BM	Basal medium
BMD	Bone mineral density
BMI	Body mass index
BSA	Bovine serum albumin
$CaCl_2.2H_2O$	Calcium chloride
cAMP	Cyclic adenosine monophosphate
CD28	Cluster of differentiation 28
CD3	Cluster of differentiation 3
CPT1	Carnitine palmitoyltransferase I
DIO	Diet induced obese
DMEM/F-12	Dulbecco's modified eagle medium: nutrient mixture f-12
DMSO	Dimethyl sulfoxide
EDTA	Ethylenediaminetetraacetic acid
EGF	Epidermal growth factor
FAO	Fatty acid oxidation
FAS	Fatty acid synthesis
FCS	Fetal calf serum
FGF	Fibroblast growth factor
FNBMD	Femoral neck bone mineral density
FoxP3	Forkhead box P3
GAPDH	Glyceraldehyde 3-phosphate dehydrogenase
GLP-1	Glucagon-like peptide-1
HEPES	4-(2-hydroxyethyl)-1-piperazineethanesulfonic acid
HOMA-B	Homeostatic model assessment for beta cell function
HOMA-IR	Homeostatic model assessment for insulin resistance
HPRT	Hypoxanthine-guanine phosphoribosyltransferase
IBMX	3-isobutyl-1-methylxanthine
IFNγ	Interferon gamma
IL-10	Interleukin 10
IL-17A	Interleukin 17A
IL-17F	Interleukin 17F

IL-1β	Interleukin 1 beta
IL-2	Interleukin-2
IL-22	Interleukin 22
IL-23	Interleukin-23
IL-4	Interleukin-4
IL-6	Interleukin-6
IR	Insulin resistance
KCl	Potassium chloride
KRP	Krebs-ringer phosphate
LIPE	Hormone-sensitive lipase
LSBMD	Lumbar spine bone mineral density
MACS	Magnetic activated cell sorting
MAP2	Microtubule-associated protein 2
MAP2K5	Mitogen-activated protein kinase 5
MAPT	Microtubule associated protein tau
MCP-1	Monocyte chemoattractant protein-1
MEF2A	Myocyte enhancer factor 2a
$MgCl_2$	Magnesium chloride
mTOR	Mechanistic target of rapamycin
NaCl	Sodium chloride
$NaH_2PO_4 \cdot H_2O$	Sodium dihydrogen phosphate monohydrate
NTF4	Neurotrophin-4
NTRK2	Neurotrophic receptor tyrosine kinase 2
OCN	Osteocalcin
ORO	Oil-red-o
OSX	Osterix
P/S	Penicillin/streptomycin
PAC	Preadipocytes
PBMC	Peripheral blood mononuclear cells
PBS	Phosphate buffered saline
PLIN1	Perilipin-1
PLIN2	Perilipin 2
PLXND1	Plexin D1
PNPLA2	Patatin like phospholipase domain containing 2
PPARγ	Peroxisome proliferator-activated receptor gamma
RORyt	RAR-related orphan receptor gamma t
RPL13A	Ribosomal Protein l13a
RUNX2	Runt-related transcription factor 2
SAT	Subcutaneous adipose tissue
SLC1A4	Solute carrier family 1 member 4
SLC2A1	Solute carrier family 2 member 1
SLITRK6	Slit and ntrk like family member 6
STAT3	Signal transducer and activator of transcription 3
STAT5	Signal transducer and activator of transcription 5
SYN1	Synapsin 1
T2D	Type 2 diabetes mellitus
T3	Triiodo-l-thyronine

TGFβ1	Transforming growth factor beta 1
Th17	T helper 17 cells
TNF-α	Tumor necrosis factor alpha
Treg	Regulatory T cells
VAT	Visceral adipose tissue
ZNF85	Zinc finger protein 85

1. Introduction

1.1. GWAS and pleiotropy

Genome-wide association studies (GWAS) compare common genetic variants in large cohorts of individuals with a given trait or disease to control individuals in order to identify variants associated with human diseases and traits (Risch and Merikangas, 1996). The primary goal of these studies is to better understand the biology of diseases, under the assumption that a better understanding will lead to better prevention and/or treatment (Visscher *et al.*, 2017).

GWAS are possible due to the identification of millions of single nucleotide polymorphisms (SNPs) across the human genome and the realization that a set of SNPs in the genome could serve as genetic marker to detect an association between a certain genomic region and a disease, regardless if the markers themselves had functional effects (Gibbs *et al.*, 2003). As such, GWAS currently rely on and exploit linkage disequilibrium (LD) (Visscher *et al.*, 2017). LD is the non-random association between alleles at different loci in a population. LD results from evolutionary forces and is broken down by recombination (Hartwell *et al.*, 2002). Generally, loci that are physically close together exhibit stronger LD than loci that are further apart on a chromosome (Visscher *et al.*, 2012).

GWAS have identified over 100,000 genetic variants associated with complex human traits and diseases (Solovieff *et al.*, 2013). However, dissecting the causal variant(s) and mechanisms responsible for increased disease susceptibility remains a challenge. The path from GWAS to biology is not straightforward because an association between a genetic variant at a genomic locus and a trait is not directly informative of the target gene or mechanism associated with phenotypic differences (Visscher *et al.*, 2017). Unlike rare, monogenic disorders involving single gene defects, where mutations are considered to be causative, the genetic contributions to common complex disorders are generally considered to be susceptibility loci, influencing but not determining the overall disease risk (Becker, 2004). In contrast to monogenic traits, complex traits have been more difficult to unravel using linkage approaches.

The fact that complex traits are associated with multiple variants at many loci makes it more likely that some of the underlying causal variants may be the same. GWAS have shown that the same genetic variants are often associated with multiple traits and diseases, even when phenotypes are measured in different individuals (Visscher *et al.*, 2017). Recent efforts in consortia-based genotyping and sequencing in the context of diverse traits and diseases, show the increasing interest in detection of pleiotropy (Sivakumaran *et al.*, 2011).

Pleiotropy is defined as the phenomenon in which a single locus affects two or more distinct phenotypic traits and was first formally described by the German geneticist Ludwig Plate in 1910 (Stearns, 2010). Pleiotropy is abundant across the human genome and a common property of SNPs and genes reported to show genome-wide association with human complex diseases and traits (Sivakumaran *et al.*, 2011). Pleiotropy can occur at the allelic level, where a single causal variant is related to multiple phenotypes (Figure 1A), or at the gene (or region) level, at which multiple variants in the same gene (or region) are associated with different phenotypes (Figure 1B) (Solovieff *et al.*, 2013; Hackinger and Zeggini, 2017). Distinguishing genuinely shared effects of single variants (pleiotropy) from those that

represent the effects of different genetic variants in high LD located in the same gene is crucial, as they imply different notions of pleiotropy and mechanistic models of shared function (Solovieff *et al.*, 2013).

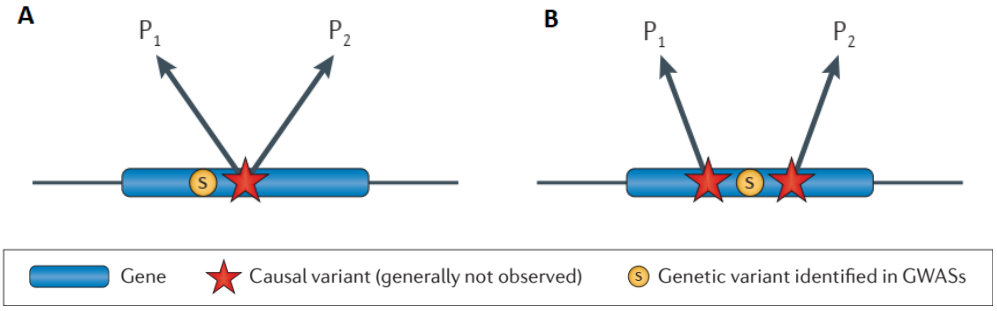

Figure 1. Different types of pleiotropy. A: a causal variant (red star) affects two different phenotypes (P_1 and P_2). B: the observed genetic variant (S) is in strong LD with two independent causal variants in the same gene that affect different phenotypes. Adapted from Solovieff et al., 2013.

1.2. Pleiotropy of bone mineral density and metabolic traits

Patients with Type 2 Diabetes have long been observed to have increased bone mineral density (BMD) but higher risk of fracture (Bonds *et al.*, 2006; Janghorbani *et al.*, 2007; Vestergaard, 2007). Studies in mice and humans have suggested several mechanisms that could explain this seemingly paradoxical phenomenon. Insulin signaling in osteoblasts has been shown to increase osteocalcin activity (Ferron *et al.*, 2010), a molecule that in mice is crucial for whole-body glucose homeostasis (Lee *et al.*, 2007). Moreover, although insulin provides an anabolic signal to osteoblasts (Ahmad *et al.*, 2017), hyperinsulinemia has been associated with lower bone strength (Srikanthan *et al.*, 2014). On the other hand, hyperglycemia has been suggested to impair bone quality by increasing collagen cross-linking and increased concentrations of advanced glycation end products, which have been tied to increased fracture risk due to decreased bone strength (Wang *et al.*, 2002). Deficits in cortical bone density and microarchitecture have also been found in subjects with type 2 diabetes (T2D) (Samelson *et al.*, 2018), further contributing to increased bone fragility and risk of fracture. The use of thiazolidinediones might also contribute to increased fracture risk by increasing activity of peroxisome proliferator-activated receptor gamma (PPARγ), which increases the commitment of pluripotent stem cells to adipocytes and inhibits the commitment to the osteoblast lineage (Angelo *et al.*, 2018). Some studies have examined genetic variants associated with BMD for association with T2D and glycemic traits in an attempt to unravel pleiotropy between both diseases (Dupuis *et al.*, 2010; Billings *et al.*, 2012; Ahmad *et al.*, 2017), but currently the cellular and molecular mechanisms underlying these traits remain largely unexplained. A recent publication by our group sheds some light on this topic, indicating an intronic variant in adenylate cyclase 5 (ADCY5) as responsible for increased pleiotropic risk for hyperglycemia and altered BMD (Sinnott-Armstrong *et al.*, 2021).

1.2.1. Biology of Adenylate Cyclase 5

ADCY5 is a member of the membrane-bound adenylyl cyclase enzymes that mediate G protein-coupled receptor signaling through the synthesis of the metabolic messenger cyclic adenosine monophosphate (cAMP) (Defer, Best-Belpomme and Hanoune, 2000). cAMP is an important molecule regulating lipolysis in adipocytes in response to nutrient and hormonal signals (Duncan *et al.*, 2007).

Single nucleotide polymorphisms in ADCY5 have been associated with T2D (Roman *et al.*, 2017), fasting glucose (Dupuis *et al.*, 2010; Vasan *et al.*, 2011), and beta cell insulin secretion (Olsson *et al.*, 2014). SNP-promoted changes in beta cell ADCY5 expression lead to impaired glucose signaling (Hodson *et al.*, 2014), thus influencing fasting glucose levels and risk of developing T2D (Olsson *et al.*, 2014). ADCY5 expression in visceral human adipose tissue is significantly higher in obese compared to lean individuals and correlates with BMI, body fat mass, circulating leptin, fat distribution, waist and hip circumference, but not with fasting plasma glucose and HbA1c (Knigge *et al.*, 2015).

1.3. Pleiotropy of Type 2 Diabetes and Alzheimer's Disease

Pleiotropy between T2D and Alzheimer's Disease (AD) is also supported by epidemiological studies, with T2D patients presenting a higher incidence of cognitive decline and AD (Akomolafe *et al.*, 2006), and over 80% of AD patients exhibiting comorbid T2D and impaired fasting glucose (Li and Hölscher, 2007). Moreover, both diseases show dysfunctions in pro-inflammatory pathways, metabolic signaling and insulin resistance (Liu *et al.*, 2011; Clarke *et al.*, 2015; Rosales-Corral *et al.*, 2015). The repurposing of antidiabetic drugs has seen positive results, with glucagon-like peptide-1 (GLP-1) mimetics producing neuroprotective and anti-inflammatory effects, including reduction of amyloid plaque in AD mouse models (Tramutola *et al.*, 2017) and prevention of brain glucose metabolism decline in AD patients (Gejl *et al.*, 2016). Carriers of the apolipoprotein E4 (APOE4) risk allele are more vulnerable to the side effects of poor glycemic control in T2D (Ravona-Springer *et al.*, 2014; Livny *et al.*, 2016).

1.3.1. Role of the immune system in T2D

Numerous studies support the importance of the immune system in the pathogenesis of T2D. In particular T cells have been shown to play an important role, with $CD4^+$ and $CD8^+$ T cell numbers being increased in obese human visceral adipose tissue (VAT) and subcutaneous adipose tissue (SAT) (McLaughlin *et al.*, 2014), with pro-inflammatory T cells more frequent in VAT compared to SAT. Moreover, obese T2D subjects have higher absolute numbers of peripheral leukocytes, mostly $CD4^+$ T cells (Van Beek *et al.*, 2014). In T2D patients, T cell content in SAT significantly correlates with waist circumference, and VAT $CD4^+$ T cell content correlates with BMI in diabetic and non-diabetic subjects (Kintscher *et al.*, 2008), suggesting that AT T cell infiltration increases with body weight.

1.3.2. T cell phenotypes in T2D

Of the multiple $CD4^+$ T cell subsets, Treg and Th17 have been shown to play an important role in T2D pathogenesis. Patients with T2D show increased levels of Th17 cells and

reduced levels of Treg cells (Zi *et al.*, 2022), with the increase in Th17/Treg ratio triggering a proinflammatory environment that promotes the development of T2D.

High Th17 cell numbers have been reproducibly shown to play an important role in T2D: the percentage of Th17 cells is elevated in the blood of T2D patients (Ip *et al.*, 2016) and their level correlates with T2D severity measured by HbA1c (Nikolajczyk *et al.*, 2011); PBMCs from T2D subjects produce higher amounts of Th17 associated cytokines (Ip *et al.*, 2016); Th17 cell numbers are significantly increased in AT from metabolically abnormal insulin-resistant obese (MAO) subjects compared to metabolically normal insulin-sensitive obese (MNO) and lean subjects (Fabbrini *et al.*, 2013).

Low Treg levels have been shown to be relevant for T2D development: Treg numbers were shown to be significantly reduced in blood from T2D patients (DiSpirito and Mathis, 2015) and in omental AT relative to SAT in obese nondiabetic humans, with the lower count being associated with higher fasting glucose, higher MCP-1 and lower ß-cell function (Gyllenhammer *et al.*, 2016); AT expression of anti-inflammatory IL-10 was inversely associated with insulin resistance in overweight human subjects (McLaughlin *et al.*, 2014).

Overall, obesity in humans results in Treg depletion in VAT due to reduced local differentiation (Deiuliis *et al.*, 2011). A loss of Tregs may potentiate inflammation through lower regulation of macrophage activation state and an increase in activated effector T cell populations.

1.3.3. Role of the immune system in AD

GWAS and pathway analysis have highlighted the importance of the immune system in AD (Lambert *et al.*, 2010; Gjoneska *et al.*, 2015). Studies have indicated that the adaptive immune system, including T cells, plays an important role in restraining AD pathology (Marsh *et al.*, 2016).

Moreover, elderly subjects and AD patients present an expansion of Aβ-reactive T cells, which may contribute to AD exacerbation (Monsonego *et al.*, 2003). Aβ has been recognized as an antimicrobial peptide (AMP) (Soscia *et al.*, 2010; Kagan *et al.*, 2012), and Aβ expression protects against fungal and bacterial infections in mouse, nematode, and cell culture models of AD (Kumar *et al.*, 2016). Aβ oligomerization, seen as a pathological hallmark of AD, may be necessary for its antimicrobial activity. It has been observed that peripheral infection increases the deposition of Aβ in the brain, which is associated with increased T cell infiltration and microglial activation in older, but not younger APP/PS1 mice (McManus and Heneka, 2017). Considering Aβ as part of the innate immune response, some studies have characterized AD as a consequence of the innate immune response to infectious pathogens (Bandea, 2013; Itzhaki *et al.*, 2016; Sochocka, Zwolińska and Leszek, 2017).

1.3.4. T cell phenotypes in AD

T cells play important physiological roles in the brain such as maintenance of hippocampal neurogenesis and spatial learning in adult mice (Kipnis *et al.*, 2004; Ziv *et al.*, 2006; Liu *et al.*, 2014). In particular, systemic $CD4^+$ T cells are involved in maintaining physiological BDNF levels in the brain and contribute to the neurogenic microenvironment without actually infiltrating the healthy brain (Wolf *et al.*, 2009).

Naive $CD4^+$ T cells do not normally penetrate the CNS because they lack expression of appropriate adhesion molecules and chemokine receptors. Once activated, T cells can enter the CNS but with regional preferences depending on the receptors expressed (Liblau *et al.*, 2013). Infiltration of activated T cells into the CNS has been shown to contribute to the chronic inflammatory status observed in AD patients (Sardi *et al.*, 2011). In addition, loss of integrity of the blood brain barrier associated with ageing and AD development facilitates T cell migration into the hippocampus (Montagne *et al.*, 2015), a region severely affected in AD.

In ageing, there is a decrease in the naive T cell population and an equivalent increase in activated T cells, which is even more striking in AD patients (McManus and Heneka, 2017). $CD4^+$ T cells are significantly increased in the peripheral blood of AD patients, consistent with upregulated expression of inflammatory cytokines such as IL-2 and IL-6 (Becher, Bechmann and Greter, 2006; Wolf *et al.*, 2009). In terms of T cell subtypes, there is evidence for Treg and Th17 cell relevance in AD development: elimination of Tregs accelerated cognitive impairment in an AD mouse model, and amplification of the Treg population restored the cognitive functions in these mice (Dansokho *et al.*, 2016); Th17 cells have been shown to infiltrate into AD brain (Ahuja *et al.*, 2017), participate in neuroinflammation and neurodegeneration by releasing proinflammatory cytokines and by direct action on neurons via apoptosis (Zhang *et al.*, 2013); Th17 differentiation factors are upregulated in AD patients (Saresella *et al.*, 2011) and animal models (Zhang *et al.*, 2015). Zhang and colleagues also observed decreased expression of Treg differentiation factors and cytokines, indicating a Th17/Treg imbalance in the brain of AD rats.

1.3.5. Biology of Treg and Th17 cells

$CD4^+$ T cells represent an important arm of the adaptive immune response and upon activation differentiate into a variety of subsets including Treg and Th17 cells. Treg cells are essential in the maintenance of immune tolerance to self and foreign antigens. After clearance of pathogens, Tregs downregulate the immune response, thereby protecting against autoimmune disease (Sakaguchi *et al.*, 2006). Their main effector cytokines include IL10 and TGF-β. IL10 is a potent inhibitory cytokine, with the ability to suppress the proinflammatory response and thus limit tissue damage (Couper, Blount and Riley, 2008).

Th17 cells are responsible for immune response against bacteria and fungi and are also involved in the pathogenesis of autoimmune/inflammatory diseases (Tabarkiewicz *et al.*, 2015). The key effector cytokines include IL17A, IL17F, and IL22. IL17A and IL17F lead to the induction of proinflammatory cytokines and proinflammatory chemokines, ensuring the chemotaxis of inflammatory cells to sites of inflammation (Moseley *et al.*, 2003). IL22 is known to mediate both inflammatory response and exhibit tissue protective properties (Rutz, Eidenschenk and Ouyang, 2013).

Figure 2 showcases the interconnection between the two T cell subsets, with both Th17 and Treg cells requiring TGF-β for differentiation. Naive $CD4^+$ T cells initially exposed to TGF-β co-express RORγt and FoxP3. From there, the TGF-β levels and cytokine microenvironment determine which subtypes the activated $CD4^+$ T cells differentiate into: high concentration of TGF-β promotes Treg differentiation through FoxP3 induction, whereas low concentration of TGF-β and the presence of pro-inflammatory cytokines favours Th17 differentiation by upregulating RORγt expression (Zhou *et al.*, 2008).

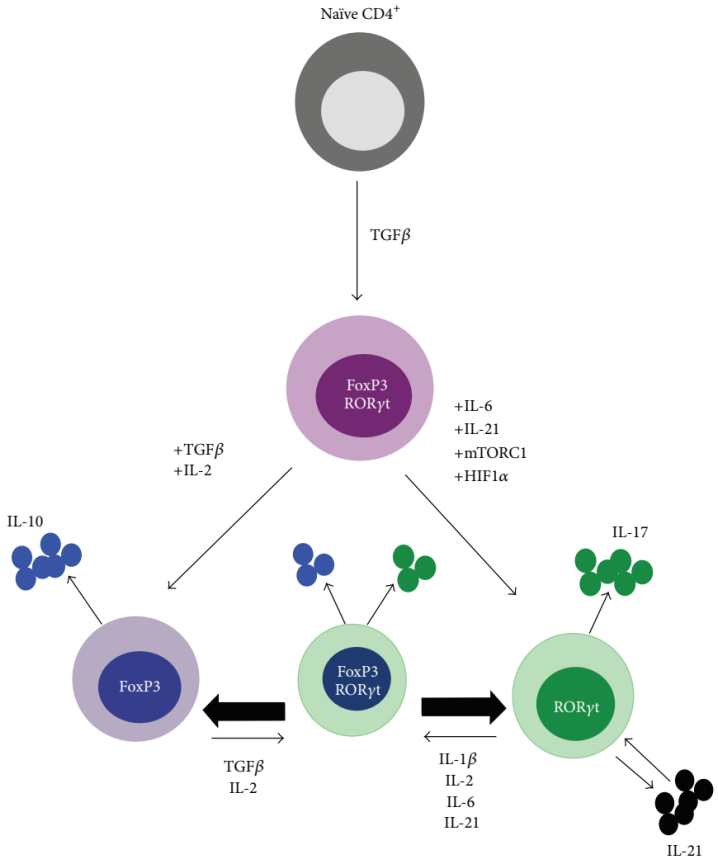

Figure 2. Interdependence and plasticity of Treg and Th17 differentiation (Diller et al. 2016).

1.3.6. MAP2K5 in T cell differentiation

The MAP2K5-ERK5 pathway has been shown to play a role in normal cell growth cycles, survival and differentiation (Drew, Burow and Beckman, 2012). During T cell development, TCR/CD3 stimulation activates the MAP2K5-ERK5 pathway and helps to regulate negative selection (Sohn, Lewis and Winoto, 2008). In peripheral primary murine T cells, silencing of the downstream target of MAP2K5, ERK5, enhances their activation (Sohn *et al.*, 2005). ERK5 plays a selective role in T-cell activation by targeting IL-2 transcriptional induction (Garaude *et al.*, 2005). Expression of a dominant-negative form of MAP2K5 in T cells leads to downregulation of LKLF, increased cell size and upregulation of activation markers such as CD25. The requirement for ERK5 in the induction of LKLF in T cells points to an important role of ERK5 in the regulation of T-cell activation and long-term survival (Sohn *et al.*, 2005).

1.4. Objectives

In this study we introduce a framework for dissecting the function of non-coding genetic variants in the context of pleiotropy, enabling the understanding of the biological mechanisms connecting causal SNPs to traits and diseases. We tested this framework in two examples of pleiotropy: 1. BMD and metabolic traits; 2. AD and T2D.

The first part of this study dissects the pleiotropy of metabolic traits and BMD mediated by an ADCY5 intronic causal variant affecting adipocyte and osteoblast metabolism and its relevance for bone mineral density and T2D.

The second part of this study explores the pleiotropy between T2D and AD mediated by the *MAP2K5* locus and its effect on $CD4^+$ T cell differentiation, particularly in Treg and Th17 cell differentiation. We hypothesize that genetic variants at the *MAP2K5* locus affect MAP2K5 expression, thereby favouring $CD4^+$ T cell differentiation towards the Th17 phenotype and contributing to the pro-inflammatory environment that promotes the development of T2D and AD.

2 Materials

2.1 Cell culture media

Table 1. Buffers for primary human cell isolation

Buffer	Composition
MACS buffer	PBS 0.5% BSA 2mM EDTA pH 7.2
4% Krebs Ringer Phosphate buffer (KRP)	126.7 mM NaCl 5.07 mM KCl 1.358 mM $CaCl_2.2H_2O$ 1.267 mM $MgSO_4.7H_2O$ 12.3 mM $NaH_2PO_4.H_2O$ 0.1% BSA, pH 7.4
KRP buffer with BSA and collagenase	4 % BSA, 50 U/ml Collagenase, pH 7.4

Table 2. T cell culture media

Medium	Composition
T cell basal medium (T cell-BM)	Gibco™ RPMI 1640 10% FCS 1% P/S
T cell expansion medium	T cell-BM 2ng/µl anti-CD3 (coated) 2 µg/ml anti-CD28 10 IU/ml IL-2
T cell Treg differentiation medium (Treg-DM)	T cell-BM 5 µg/ml anti-CD3 (coated) 1 µg/ml anti-CD28 5 ng/ml TGFβ1 5 ng/ml IL-2
T cell Th17 differentiation medium (Th17-DM)	T cell-BM 5 µg/ml anti-CD3 (coated) 1 µg/ml anti-CD28 2.5 µg/ml anti-IL4 1 µg/ml anti-IFNγ 2.25 ng/ml TGFβ1 30 ng/ml IL-6 20 ng/ml IL-1β 30 ng/ml IL-23

Table 3. Adipocyte and preadipocyte culture media

Medium	Composition per 100 ml
Adipocyte basal medium (AC-BM)	99 ml DMEM/F-12 1 ml P/S

Preadipocyte basal medium (PAC-BM)	98 ml DMEM/F-12 1 ml P/S 1 ml B/P (B/P = 0.8 mg/ml Biotin and 0.4 mg/ml Pantothenate in DMEM/F-12)
Preadipocyte proliferation medium (PAC-PM)	97.1 ml PAC-BM 2.5 ml FCS 7.7 µl Insulin 1.722 mM 200 µl EGF 5 µg/ml 200 µl FGF 0.5 µg/ml
Preadipocyte induction medium (PAC-IM)	98.6 ml PAC-DM 50 µl Rosiglitazone 100 µl Dexamethasone 1250 µl IBMX
Preadipocyte differentiation medium (PAC-DM)	98.8 ml PAC-BM 50 µl Insulin 1.722 mM 50 µl T3 2 µM 100 µl Cortisol 100 µM 1000 µl Transferrin 1 mg/ml
Osteogenic differentiation medium (PAC-OM)	87 ml αMEM 10 ml FCS 1 ml P/S 1 ml β-GP 1M stock 1 ml HC 40µM stock

Table 4. SH-SY5Y cell line culture media

Medium	**Composition**
Proliferation medium	DMEM F12 10% FCS 1% P/S 2mM L-glutamine
Differentiation medium 1 (day 0 - 3)	DMEM-F12 2mM L-glutamine 1% P/S 10 µM RA
Differentiation medium 2 (day 3 - 6)	Neurobasal medium B27 supplement 1% P/S 2mM L-glutamine 50 ng/ml BDNF

Table 5. Nuclear extract preparation buffers

Buffer A	**Final conc. [mM]**	**Buffer C**	**Final conc. [mM]**
HEPES	10	HEPES	20
KCL	10	NaCl	400
EDTA	0.1	EDTA	1
EGTA (freezer 1)	0.1	EGTA (freezer 1)	1
PMSF	0.5	glycerol	20%

DTT	1	PMSF	1
protease inhibitor	1 tablet/ml	DTT	1
phosphatase inhibitor	1 tablet/ml	protease inhibitor	1 tablet/ml
		phosphatase inhibitor	1 tablet/ml

Table 6. EMSA buffers and gel

TBE 5x	**Gel 5.3%**	**1 x**
54 g Tris Base	TBE 5x	5 ml
27.5 g boronic acid	H2O	35.6 ml
20 ml EDTA 0.5M pH 8.0	86% v/v Glycerol	1.45 ml
Ad 1 L water and adjust	10% APS	375 µl
final pH to 8.3		
	TEMED	25 µl
	37.5:1 acrylamide/bisacrylamide (40% w/v)	6.5 ml

5X Gel Binding Buffer	**10X Loading Buffer**
Final concentration	**Final concentration**
20% v/v glycerol	250 mM TrisHCl pH 7,5
5 mM MgCl2	0.2% OrangeG
2.5 mM EDTA	40% v/v glycerol
2.5 mM DTT	
250 mM NaCl	
50 mM TrisHCl pH 7,5	
0.25 mg/ml poly(dI-dC):poly(dI-dC)	

2.2 Chemicals and Consumables

Table 7. Chemicals

Product	**Supplier**
BCIP/NBT tablets (SigmaFast™ BCIP-NBT)	Sigma-Aldrich, Germany
Biocoll	Biochrom, Germany
Biotin	Carl Roth, Germany
BSA	Sigma-Aldrich, Germany
Calcium chloride ≥98% dried power	Carl Roth, Germany
CD14 MicroBeads, human	Miltenyi Biotec
CD28 Monoclonal Antibody (CD28.2), Functional Grade	ThermoFisher Scientific, Germany
CD3 Monoclonal Antibody (OKT3), Functional Grade	ThermoFisher Scientific, Germany
CD4 MicroBeads, human	Miltenyi Biotec
Collagenase	Biochrom, Germany
Cortisol	Sigma-Aldrich, Germany
Dexamethasone	Sigma-Aldrich, Germany
DMEM/F-12	ThermoFisher Scientific, Germany
DMSO	Carl Roth, Germany
DNase I	QIAGEN, Germany
EDTA	Merck, Germany

EGF	Bio-Techne, USA
Ethanol (99%)	CLN, Germany
FCS	Sigma-Aldrich, Germany
FGF	Bio-Techne, USA
Gibco™ optiMEM	ThermoFisher Scientific, Germany
Gibco™ RPMI 1640 Medium	ThermoFisher Scientific, Germany
HEPES	Sigma-Aldrich, Germany
Hydrocortisone 21-hemisuccinate sodium salt	Sigma-Aldrich, Germany
IBMX (3-isobutyl-1-methylxanthine)	Sigma, Germany
IFN gamma Monoclonal Antibody (NIB42), Functional Grade	ThermoFisher Scientific, Germany
IL1B Recombinant Human Protein	ThermoFisher Scientific, Germany
IL2 Recombinant Human Protein	ThermoFisher Scientific, Germany
IL23 Recombinant Human Protein	ThermoFisher Scientific, Germany
IL-4 Monoclonal Antibody (MP4-25D2), Functional Grade	ThermoFisher Scientific, Germany
IL6 Recombinant Human Protein	ThermoFisher Scientific, Germany
Insulin human	Sigma, Germany
Isopropanol	J.T. Baker, USA
Magnesium chloride ($MgCl_2$)	Carl Roth, Germany
Nuclease free water	Carl Roth, Germany
Pantothenate	Sigma, Germany
PBS without Ca^{2+} and Mg^{2+}	Biochrom, Germany
Penicillin/ Streptomycin (P/S)	Sigma-Aldrich, Germany
Potassium chloride (KCl)	Carl Roth, Germany
Rosiglitazone	Cayman Chemical, USA
Sodium chloride (NaCl)	Carl Roth, Germany
Sodium dihydrogen phosphate monohydrate ($NaH_2PO_4 \cdot H_2O$)	Merck, Germany
ß-mercaptoethanol	Sigma-Aldrich, Germany
SYBR green master mix	ThermoFisher Scientific, Germany
TGFβ1 Recombinant Human Protein	ThermoFisher Scientific, Germany
Transferrin	Sigma-Aldrich, Germany
Triiodo-L-Thyronine (T3)	Sigma-Aldrich, Germany
Trypsin-EDTA solution	Sigma-Aldrich, Germany

Table 8. Consumables

Product	**Distributor**
24-well cell culture plates (suspension cells)	Greiner Bio-One, Austria
6-well cell culture plates (adherent cells)	Corning, USA
6-well cell culture plates (suspension cells)	Greiner Bio-One, Austria
Corning® Costar® Snapwell cell culture inserts	Sigma-Aldrich, Germany
Filters (0.22 µm)	Millipore, Eschborn
MS Columns	Miltenyi Biotec
Nylon mesh 200 µm	VWR, USA
Nylon mesh 2000 µm	VWR, USA

Octo MACS Separator Starter Kit	Miltenyi Biotec
Pasteur pipettes	Brand, Wertheim
PCR 96-well plates	4titude, UK
PCR tubes (200 µl)	4titude, UK
Pipette tips (0.1 – 1000 µl) (Tip One Filter Tips)	Sarstedt, Germany
Safelock micro test tubes (1.5 ml and 2 ml)	Eppendorf, Hamburg
Serological pipettes (5 ml, 10 ml, 25 ml, 50 ml)	Greiner Bio-One, Austria
T25 flasks (suspension cells)	Greiner Bio-One, Austria
Test tubes (15 ml and 50 ml)	Greiner Bio-One, Austria

3 Methods

3.1 Bivariate GWAS analysis

3.1.1 Cross-phenotype association analysis (CPASSOC)

CPASSOC combines GWAS summary statistics to search for variants that contribute to multiple traits (Zhu *et al.*, 2015). We used summary statistics from a large FNBMD GWAS study performed by the GEFOS Consortium (Estrada *et al.*, 2012); n(FNBMD) = 32,961 and n(LSBMD) = 31,800, and from large GWAS studies from the MAGIC GWAS Consortium (Dupuis *et al.*, 2010; Alisa K. Manning *et al.*, 2012); glycemic trait sample n(FASTING GLUCOSE) = 46,186, n(FASTING INSULIN) = 38,238, n(HOMAIR) = 37,037, n(HOMAB) = 36,466. We reported potential pleiotropic SNPs based on a suggestive significance level of (1) $P \leq 5x10^{-06}$ from the bivariate GWAS analyses; (2) the bivariate p-value divided by the univariate p-value is less than 0.05; and (3) univariate $P \leq 0.05$ for both phenotypes.

3.1.2 Multi-Trait Analysis of GWAS (MTAG)

MTAG is a method used for combined analysis of GWAS summary statistics from different traits in a flexible framework which takes into account the genetic correlation of the traits and potential sample overlap (Turley *et al.*, 2017).

3.1.3 eLX

Bivariate GWAS analysis was performed using the empirical-weighted linear-combined test statistics method (eLC) implemented in the eLX package using summary statistics from univariate GWAS meta-analyses (Chen and Hsu, 2017). The eLC directly combines correlated test statistics (or p-values) obtained from variant-phenotype association or GWAS analyses with a weighted sum of univariate test statistics. eLC maximizes the overall association signals by accounting for the correlation between phenotypes.

3.1.4 Chromatin state segmentation and visualization

Chromatin state segmentations were obtained from the Roadmap Epigenomics Project (Claussnitzer *et al.*, 2014; Roadmap Epigenomics Consortium *et al.*, 2015) and visualized in the WashU Epigenome Browser (Zhou *et al.*, 2011). Specifically, imputed chromatin state calls from a 25-state model based on imputed datasets from 12 chromatin marks were used (Ernst and Kellis, 2012). Split panels were constructed using the epigenome browser's JSON-based configuration system. Shown are chromatin state calls across all epigenomes, as well as putative regulatory region delineations from the Roadmap Epigenomics Project.

3.1.5 Hi-C data processing and visualization

Hi-C data from human H1-hESC derived MSC cultured cells (Dixon *et al.*, 2015) were downloaded from SRA (SRR1030739-SRR1030744) and reprocessed at 10kb resolution. Experiments from the ENCODE (DHS-seq and CTCF ChIP-seq) and Roadmap (chromatin state) projects were visualized using the WashU Epigenome Gateway (Zhou et al. 2011; interactive session 2apaIcl6nH).

3.1.6 Phylogenetic Module Complexity Analysis (PMCA)

The PMCA method described in (Claussnitzer *et al.*, 2014) analyses evolutionary conservation of cis-regulatory modules across related species to predict the causal variant

associated with a trait or disease. This method was used with several modifications: multi-way MULTIZ alignment to hg38 at UCSC (Blanchette *et al.*, 2004) was used to define orthologous regions in 20 vertebrate species. Each region's sequence was extracted and aligned to each other using CLUSTALW. Transcription factor positions were selected based on matches of the given motifs to the hg38 sequence. 972 position weight matrices from the Catalog of Inferred Sequences of Binding Preferences (CIS-BP) were grouped in 192 motif matrix families using TomTom (Maurano *et al.*, 2015), and families were further overlapped by motif name to create a many-to-many mapping where individual TFs had multiple motifs annotated. MOODS (Korhonen *et al.*, 2009) was used to scan 120bp variant-flanking regions of the human reference genome (variant at mid-position) and its orthologous regions for cross-species conserved groups of transcription factor binding site motifs, so called groups of transcription factor binding site motifs, or motif modules. A module is defined as a set of binding site motifs, whose order and distance range is conserved across species. Enrichments of motifs in conserved modules are computed using 10,000 permutations of orthologous sets. The PMCA method counts instances of conserved motifs within conserved modules within the 120bp sequence context of a given variant. The scores have a minimum of 0 (no conserved motif modules), with scores indicating the count of non-overlapping jointly conserved transcription factor binding site motifs whose relative positions within the window are conserved.

3.1.7 Basset CNN

To identify the regulatory elements surrounding rs56371916, the Basset CNN model (Kelley, Snoek and Rinn, 2016) was used to analyse the effect of altering each base within a 20bp window centered on the SNP. The Basset method predicts the change in accessibility resulting from mutation at every position to each alternative nucleotide, which highlights the individual nucleotides most critical to a sequence's activity. *In silico* mutagenesis produces heatmaps that display the change in predicted accessibility for any of the four possible nucleotides. The loss score measures the largest possible decrease while the gain score measures the largest possible increase for mutation to any other non-reference nucleotide at a given position.

3.2 Study information T cell samples

3.2.1 Ethics statement

The study protocol was reviewed and approved by the ethics committee of the Faculty of Medicine of the Technical University of Munich (#5499/12). The study was registered in the German Clinical Trial Register (DRKS00014182). Written informed content was obtained from all participants before study inclusion. The study was conducted under the guidelines of the International Conference on Harmonization of Good Clinical Practice and the declaration of Helsinki (in the revised version of Seoul, South Korea 2008).

3.2.2 Study design

The human explorative study was an uncontrolled, single-arm monocentre study. The study centre was in Freising-Weihenstephan, Germany. The study included an appointment of approximately 30 minutes. The subjects were instructed to abstain from caffeine and sports

24 hours before the appointment and to fast during the 12 hours prior to the blood collection (no food consumption, water was allowed). On the morning of the appointment the subjects came fasted to the study centre. There, approximately 50 ml of blood was drawn. In addition, height, waist circumference and body composition were determined according to SOPs (Annex 1).

3.2.3 Study population

Seventeen male participants aged 18 to 40 years with a BMI between 18.5 and 30 kg/m² were recruited via flyers at the TUM campus Weihenstephan in Freising, Germany. The participant's eligibility was assessed with a detailed screening questionnaire (Annex 1.3). Volunteers were assigned to the study only after checking the inclusion and exclusion criteria (Table 9), after being informed of the purpose and possible risks of protocols, and after giving written informed consent (Annex 1.4 and 1.5). The average characteristics of the study population are summarized in Table 10.

Table 9. Inclusion and exclusion criteria for the study

Inclusion criteria	Exclusion criteria
Healthy male	Type 1 and 2 Diabetes
Age between 18 and 40 years	Smoking
BMI between 18,5 und 30 kg/m²	Cardiovascular disease
Non-smoker	Chronic and serious diseases (such as cancer)
Written informed consent	Blood transfusion in the previous 3 months
	Antibiotic use in the previous 6 months

Table 10. Characterization of the study population

Parameter	Average	SD
Age (years)	26.2	3.9
BMI (kg/m^2)	22.6	2.2
Waist circumference (cm)	82.7	6.6
Fasting glucose (mg/dL)	94.1	6.3
% CD4$^+$ T cells	19.8	4.9

3.2.4 Anthropometric measurements

All anthropometric and clinical measurements were performed in a standardized manner between 9 and 10 am in the morning following an overnight fast. Body height (cm) was measured using a stadiometer (Seca, Hamburg, Germany). Body weight and body composition were measured using the Seca mBCA 515 from seca® (Hamburg, Germany). The measurements were performed barefoot, without outdoor clothing and with an empty bladder. BMI was calculated by dividing weight in kg by height in meter squared (kg/m²). Waist was measured with a soft tape midway between the lowest rib and the iliac crest. Hip circumference was measured at the widest part of the gluteal region.

3.2.5 Data and sample collection

All data and samples were pseudonymized with 3 digit code. For confidential reasons the subject identification list was kept in the study centre in a locked cupboard. The data was

documented in a pseudonymized manner in Case Report Forms (CRF) (Annex 1.6) and analyzed using in MS Office Excel (version 2016).

3.3 Cohort information of adipose tissue samples

Cohort 1: primary AMSC, n=41 (TT: 23, CT: 18) (Technical University Munich and University Hohenheim, Germany)
Cohort 2: subcutaneous adipose tissue, n=30 and AMSC n=24 (not genotyped, University Bergen, Norway)
Cohort 3: subcutaneous adipose tissue, n=12 (TT: 8, CT: 1, CC: 2, NA: 1) (University Bergen, Norway)
Cohort 4 (subcohort of Cohort 1): primary AMSC, n=8 (TT: 4, CT: 4) (Technical University Munich and University Hohenheim, Germany)
Cohort 5: adipose tissue, n=237 obese and n=85 non-obese (not genotyped), pairwise subcutaneous and visceral samples (University Bergen, Norway)

3.4 Cell culture

3.4.1 Isolation of human primary $CD4^+$ T cells

Three sequential protocols were performed for the isolation of primary $CD4^+$ T cells from freshly collected human blood. Peripheral Blood Mononuclear Cells (PBMCs) were initially separated from the other major blood components (plasma and erythrocytes) by gradient centrifugation. Secondly, CD4-weakly expressing $CD14^+$ cells were depleted from the PBMC cell fraction using magnetic columns and $CD14^+$ antigen coated MicroBeads. Lastly, $CD4^+$ T cells were positively selected using $CD4^+$ antigen-coated MicroBeads and magnetic columns. The cells in the final eluent were counted with the Invitrogen Countess automatic counting chamber and plated in 12- or 24-well plates, adequate for suspension cell culture (Suspension 12/24 well culture plates, Cellstar®, Greiner bio-one).

3.4.1.1 Peripheral Blood Mononuclear Cell (PMBC) isolation

Blood was drawn from volunteers into 9-ml Heparin monovettes by a medical doctor in the Human Study Unit. The donors were healthy, aged between 18 and 40 years and were asked to fast for a minimum of 12 hours prior to blood collection and extraction. All procedures had passed ethical scrutiny and the donors gave full written consent for the use of their blood samples. Between 6 and 8 samples of 9-ml Heparin blood monovettes were harvested, this total volume of blood being within the established limits which would neither interfere in the volunteers' normal blood cell production and turnover nor make them feel weak or indisposed after the withdrawal.
Following blood draw the 9-ml Heparin blood monovettes were shaken gently to ensure proper mixture of the blood with the heparin beads and prevent blood coagulation. All subsequent steps were carried out under a sterile bench in a Biosafety Laboratory 2 (BSL-2). Blood from one monovette was diluted with an equal volume of sterile Dulbecco's-PBS without Ca^{2+} or Mg^{2+} warmed at room temperature (RT). The PBS used was depleted of Ca^{2+} and Mg^{2+} as these two ions facilitate cell binding and clumping. The separation of the different blood components was achieved using a density gradient medium (Biocoll separating solution, Biochrome, density 1.077 g/ml) that promotes differential migration of

blood cells through the medium during centrifugation. The diluted blood (16 ml) was carefully layered on top of 16 ml of Biocoll in a 50-ml Falcon tube and centrifuged at 400 *g* for 25 minutes, with acceleration set to 1 (minimum) - to promote slow cell migration and formation of the PBMC ring - and brake switched off - to avoid pellet formation at the bottom of the tube. After centrifugation the blood components were separated into 4 layers: the bottom layer was made up of the heaviest cells, erythrocytes, followed by granulocytes, the layer of Biocoll, the white ring of PBMCs at the interphase between the Biocoll and the plasma, which was the top layer. The cloudy white PBMC ring was carefully recovered with a plastic Pasteur pipette. The lymphocytes from two tubes were pooled into one 50-ml Falcon tube and washed with sterile PBS at RT, adding enough to reach the 50-ml mark. The tubes were centrifuged at 300 *g* for 10 minutes with acceleration 5 and brake 9 to promote pellet formation at the bottom of the tube. Afterwards, the supernatant was discarded and the pellet resuspended thoroughly in 10 ml of sterile PBS. At this point the PBMC yield was calculated by mixing a 15-µl aliquot of the cell solution with 15 µl of Trypan Blue and counted with an Invitrogen Countess automatic counter.

3.4.1.2 Depletion of $CD14^+$ cells

Enrichment of the PBMC cell suspension in $CD4^+$ T cells was achieved using magnetic activated cells sorting (MACS). MACS® Separation columns, $CD14^+$ MicroBeads and a MACS Separator magnet from Miltenyi Biotec were used for the depletion of $CD14^+$ cells. This step was performed to exclude $CD4^{low}$ $CD14^+$ monocytes and guarantee a higher purity of our final $CD4^+$ T cell population.

The PBMC cell suspension was first labelled with $CD14^+$ antigen coated magnetic MicroBeads. For this, the cell suspension was centrifuged at 300 *g*, acceleration 5 and brake 9, for 10 minutes. The supernatant was discarded and the pellet was resuspended in 80 µl of ice-cold MACS buffer and 20 µl of $CD14^+$ MicroBeads per 10^6 cells was added to label the $CD14^+$ cells. The tubes were incubated in the dark (the microbeads are light sensitive) at 4 °C for 15 minutes. After the incubation period, the cells were washed with 1 ml of cold MACS buffer per 10^6 cells and centrifuged at 300 *g*, acceleration 5 and brake 9, for 10 minutes to remove excess microbeads. During this centrifugation step, MACS® Separation columns were placed in the MACS Separator magnet and prepared by adding 500 µl of cold MACS buffer. The number of columns used was adjusted based on a single column capacity of 10^6 cells and the initial PBMC count. The pellet was resuspended in 500 µl of cold MACS buffer per column and the total volume was loaded onto the MACS® Columns. The magnetically labelled $CD14^+$ cells were retained within the column while the unlabeled cells ran through and were collected in 50-ml Falcon tubes. The columns were washed three times with 500 µl of cold MACS buffer. Once all the buffer had run through, the columns were discarded and the negative fraction, depleted of $CD14^+$ cells and containing the unlabeled cells of interest, was kept for further enrichment.

3.4.1.3 Positive selection of $CD4^+$ T cells

The cell fraction resulting from the $CD14^+$ cell depletion protocol was centrifuged at 300 *g*, acceleration 5 and brake 9, for 10 minutes. The supernatant was discarded and the pellet was resuspended in 160 µl of ice-cold MACS buffer and 40 µl of $CD4^+$ MicroBeads per 10^6 cells to magnetically label $CD4^+$ cells. The tubes were incubated in the dark at 4 °C for 15 minutes. Afterwards the cells were washed with 2 ml of cold MACS buffer per column and centrifuged at 300 *g*, acceleration 5 and brake 9, for 10 minutes to remove the excess microbeads. During this centrifugation step, new columns were set up in the MACS

Separator magnet and prepared by washing with 500 µl of cold MACS buffer per column. The pellet resulting from the centrifugation was resuspended in 500 µl of cold MACS buffer per column and loaded onto the MACS® Columns. The $CD4^+$ labelled cells were retained within the columns while the unlabeled cells flowed through and were collected in 50-ml Falcon tubes. The columns were washed three times with 500 µl cold MACS buffer per column. Once all the buffer had run through, the columns were removed from the magnet and the retained $CD4^+$ cells were expelled from the columns by adding 1 ml of MACS buffer and gently applying pressure with the plunger provided. Finally, the positively selected $CD4^+$ T cell yield was calculated by taking 15 µl of the expelled cell fraction mixed with 15 µl of Trypan Blue for cell counting using the Invitrogen Countess automatic counter.

3.4.2 Expansion and differentiation of naive $CD4^+$ T cells to Treg and Th17 phenotypes

In order to activate and expand the cell population, $CD4^+$ T cells were incubated in plates coated with anti-CD3 and soluble anti-CD28 to promote T cell activation, and IL-2 to prevent cell clumping and improve cell survival. Suspension 24- or 12-well culture plates were coated with 200 µl/well of 2.5 µg/ml anti-CD3 solution in PBS. The plates were incubated at 37 °C for two hours, wrapped in Parafilm to avoid evaporation. Afterwards, the anti-CD3 solution was removed and the wells were washed with 500 µl of warm PBS. Cell suspension resulting from the $CD4^+$ T cell isolation protocol was centrifuged at 200 *g*, acceleration 5 and brake 9, for 10 minutes to remove the elution buffer. The supernatant was discarded and the pellet was resuspended in basal medium (RPMI 1640 medium supplemented with 10% FCS and 1% P/S) with 2.5 µg/ml anti-CD28 and 10 IU/ml IL-2. Cells were plated at a density of $1x10^6$/ml in 500 µl in a 24-well plate or 1 ml in a 12-well plate. Cells were kept in expansion medium for 3-7 days until the desired cell number was achieved.

Differentiation protocols for the specific phenotypes of interest were optimized based on the scientific literature. The appropriate differentiation medium to promote cell differentiation into Treg and Th17 phenotypes is described in Table 2. Basal medium containing only anti-CD3 and anti-CD28 stimulation factors, which induces unspecific differentiation, was used as comparison to check for enrichment of Treg and Th17 populations with the specific differentiation media. Cells were incubated at 37 °C, 5% CO_2 and differentiated for 7 days. For Treg differentiation fresh medium was added on day 3 of differentiation; Th17 cells were left untouched for 7 days.

3.4.3 Transfection of $CD4^+$ T cells

An initial test was performed using chemical transfection. Cells were plated at 200.000 cells per well and incubated with 100 nM ON-Target plus Human MAP2K5 siRNA SMART pool from Dharmacon in the presence of HiPerFect Transfection Reagent from QIAGEN and Opti-MEM. Knock down efficiency was assessed after 48 hours incubation by qPCR.

Electroporation was also tested for siRNA delivery. Transfection of CD4+ T cells was tested using Amaxa® Human T Cell Nucleofector® Kit and Nucleofector™ 2b Device from Lonza. CD4+ T cells were transfected after isolation using program U-014 and following the manufacturer instructions. Cells were rested for 5 hours before transfer to differentiation media. Knock down efficiency was assessed after 48 hours incubation by qPCR.

Finally, loss of function experiments were performed using Accell™ siRNA technology from Dharmacon. Self-delivering siRNA was reconstituted using 1x siRNA resuspension buffer from Dharmacon under sterile conditions to make a 100 µM stock solution. T cells were harvested after 2 days in expansion medium (Table 2) and resuspended in Accell siRNA

delivery medium at a final concentration of $1x10^6$ cells/ml. The cells were plated in 24-well plates in Accell siRNA delivery media and siRNA was added to a final concentration of 1 µM per well (500 µl) in triplicates. The plate was then incubated for 72 hours at 37 °C, 5% CO_2.

3.4.4 Differentiation of SH-SY5Y

The neuronal cell line SH-SY5Y is a subclone of the parental SK-N-SH cell line originally isolated from the neuroblastoma of a 4-year old female. It has been used as a model for human neuronal systems due to its proliferation capacity and ability to differentiate into neuronal-like cells. The cell line was purchased from the European Collection of Authenticated Cell Cultures (ECACC catalogue no. 94030304). It was maintained in culture in proliferation medium and differentiated using retinoic acid and BDNF (Table 4). Experiments were performed below passage 20 to prevent loss of neuronal characteristics.

3.4.5 Isolation of primary human preadipocytes from liposuction material

Human liposuction material was collected from a collaborating private plastic surgery clinic Medaesthetic Privatklinik Hoffmann & Hoffmann in Munich, Germany. Patient profiles varied, but the majority were aged less than 50 and with a BMI under 30 kg/m². Harvested subcutaneous liposuction material was used for isolation of preadipocytes. Krebs-Ringer Phosphate (KRP) buffer was prepared containing 200 U/ml of collagenase and 4 % heat shock fraction BSA and sterilized by filtration using a Bottle-Top Filter 0.22 µM. After reaching RT, 12.5 ml of liposuction material was aliquoted into sterile 50-ml tubes with plug seal caps. The tubes were filled to 47.5 ml with warm KRP-BSA-collagenase buffer and the caps were securely tightened and wrapped in Parafilm to avoid leakage. The tubes were incubated in a shaking water bath for 30 minutes at 37 °C with strong shaking. After 30 minutes, the oil on top was discarded and the supernatant was initially filtered through a 2000-µm nylon mesh. The supernatant of all tubes was combined after filtration and centrifuged at 200 g for 10 minutes. The supernatant was discarded and each pellet was resuspended with 3 ml of erythrocyte lysis buffer, then all the pellets were pulled in one tube and incubated for 10 minutes at RT. The cell suspension was filtered through a 250 µm filter and then through 150 µm filter, followed by centrifugation at 200 g for 10 minutes. The supernatant was discarded and the pellet containing preadipocytes was resuspended in an appropriate amount of DMEM/F12 with 1% P/S and 10% FCS, seeded in T75 cell culture flasks and stored in the incubator (37 °C, 5% CO2). The next day the medium was changed to PAC-PM (Table 3).

3.4.6 Preadipocyte differentiation into adipocytes

Once preadipocytes reached 100% confluency in T25 or T75 flasks they were split into 6-well plates at a seeding density on 250 000 cells per plate in PAC-PM. Once they reached 100% confluency, PAC-IM was prepared fresh and added to the preadipocytes to induce differentiation. On day 3 after induction, the medium was changed to PAC-DM and replaced twice a week.

3.4.7 Co-culture of T cells with differentiated PAC and SH-SY5Y

Preadipocytes and SH-SY5Y were plated in 6-well plates and differentiated for 10 and 7 days respectively. T cells were then counted and the same number of T cells of each KD and differentiation condition was added to each well of PAC and SH-SY5Y. Co-culture with T cell supernatant was set up by equally distributing the volume of supernatant of each T cell condition per well of PAC and SH-SY5Y.

3.4.8 Preadipocyte differentiation into osteoblasts

Considering the common lineage of adipocytes and osteoblasts, we used PAC as mesenchymal stem cells and induced their differentiation into osteoblasts using ß-glycerol phosphate and hydrocortisone. PAC were seeded in 6-well cell culture plates and allowed to grow in PAC-PM until 80% confluency. Osteogenic differentiation was then promoted by changing the medium to PAC-OM containing hydrocortisone and β-glycerophosphate (Table 3). Medium was replaced twice a week and cells were kept at 37 °C, 5% CO2.

3.4.9 Staining of differentiated adipocytes and osteoblasts

3.4.9.1 Oil Red-O staining

Lipid droplets are lipid-storage organelles predominantly present in differentiated adipocytes. Oil Red O selectively stains neutral lipids, such as cholesteryl esters, triglycerides, and fatty acids, in cultured differentiated adipocytes, serving as a good measurement for the degree of differentiation. At day 10 of differentiation, the culture medium was removed and the differentiated adipocytes were carefully washed with PBS. The cellular monolayer was then covered with 3.7% Formaldehyde to fix the cells. After 1 hour, the formaldehyde was removed and the cells were stained with Oil-Red-O (ORO) staining solution (0.3% Oil-Red-O in 60 ml Isopropanol and 40 ml H_2O, filtered before use) and left to incubate for 1 hour. Afterwards, the ORO solution was removed and cells were washed twice and kept in PBS. Differentiated adipocytes full with lipid droplets showed a strong red color. Quantification of lipid accumulation was done by removing the PBS, adding 500 µl isopropanol and incubating 15 min at RT. Afterwards, 75 µl per well were transferred to a 96-well plate for measuring absorbance at 492 nm using the Tecan Infinite® 200 Pro Nanoquant microplate reader.

3.4.9.2 Alkaline Phosphatase staining

Proliferating osteoblasts show alkaline phosphatase (AP) activity, which is greatly enhanced during *in vitro* bone formation. AP activity is therefore a practical marker for osteoblast differentiation. AP can easily be detected using the substrate 5-bromo-4-chloro-3-indolyl phosphate (BCIP)/nitro blue tetrazolium (NBT), which stains cells blue-violet in the presence of AP. At day 10 of differentiation, culture medium was removed and the cells were carefully washed with PBS. The cellular monolayer was covered with neutral buffered formalin 10% for 60 seconds, then washed with 0.05% Tween 20 in PBS without Ca^{2+} or Mg^{2+} (washing buffer). Cells were incubated with BCIP/NBT substrate solution (1 tablet dissolved in 10 ml distilled water) at RT in the dark for 5 to 10 minutes, checking the staining progress every 2 to 3 minutes. Afterwards, the substrate solution was removed, cells were washed with washing buffer and finally kept in PBS. AP positive cells presented a dark blue-violet color, whereas AP negative cells were colorless or faintly bluish.

3.4.9.3 Alizarin Red S staining

Osteoblasts can be induced to produce vast extracellular calcium deposits *in vitro*, a process called mineralization. Calcium deposits are an indication of successful in vitro bone formation and can specifically be stained bright orange-red using Alizarin Red S. For staining, the Alizarin Red S staining solution was prepared by dissolving 2 g of Alizarin Red S in 100 ml distilled water and adjusting the pH to 4.1-4.3 with 0.1% NH_4OH. After filtration, the solution was stored in the dark. At day 10 of differentiation, the culture medium was removed and

cells were carefully washed with PBS without Ca^{2+} or Mg^{2+}. The cellular monolayer was covered with neutral buffered formalin 10% for at least 30 minutes, then washed with distilled water and incubated with Alizarin Red S staining solution at room temperature in the dark for 45 minutes. Afterwards, the substrate solution was removed, cells were washed 4 times with 1 ml distilled water and finally kept in PBS. Undifferentiated cells, without extracellular calcium deposits, were slightly reddish, whereas mineralized osteoblasts, with extracellular calcium deposits, were bright orange-red.

3.4.10 Viability assay CCK-8

Viability of differentiated PAC and SH-SY5Y was assessed using the Cell Counting Kit-8 from SIGMA. This assay is based on the reduction of the highly water-soluble tetrazolium salt WST-8 to formazan, a yellow colored product which is soluble in tissue culture medium. The amount of the formazan dye generated by the activity of cellular dehydrogenases is directly proportional to the number of living cells. The detection sensitivity of CCK-8 is higher than other tetrazolium salts. This assay was also selected due to the low toxicity of CCK-8, so that after the assay the same cells could be used for other readouts.
The assay was performed by adding 10% of the total volume present in a well of CCK-8 solution and incubating for 4 hours at 37 °C. Afterwards, the absorbance at 450 nm and 650 nm (reference to account for turbidity in the medium) was measured using the Tecan Infinite® 200 Pro Nanoquant microplate reader and the calculated difference was used for analysis.

3.4.11 CRISPR/Cas9 genome editing

Plasmids: hCas9 and the gRNA cloning vector were purchased from Addgene (Plasmid ID #41815 and #41824, respectively). Genomic DNA was amplified from one rs56371916 CC allele carrier and one-TT allele carrier. Site-directed mutagenesis was performed using the Q5 Site-Directed Mutagenesis Kit (New England Biolabs). The guide RNAs (gRNAs) were designed using the CRISPR design online tool from the Zhang lab (http://crispr.mit.edu/). 2 guide RNAs were used: 5'-TAGAGGTCTCACCCCACTCA-3', 5'-GAGGGGACACCTATTCCTAG-3'. For transfection, we co-transfected GFP- and hCas9- and sgRNA expression vectors, and the pMACS plasmid 4.1 (Milteny) in human AMSCs using the Amaxa-Nucleofector device (program T-030) (Lonza). We sorted cells using the MACSelectTM Transfected Cell Selection cell sorting kit (Miltenyi). Sorted cells were cultured for 3–5 days and clones propagated from single cell were picked out. Nucleotide exchange was confirmed by Sanger sequencing and lack of random indels was confirmed by sequencing the 1000 bp genomic DNA flanking the rs56371916 targeted site. We further sequenced the top four predicted off-target sites, as computationally predicted by the CRISPR design tool (crispr.mit.edu) and the CRISPR-OFF tool (https://rth.dk/resources/crispr/crisproff/submit), and as such we have studied all predicted off targets with a CRISPR-OFF score above 12 and predicted critical off targets based on the CRISPR-off algorithm.

3.4.12 Lipolysis assay

Glycerol was measured in the medium after the 18-h incubation. Glycerol was measured spectrophotometrically using a glycerol 3-phosphate oxidase trinder kit (Sigma). For stimulated lipolysis measurements, 1 mmol/l isoproterenol (Sigma) was added for 1 h.

3.4.13 Luciferase reporter assay

For the promoter construct, we cloned a 752 bp thymidine kinase (TK) promoter upstream of the firefly luciferase gene into the EcoRV and BglII sites of the pGL4.22 firefly luciferase reporter vector (Promega). We then subcloned the following non-coding genomic regions upstream of the TK promoter into the KpnI and SacI sites of the pGL4.22-TK vector in forward orientations: (i) To assay haplotype enhancer activity we used 10 kb genomic regions flanking rs56371916 synthesized as plasmid vectors (Life Technologies) for both the ancestral and derived haplotype using HapMap individuals information; (ii) To assay rs56371916 allelic activity 1 kb genomic regions flanking rs56371916 carrying both alternate alleles at rs56371916 were synthesized. We cloned genomic DNA segments upstream of the TK promoter into the KpnI and SacI sites of the pGL4.22-TK vector in forward orientation. All constructs were verified by Sanger sequencing of plasmids. We performed transfection in different cell types as described below.

Human Huh7 hepatoma, mouse C2C12 myoblasts, HT22 neuronal cells, Clonetics™ Normal Human Articular Chondrocytes (NHACkn), and human K562 lymphoblastoid lymphoblastoid cell lines were cultured in DMEM medium (supplemented with P/S and 10 % FBS). The human pre-adipocyte SGBS (Simpson–Golabi–Behmel Syndrome) cell line was cultured as previously described (Claussnitzer *et al.*, 2014) in DMEM/F12 (1:1) medium (supplemented with 10% FCS, 17 mM biotin, 33 mM pantothenic acid and 1% P/S). To promote adipose differentiation of the SGBS cell line, cells were grown to confluence. For induction of adipocyte differentiation cells were cultured in serum free MCDB-131/DMEM/F12 (1:2) medium supplemented with 11 mM biotin, 22 mM pantothenic acid, 1% P/S, 10 mg/ml human transferrin, 66 nM insulin, 100 nM cortisol, 1nM triiodothyronine, 20 nM dexamethasone, 500 mM 3-isobutyl-1-methyl-xanthine (Serva, Germany) and 2 mM rosiglitazone (Alexis, Germany). All cells were maintained at 37°C and 5% CO_2. Huh7 cells (96-well plate, 1.1 x 10^4/ well) were transfected one day after plating with approximately 90% confluence, K562 cells (12-well plate, 8 x 10^4/ well) were transfected three days after plating with approximately 90% confluence, SGBS adipocytes (12-well plate, 8 x 10^4/ well) were transfected at day eight after the induction of differentiation with approximately 80% confluence and C2C12 cells (12-well plate, 2 x 10^5/ well) were transfected at day four after induction of differentiation with approximately 90% confluence. MC3T3 osteoblasts were seeded (seeding density: 250,000 cells/well) in a 6-well plate. Cells were differentiated using αMEMmedium supplemented with 10% FBS, 1% P/S, 50 µg/ml ascorbic acid, and 10 mM beta-glycerophosphate. Huh7 were transfected with 0.5 mg of the respective firefly luciferase reporter vector and 1 ml Lipofectamine 2000 transfection reagent (Invitrogen, Darmstadt, Darmstadt, Germany), differentiated C2C12 myocytes were transfected with 1 mg of the respective pGL4.22-TK construct and 2 ml Lipofectamine reagent, and both K562-cells and differentiated SGBS adipocytes were transfected with 2 mg of the respective pGL4.22-TK construct and 2 ml Lipofectamine reagent. The firefly luciferase constructs were co-transfected with the ubiquitin promoter-driven Renilla luciferase reporter vector pRL-Ubi to normalise the transfection efficiency. Twenty-four hours after transfection, the cells were washed with PBS and lysed in 1x passive lysis buffer (Promega, Germany) on a rocking platform for 30 minutes at room temperature. Firefly and Renilla luciferase activity were measured (substrates D-luciferin and Coelenterazine from PJK, Germany) using a Luminoscan Ascent microplate luminometer (Thermo) and a Sirius tube luminometer (Berthold), respectively. The ratios of firefly luciferase expression to Renilla luciferase expression were calculated and normalized to the TK promoter control vector, i.e. enhancer activity. For overexpression ADCY5 cDNAs derived from SGBS total cDNA were inserted

into the doxycycline-inducible Tet-On® Advanced Inducible Gene Expression System (BD Biosciences, Clontech, San Diego, CA). P-values comparing luciferase expression from risk and non-risk alleles were calculated using paired t-tests.
This assay was performed by Nasa Sinnott-Armstrong at the Broad Institute of MIT and Harvard, Cambridge, MA 02142, USA.

3.5 Molecular biology

3.5.1 RNA isolation from human primary CD4$^+$ T cells

Cell harvest for RNA isolation was performed using the lysis buffer RTL provided with the RNA isolation kit from QIAGEN, supplemented with 10% β-mercaptoethanol to ensure complete RNase inhibition and RNA protection. CD4$^+$ T cells were harvested in 150 µl buffer RLT and stored in 1.5 ml Eppendorf tubes at -80 °C until processing. PAC and SH-SY5Y were harvested in 350 µl of RLT buffer. The RNA isolation was performed under an extraction hood due to β-mercaptoethanol toxicity. This isolation method is based on the principle of RNA solubility in water and insolubility in ethanol.
The 1.5 ml Eppendorf tubes were thawed on ice, then 150 µl of ice-cold 70% ethanol was added to each sample and vortexed. The entire volume was transferred to RNeasy Mini spin columns placed inside collection tubes and centrifuged for 30 seconds at 9000 *g* to promote RNA binding to the membrane (flow through discarded). Several washing steps were performed to remove any contaminants and ensure purity of the RNA. First 350 µl of RW1 buffer was added to the columns and centrifuged for 30 seconds at 9000 *g* (flow through discarded). A DNase I solution was added and the columns were incubated for 15 minutes at RT to digest the genomic DNA. Several washing steps and centrifugations followed with different volumes of RW1 and RPE buffer following protocol steps provided by the company, in order to eliminate any contaminants. After the various washes, 20 µl of RNase-free water was added to each column, which were then incubated at 37 °C for 8 minutes to promote RNA dissolution into water. The columns were centrifuged and the RNA eluate was recovered from the bottom of the collection tube and reapplied on top of the column filter to repeat the elution and achieve a higher RNA concentration. From this point onwards, the samples were kept on ice to prevent RNA degradation and frozen at -80 °C overnight to improve RNA stability and quantification measurements.

3.5.2 RNA quantification

The Tecan Infinite® 200 Pro Nanoquant device was used for quantification of nucleic acid in small volumes of sample by absorbance measurements. RNase-free water was measured as blank for quality control, then 1 µl of the samples was measured and calculations of the nucleic acid content and purity using the 260/280 ratio were performed automatically by the device's software. The absorbance of nucleic acid samples was measured at 260 nm and, in conjunction with a 280 nm reading, was used to estimate the relative purity of the sample. For RNA, a pure sample would have a 260/280 ratio value of 2.0 - between 1.8 and 1.9 was acceptable, but lower values indicate poor quality of the RNA due to contaminants, including protein and other chemicals, or degradation.

3.5.3 cDNA synthesis

Reverse transcription of total RNA to single-stranded cDNA was achieved using the High Capacity cDNA Reverse Transcription kit by Applied Biosystems, with a reaction size of 20 µl

and a Thermal cycler. Following the manufacturer's instructions, a 2x reverse master mix was prepared and 10 µl was added to 10 µl of RNA solution (approx. 500 ng), mixed and placed in a thermal cycler (Table 11). The synthesized cDNA solution was diluted 1:10 to a final volume of 200 µl by adding 180 µl of RNase-free water.

Table 11. Thermal cycling conditions for cDNA synthesis

	Temperature	**Time**
Step 1	25 °C	10 min
Step 2	37 °C	120 min
Step 3	85 °C	5 min
	4 °C	hold

3.5.4 SYBR Green based quantitative PCR (qPCR)

Quantitative PCR analysis was performed using Maxima SYBR Green/ROX qPCR Master Mix (2X) from Thermo Fisher and the Mastercycler ep Realplex thermal cycler by Eppendorf. A master mix was prepared according to the manufacturer's instructions (Table 12), mixing 8 µl of master mix with 2 µl of cDNA. The qPCR thermal profile applied is described in Table 13. The primers were designed using Primer-BLAST, an online tool from NCBI (https://www.ncbi.nlm.nih.gov/tools/primer-blast/). Annealing temperatures and sequences of the primer pairs used are indicated in Table 14. RT-PCR data was analysed using the double delta Ct (ΔΔCt) method, in which the Ct values obtained from different experimental RNA samples were normalized directly to a housekeeping gene and then compared. This method assumes that the amplification efficiencies of the gene of interest and the housekeeping gene are close to 100%. First, the difference between the Ct values (ΔCt) of the gene of interest and the housekeeping gene was calculated for each experimental sample. Then, the difference in the ΔCt values between the experimental and control samples (ΔΔCt) was calculated. The fold-change in expression of the gene of interest between the two samples is thus equal to 2^(-ΔΔCt). Relative mRNA expression was expressed as fold-change expression over the average control gene expression taken as one. Fold-change values were then $\log_2$ transformed and plotted in a column graph using GraphPad Prism software. GAPDH or RLP13A expression was used as a reference housekeeping gene for normalization for PAC/SH-SY5Y or T cell marker detection respectively.

Table 12. Composition of SYBR Green qPCR master mix

Component	**Volume (µl) per reaction**	**Final concentration**
PCR grade H2O	2.4	
Maxima SYBR 2x	5.0	1x
Primer for (10 µM)	0.3	0.3 µM
Primer rev (10 µM)	0.3	0.3 µM
Total volume per reaction	8.0	

Table 13. qPCR cycling conditions

Number of cycles	**Step**	**Temperature**	**Time**
1 cycle	Pre-denaturation	95 °C	10 min

40 cycles	Denaturation	95 °C	15 sec
	Annealing	(Primer specific)	40 sec
1 cycle	Melting curve	65 °C-95 °C	(0.5 °C/step)

Table 14. Primer sequences and annealing temperatures

Target	Ta (°C)	Forward Primer	Reverse Primer
ACACA	60	ATGCTCCTGGAACGTCGAAAT	CCAAAAAGACCTAGCCCTCAAGA
Adiponectin	61	GGTGAGAAGGGTGAGAAAGGA	ACACTGAATGCTGAGCGGTA
AMPK	60	TCGGAGCCTTGATGTGGTAG	TTCATCCAGCCTTCCATTCTT
APP2	60	AACGAAGGTTCTGGGTTGACA	TGATGACGATCACTGTCGCT
CPT1	61	CCCCTCCAGTTGGCTTATCG	CATGCAGTTGGCCGTTTCC
FoxP3	62	CCTCCTCTTCTTCCTTGAACCCC	GAGAGCTGGTGCATGAAATGTGG
GAPDH	60	GATCATCAGCAATGCCTCCTGC	ACAGTCTTCTGGGTGGCAGTGA
IL-10	60	GGCACCCAGTCTGAGAACAG	GGCAACCCAGGTAACCCTTAAA
IL-17A	60	CAGGCACAAACTCATCCATCC	GCAGTAGCAGTGACACCAATG
IL-17F	62	CCTGGAATTACACTGTCACTTGG	TCTCTTGCTGGATGGGAACG
IL-22	62	CCACGGAGTCAGTATGAGTGAG	ACATGTGCTTAGCCTGTTGC
IL-6	60	ATCTGGATTCAATGAGGAGACTTG	GCAGGAACTGGATCAGGACTT
Leptin	62	TCCAAGATGACACCAAAACCC	ACGTGAAGAAGATCCCGGAG
LIPE	59	TCCTCATGGCTCAACTCCTT	AAGTCCCTCAGGGTCAGGTT
MAP2	61	TTTCTGCGCCCAGATTTTATTGA	GTTCGTTGTGTCGTGTTCTCA
MAP2K5	61	GTCACTCCCCTTGTCACCTCT	AACCTGGCCTATCACATCCAGC
MAPT	61	TAGCAACGTCCAGTCCAGTG	GGCCACCTCCTGGTTTATGAT
MCP-1	58	GCAATCAATGCCCCAGTC	GGTGGTCCATGGAATCCTGA
MEF2A	62	GAACCGACAGGTCACTTTTACA	TCCGAGTTGGTTCTGCTTTCA
mTOR	60	CGCGAACCTCAGGGCAAG	TGACTCATCTCTCGGAGTTCCA
MYC	60	TTCCCCTACCCTCTCAACGA	TTCTTGTTCCTCCTCAGAGTCG
NTF4	61	CTGACAGGTGCTCCGAGAGAT	GGGAGAGAAGGTCCCACTCA
NTRK2	62	TGACGATGGTGCAAACCCAA	AGACCGAGAGATGTTCCCGA
PLIN1	61	TTTCTGCCTGAGGAGACACTC	CCATCCTCGCTCCTCAAGT
PLXND1	62	TATGGGAACAACATCCGCAC	ACATCTCAACAGTCACGTGGT
PNPLA2	60	CCAATGTCTGCAGCGGTTTC	GACAGATGTCACTCTCGCCC
RORγt	62	GAGCTAGGTGCAGAGCTTCAG	GGGATCACTTCAATTTGTGTTCTCA
RPL13A	60	GAACACCAACCCTTCCCGAG	AACCACCATCCGCTTTTTCTTG
SLC1A4	60	TGAAAAGATCCCCATAGGCAC	TCACCAGCACGATGATGTCT
SLC2A1	62	GAACTCTTCAGCCAGGGTCC	ACCACACAGTTGCTCCACAT
SLITRK6	61	AGTACGCAGTGGTTGGTGTT	TCCGATTCTGTAAAGCAGAGACT
STAT3	60	CTGCCCCATACCTGAAGACC	GTGAGGGACTCAAACTGCCC
STAT5	62	AAGCAAGTGGTCCCTGAGTTT	CCATTGGTCGGCGTAAGAGT
SYN1	59	GACCAATACTGGCTCTGCGA	GAGGAACCCACCACCTCAAT
TGF-β	60	TTGAGGGCTTTCGCCTTAGC	GGTAGTGAACCCGTTGATGTCC
ZNF85	61	GCCAAACCCACAGGTTGTCT	TATTCTGCTCCGGCCAAAGG

3.5.5 Nuclear protein extract preparation

Nuclear extracts were prepared from preadipocytes differentiated into adipocytes and osteoblasts. All buffers and equipment were cooled to 4 °C to minimize protein denaturation and improve protein yield. Cell culture medium was removed and cells were washed with cold PBS twice, then 200 µl of buffer A (Table 5) was added to each well to collect cells with a rubber scraper. Cells were homogenized twenty times in a potter and passed through an insulin needle five times, then transferred to a 1.5 ml test tube and incubated on ice for 15 minutes. Afterwards, Nonidet NP-40 was added to a final concentration of 0.5%, the tubes were vortexed shortly and centrifuged at over 21000 g for 5 minutes. The supernatant containing the cytoplasmic fraction was discarded and any visible fat was removed. The resulting pellet was washed twice with buffer A to remove Nonidet NP-40, which could interfere with protein DNA-interaction, and centrifuged at over 21000 g for 3 min. The supernatant was discarded completely and buffer C was added to the pellet, adjusting the volume to the size of the pellet to yield a higher concentration. The pellet was incubated for 30 minutes at 4 °C shaking vigorously. Afterwards the tubes were centrifuged at over 21000 g for 5 minutes and the supernatant containing the nuclear fraction was recovered and aliquoted. A dilution of 1:10 was aliquoted for protein measurement using the Bradford method.

3.5.6 Nuclear protein extract quantification

Protein measurement was performed using the Bradford method to ensure buffer compatibility. Standards were prepared in 10% buffer C containing decreasing concentrations of BSA: 2 mg/ml, 1 mg/ml, 0.5 mg/ml, 0.25 mg/ml, 0.125 mg/ml, 0.0625 mg/ml, 0.03125 mg/ml and 0.015625 mg/ml. The blank was 10% buffer C in water. Standards and samples were measured in duplicates, diluting 5 µl of standard or sample in 45 µl water. Roti-Quant solution was prepared by mixing 5.5 parts water and 2 parts Roti-Quant and 200 µl was added to each well, incubating for 5 minutes at room temperature. Colour development was measured at 595 nm and sample concentration was calculated using linear regression.

3.5.7 Electrophoresis mobility shift assay (EMSA)

EMSA is a technique used for determining interactions between protein complexes and nucleic acids. It is based on the observation that the electrophoretic mobility of a protein-nucleic acid complex is typically less than that of the free nucleic acid. It can be used qualitatively to identify sequence-specific, DNA-binding proteins (such as transcription factors) in nuclear protein extracts. Gels containing 5.3% polyacrylamide were prepared according to Table 6 and pre-ran at 180 V at 4 °C for 1 hour. The protein-DNA binding reactions were prepared on ice as follows: water, 5x gel binding buffer, poly dI:dC and nuclear protein extract were first incubated for 10 minutes, then labelled DNA probes were added and the reaction was incubated an extra 20 minutes protected from light. For competition EMSA, the competition probes were added shortly before the Cy5 labelled DNA probe and incubated at the same time. For supershift EMSA, the antibody and nuclear protein extract were incubated initially for 30 minutes before adding water, 5x gel binding buffer and poly dI:dC. Lastly, 10x gel loading buffer was added and the reactions were loaded on the gel, which ran for approximately 3 hours at 200 V and 4 °C. Detection of electrophoretic bands was done by scanning the gels using a TYPHOON scanner from GE Life Sciences. The settings used were as follows: fluorescence Cy5, 650 PMT, normal sensitivity, resolution 50 microns.

Table 15. EMSA oligonucleotides

rs56371916_C_for	Cy5-TGGCCCCAGAGCAGAGTGGC**C**GGCGTGAGTGAAGATGATGA-3’
rs56371916_C_rev	5’-TCATCATCTTCACTCACGCC**G**GCCACTCTGCTCTGGGGCCA-3’
rs56371916_T_for	Cy5-TGGCCCCAGAGCAGAGTGGC**T**GGCGTGAGTGAAGATGATGA-3’
rs56371916_T_rev	5’-TCATCATCTTCACTCACGCC**A**GCCACTCTGCTCTGGGGCCA-3’
Srebp1-competitor-for	5’-GTGGCCCCAGAGCAG**GTGGGGTGAT**GAAGATGATGAACTGG-3’
Srebp1-competitor-rev	5’-CCAGTTCATCATCTTCATCACCCCACCTGCTCTGGGGCCAC-3’

4 Results

4.1 Pleiotropy of BMD and metabolic traits

4.1.1 GWAS identifies bivariate loci for BMD and glycemic traits

GWAS summary statistics from the MAGIC consortium (Dupuis *et al.*, 2010; Alisa K Manning *et al.*, 2012) and the GEFOS consortium (Estrada *et al.*, 2012) were used to discover genetic loci with possible pleiotropic effects on BMD and glycemic traits. The MAGIC consortium included measures of HOMA-IR, HOMA-B, fasting glucose levels and fasting insulin levels, whereas the GEFOS consortium included measures of femoral neck BMD (FNBMD) and lumbar spine BMD (LSBMD). All pairs of glycemic and BMD traits were analyzed using the cross-phenotype association analysis (CPASSOC) program (Park *et al.*, 2016), which identified 8 distinct bivariate loci (p-value ≤ 5×10^{-6}) (Figure 3, Annex Table S1). A locus within an intron of the *ADCY5* gene was associated with FNBMD and glucose levels (lead SNP rs2124500, bivariate GWAS p-value = 1.83×10^{-7}) (Figure 4A), as well as FNBMD and HOMA-B (Annex Table S1). The bivariate association of this locus was also confirmed by two other methods: MTAG (Turley *et al.*, 2017) (p = 3.22×10^{-9}) and eLX (Chen and Hsu, 2017) (p = 5.73×10^{-9}) (Annex Table S2). Moreover, the locus showed bivariate association (CP-ASSOC p = 1.35×10^{-7}; eLX p = 4.35×10^{-11}; MTAG p = 6.03×10^{-9}) in independent data from the UK Biobank for heel BMD (n = 194,398) and diagnosed diabetes (n = 336,473), and was recently associated with heel BMD (UK Biobank, p=1.15×10^{-10} , n=435,039) (Morris *et al.*, 2019).

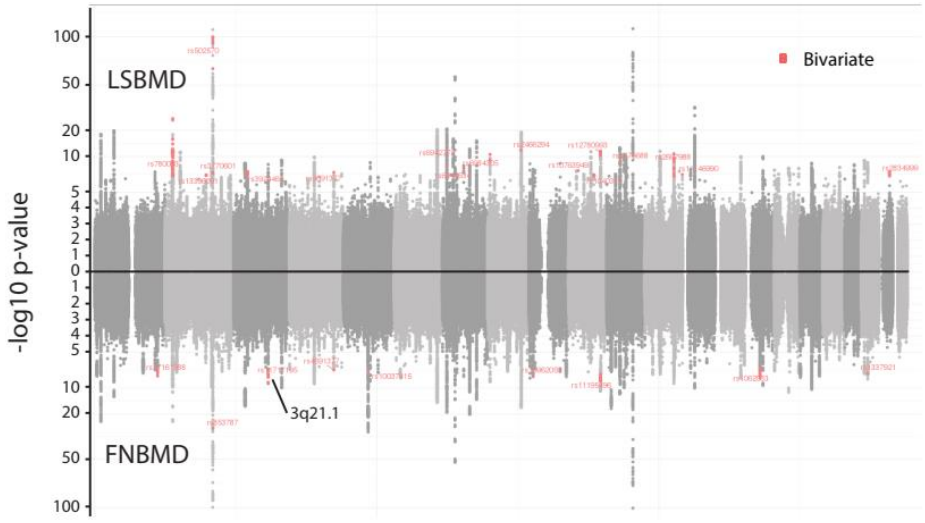

Figure 3. Manhattan plot of genome-wide association results for bone density and glycemic traits using CP-ASSOC. Bivariate associations were computed for two bone density traits (FNBMD and LSBMD) and four glycemic traits (HOMA-IR, HOMA-B, fasting glucose levels, and fasting insulin levels). The x-axis indicates the chromosomal position, and the y-axis the significance on a −log10 scale, directionally split by LSBMD and FNBMD.

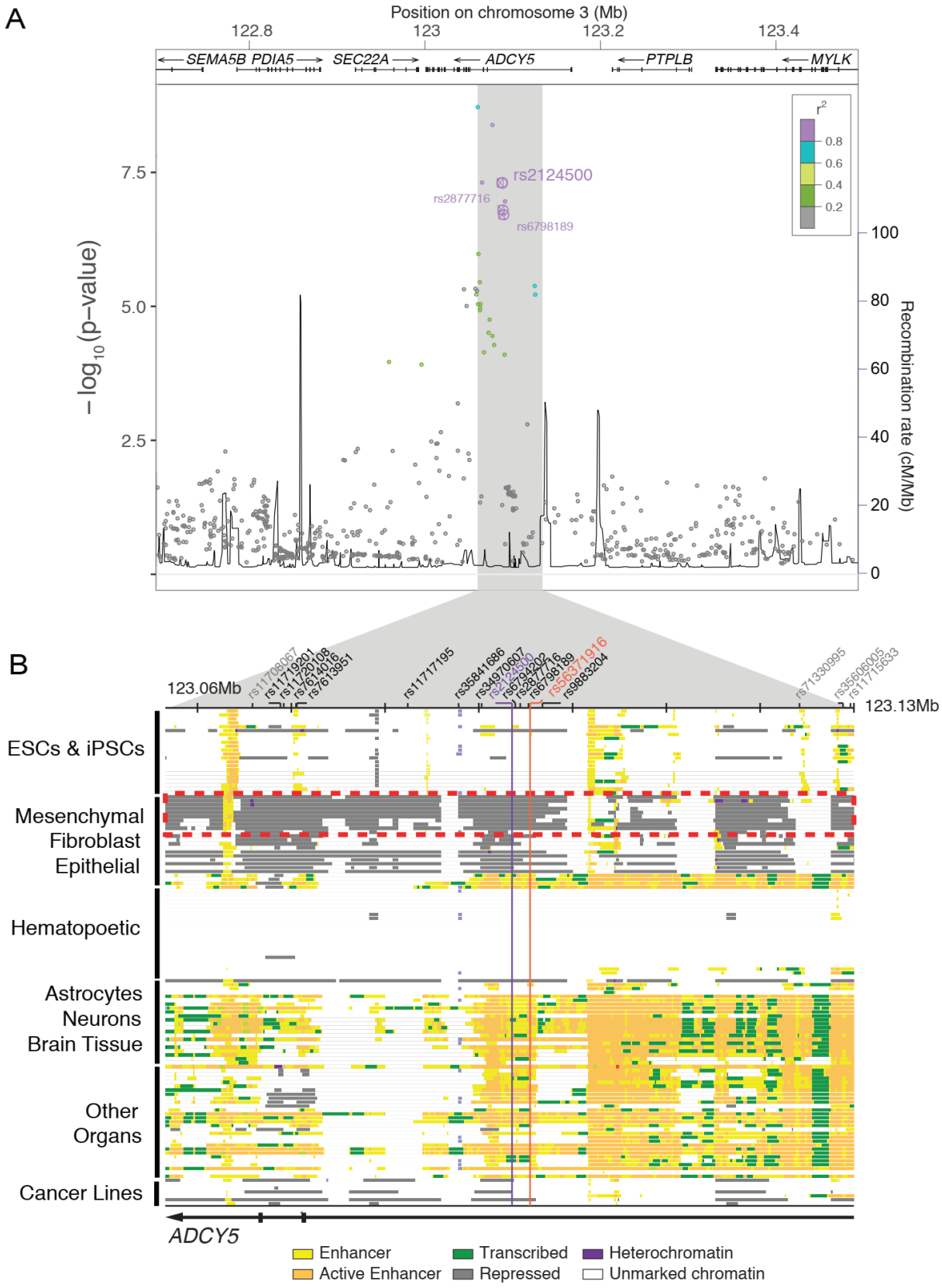

(Legend in next page)

Figure 4. A: Genetic association with FNBMD and fasting glucose levels for ADCY5 locus variants. Bivariate association (y-axis) and genomic coordinates (x-axis) for all common single nucleotide polymorphisms (SNPs = circles) in a 100kb window of chromosome 3 centered on the ADCY5 bivariate locus. The region of association localizes to a 65kb interval in intronic regions of the ADCY5 gene containing 13 variants in high linkage disequilibrium in Europeans (1000 Genomes r^2, dot color) with the bivariate tag SNP rs2124500. SNPs that meet bivariate criteria are marked by bolded purple dots. **B:** Chromatin state annotations for the 65kb-long bivariate locus. Genomic intervals are shown across 127 human cell types and tissues reference epigenomes profiled by the Roadmap Epigenomics projects, based on a 25-state chromatin state model (colours) learned from 12 epigenomic marks using imputed signal tracks at 25-nucleotide resolution (Roadmap Epigenomics Consortium et al., 2015). Chromatin states considered here include Polycomb repressed states (grey, H3K27me3), weak enhancers (yellow, H3K4me1 only), strong enhancers (orange, also H3K27ac), and transcribed enhancers (lime, also H3K36me3). Polycomb-repressed segments in mesenchymal cells are denoted with a dotted red box. The tagSNP rs2124500 (purple), the predicted causal variant rs56371916 (red) and 11 other variants (black) in high LD with rs2124500 are indicated.

4.1.2 Haplotypes at *3q21.1* differ in regulatory activity

The *3q21.1* locus is located within the 95 kb-long first intron of *ADCY5* (Figure 4A), consisting of 65 kb containing 13 non-coding SNPs in strong LD ($r^2 > 0.8$, 1000G Phase 1 EUR). These 13 candidate regulatory variants define two alternative haplotypes: the ancestral haplotype 1 (frequency 77% in European individuals), associated with higher FNBMD and higher fasting glucose levels, and haplotype 2 (frequency 23% in European individuals), associated with lower FNBMD and lower fasting glucose levels.

Chromatin state maps of the *3q21.1* locus were examined across 127 human cell types (Roadmap Epigenomics Consortium *et al.*, 2015) in order to identify the cell types affected by the candidate variants (Figure 4B). The data revealed that the entire locus was spanned by Polycomb-repressed chromatin (marked by H3K27me3) in mesenchymal lineages, while it was unmarked or active in non-mesenchymal cell types. Among the mesenchymal lineages, we focused on adipocytes, osteoblasts, and mesenchymal stem cell (MSC) precursors, which can give rise to adipocytes, osteoblasts, myocytes, and chondrocytes (Chen *et al.*, 2016), as they presented the highest levels of enrichment for Polycomb-repressed chromatin.

Differences in regulatory activity of the two haplotypes were tested using plasmid-based luciferase-reporter assays in osteoblasts and adipocytes. Analysis of a 10 kb region containing the 10 candidate regulatory SNPs in tightest LD with rs2124500 ($r^2 > 0.9$) revealed that haplotype 1 had greater transcriptional activity in osteoblasts and adipocytes (1.9-fold and 1.8-fold respectively) (Figure 5). In contrast, hepatocytes, lymphocytes, differentiated muscle cells and pancreatic beta cells showed no haplotype-specific regulatory differences.

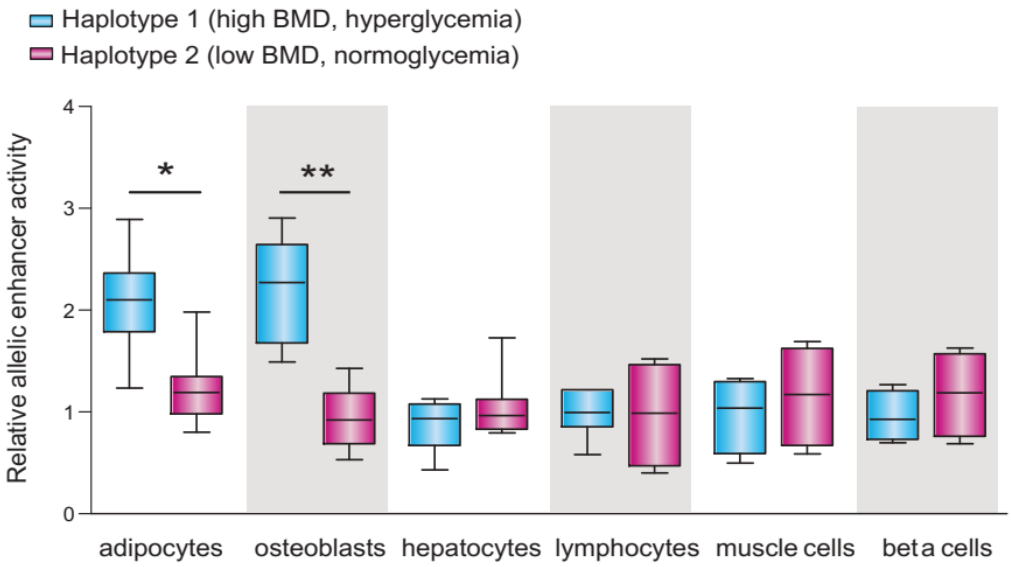

Figure 5. Haplotype-specific luciferase assays for 10 kb fragments containing 10 candidate regulatory SNPs from each haplotype in tightest LD with rs2124500 (r^2 > 0.9) in adipocytes, osteoblasts, hepatocytes, lymphocytes, differentiated muscle cells and pancreatic beta cells.

4.1.3 Regulatory region targets ADCY5

In order to identify potential regulatory target(s) of the locus, three-dimensional genome folding maps from Hi-C assays in embryonic stem cell-derived MSCs (Dixon *et al.*, 2015) were examined. The locus lies in a well-defined 300-kb contact domain containing only the genes *ADCY5* and *PTPLB* (Figure 6). For the assay, the six genes within a larger 1 Mb region centered on the locus were considered (*PDIA5*, *SEC22A*, *ADCY5*, *PTPLB*, *MYLKAS1*, and *MYLK*) (Figure 6).

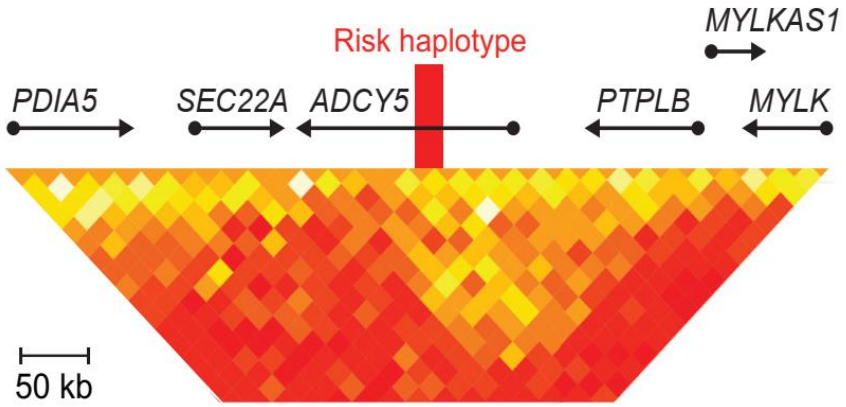

Figure 6. Genome-wide higher order chromatin interactions for the ADCY5 locus analyzed by Hi-C assays in human embryonic stem cell derived MSCs from an individual homozygous for haplotype 1.

AMSCs were isolated from 41 normal-weight individuals consisting of 18 heterozygous individuals (haplotypes 1/2) and 23 homozygous individuals (haplotypes 1/1). These AMSCs were differentiated into mature osteoblasts and adipocytes, with the phenotypes confirmed by marker-gene expression, bright field microscopy, and colorimetric assays (Table 16, Figure 7).

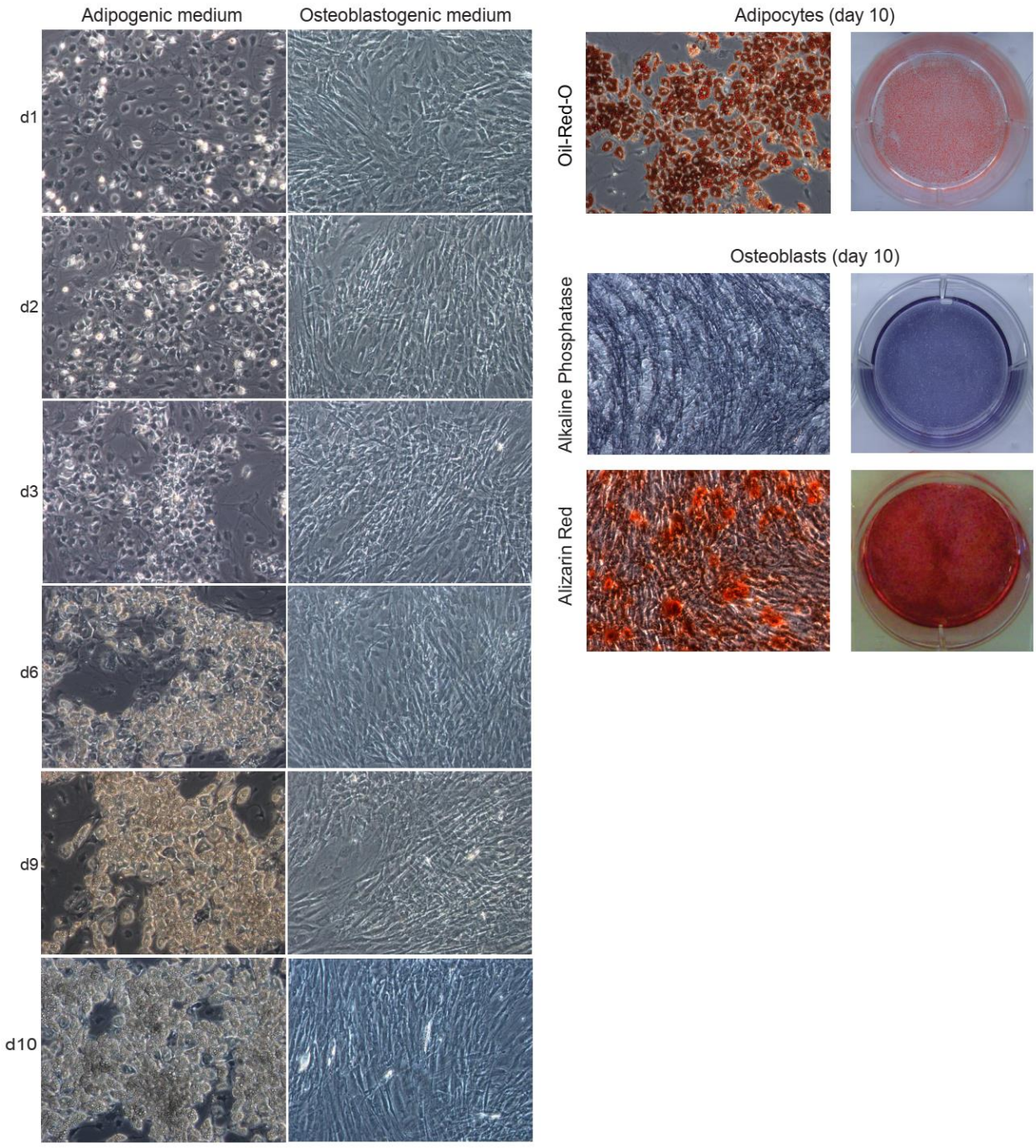

Figure 7. Morphological changes of primary human AMSCs during differentiation into mature adipocytes and osteoblasts, respectively. Unstained bright field microscopy-based pictures are shown (**left**) as well as Oil-Red-O based lipid staining for adipocyte differentiation, and Alkaline Phosphatase staining and Alizarin Red staining for osteoblast differentiation (**right**). Micrographs were taken at 10x magnification under an Inverted Laboratory Microscope LEICA DM IL LED.

Table 16. Relative mRNA levels in AMSCs differentiated to osteoblasts (n=5) and adipocytes (n=5).

	Marker Gene	Diff day 0	Diff day 6	Diff day 14
Osteoblasts	*RUNX2*	1.1±0.03	1.6±0.09	3.4±0.08
	OCN	1.1±0.12	1.0±0.15	2.9±0.38
	OSX	1.0±0.01	1.3±0.07	2.2±0.08
Adipocytes	*CEBPA*	0.9±01	*3.1±0.03*	3.2±0.2
	PPARG	1.1±0.07	2.8±0.15	3.5±0.05
	ADIPOQ	1.0±0.2	1.3±0.07	5.2±0.2

Among the six genes, only *ADCY5* showed haplotype-specific differences in gene expression (Figure 8 Left), with haplotype 1 being associated with 2.7-fold higher expression in both adipocytes and osteoblasts (p = 0.007, Figure 8 Right). These results implicated *ADCY5* as the likely regulatory target of the *3q21.1* locus.

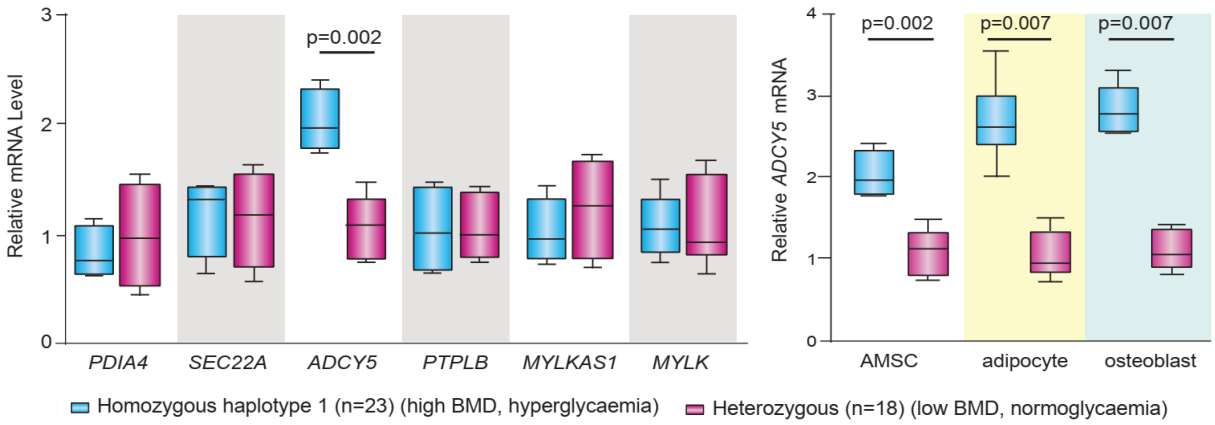

Figure 8. Quantitative PCR mRNA levels (y-axis, HPRT normalized) in primary cells from individuals heterozygous (dark grey, n=18) and homozygous (light grey, n=23) for haplotype 1 (Cohort 1). **Left**: Haplotype-dependent differential gene expression for six potential target genes across a 1Mb region centered on the 3q21.1 locus. Box plots depict relative gene expression + SD. Assays were performed at day 3 of osteoblast differentiation. **Right**: Haplotype-dependent differential gene expression of ADCY5 in undifferentiated adipose-derived AMSCs, differentiated adipocytes and osteoblasts.

4.1.4 Variant prioritization and effect analysis: rs56371916

Two orthogonal computational approaches were used to prioritize variants which could be responsible for the differential expression of *ADCY5.* Both approaches highlighted the same SNP, rs56371916 (Annex Table S3). The SNP rs56371916 was predicted to have the greatest effect, with the T-to-C substitution predicted to disrupt a highly conserved second position in a sterol regulatory-element-binding protein 1 (SREBP1) motif in fully differentiated adipocytes (Mabbott *et al.*, 2013; Weirauch *et al.*, 2014) (Figure 9). At day 0 of AMSC differentiation, the rs56371916 T allele (haplotype 1) has little effect and there is no substantial predicted change in accessibility (Figure 9B). By day 24, however, the accessibility has increased substantially with the rs56371916 T allele, the most critical nucleotide for 20bp sequence accessibility in terminally differentiated AMSC. Changes at rs56371916 are likely to reduce this accessibility, particularly if the T allele is changed to C, carried on haplotype 2 (Figure 9C). This is consistent with the overlapping SREBP1 motif, which is conserved across species (Figure 9A). The alternate C allele decreases accessibility by disrupting a SREBP1 motif.

Electrophoretic mobility shift assay (EMSA) confirmed that rs56371916 alters protein binding to the surrounding DNA sequence, with the C allele causing decreased protein binding (Figure 10). SREBP1 protein-binding to rs56371916 was confirmed by competition with an excess of probe containing a consensus binding sequence for SREBP1 (Figure 11).

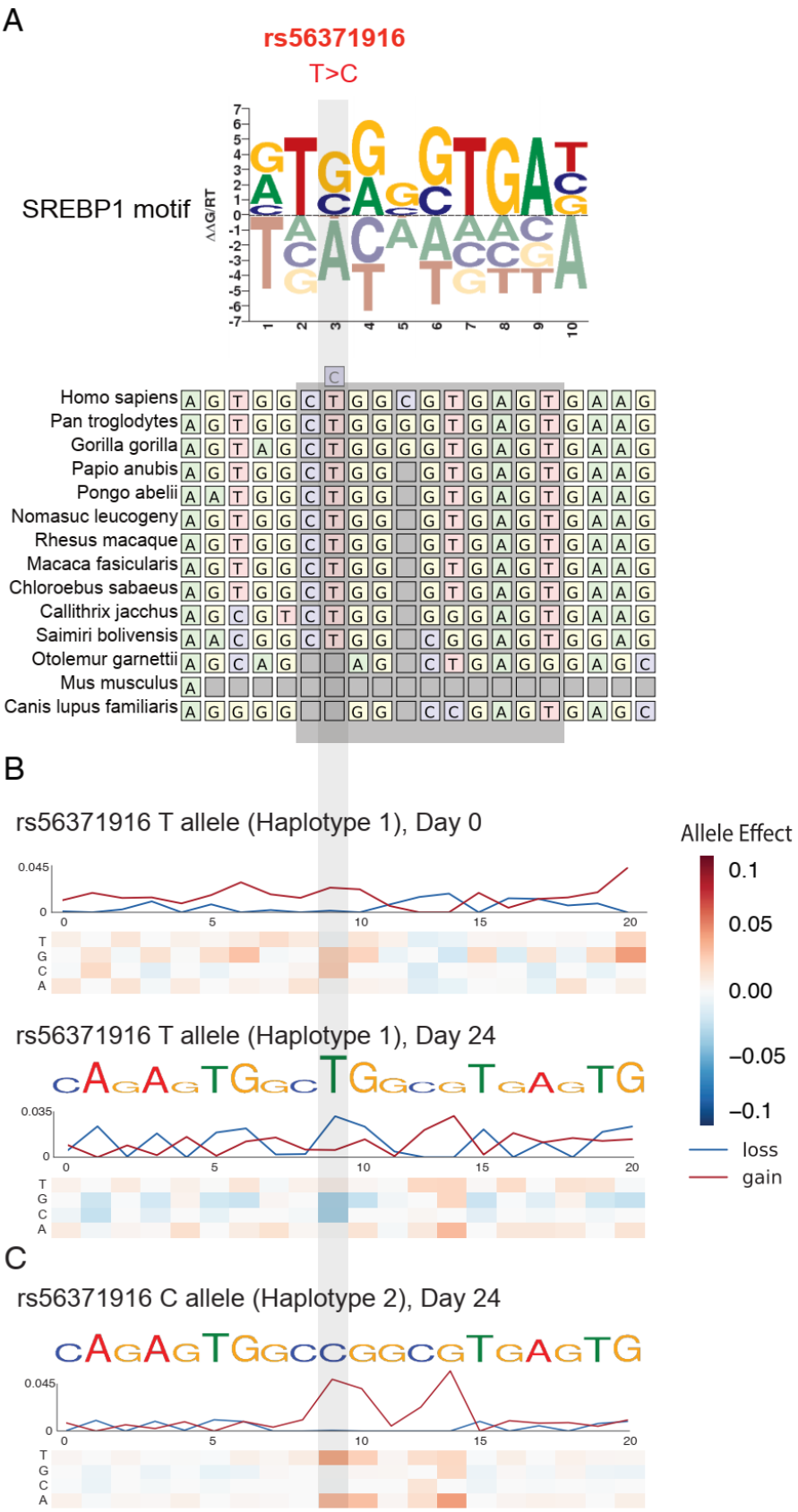

Figure 9. A: Multi-way multiz alignment of orthologous regions of the SREBP1 motif in rs56371916 in different species. **B-C:** *In silico* saturated mutagenesis for chromatin accessibility of 20 bp centered on rs56371916 for haplotype 1 (T allele, B) and haplotype 2 (C allele, C). The heatmaps display the change in predicted accessibility for any of the four possible nucleotides at day 0 and day 24 of differentiation.

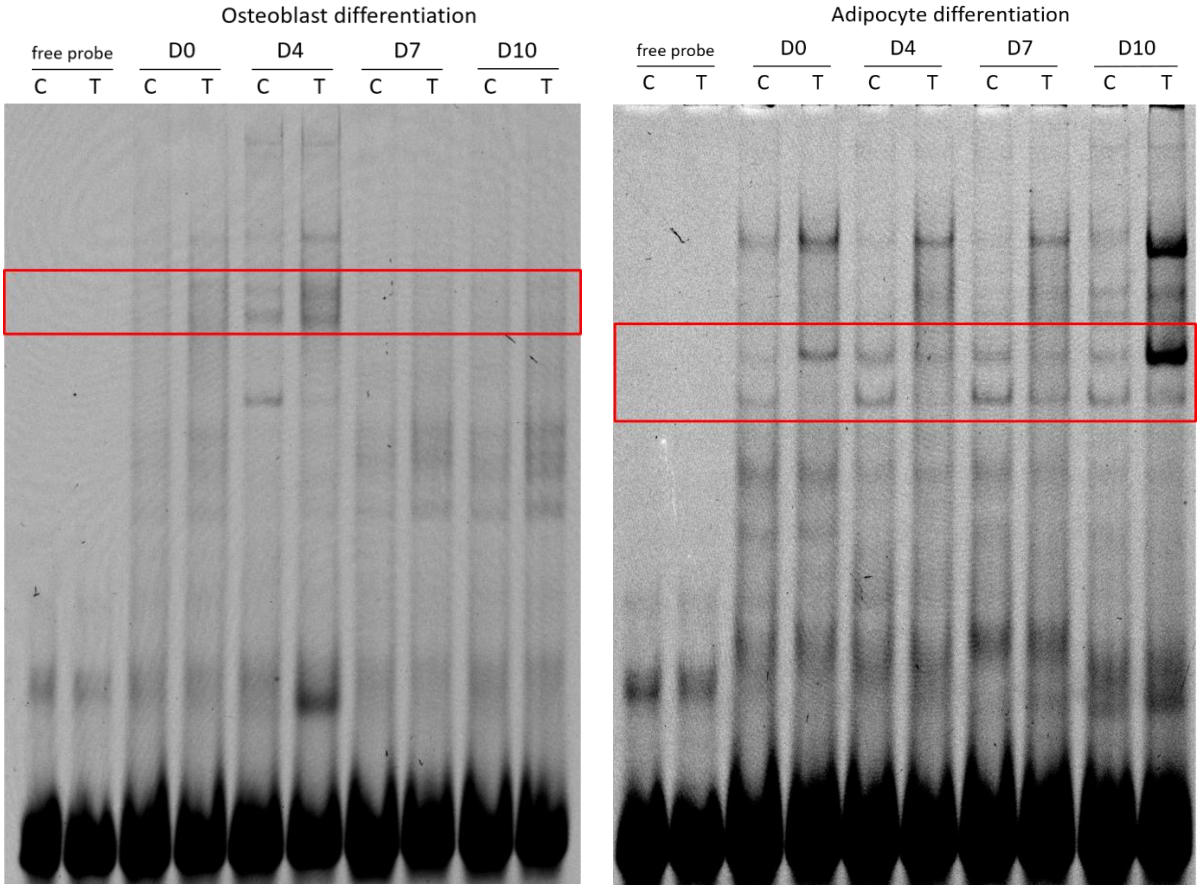

Figure 10. Electrophoretic mobility shift assays (EMSA) for 40bp oligonucleotides centered on rs56371916 using MC3T3 osteoblast (left) and AMSC-derived adipocyte (right) nuclear extract at different stages of differentiation (day 0, 4, 7, and 10). The upper bands correspond to the membrane bound form of SREBP1, while the double bands in the red box correspond to the cleaved active forms SREBP1-a and SREBP1-c (Bitter *et al.*, 2015).

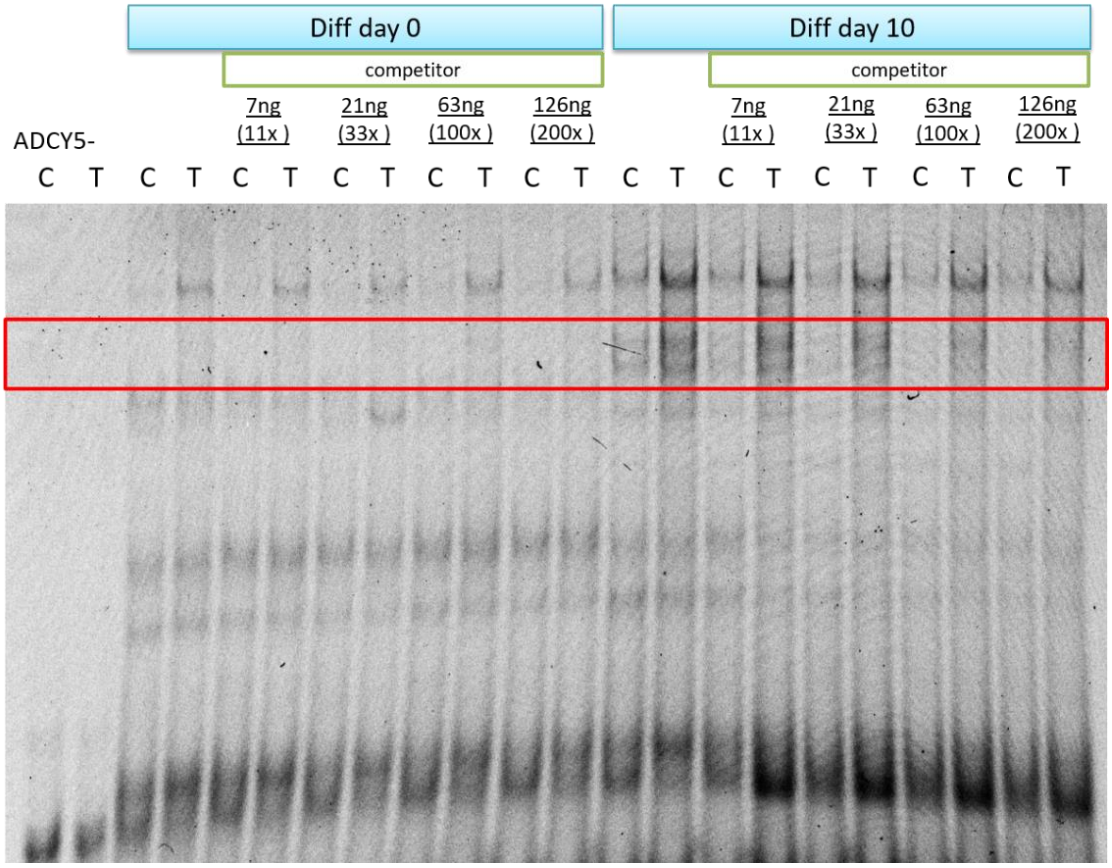

Figure 11. Competition EMSA assays using adipocyte nuclear extract. Competition assays were performed by adding 11-, 33-, 100-, and 200- molar excess of unlabeled probes. Differential binding of SREBP1 to the T allele was competed away with increasing amount of unlabeled probe, clearly visible with nuclear extract from day 10 of differentiation. The upper bands correspond to the membrane bound form of SREBP1, while the double bands in the red box correspond to the cleaved active forms SREBP1-a and SREBP1-c (Bitter *et al.*, 2015).

4.1.5 Genome editing of rs56371916 confirms its effect on ADCY5 expression

CRISPR-based genome editing was performed to directly confirm that the haplotype-specific effects on ADCY5 gene expression and cellular properties described above are mediated by rs56371916. AMSCs from a homozygote for haplotype 2 (genotype CC at rs56371916) were edited to create isogenic AMSCs with genotype TT. Following osteoblast induction, TT homozygous cells showed higher ADCY5 expression levels (1.6-fold) (Table 17) and higher expression of osteoblast differentiation marker genes (RUNX2, OCN and OSX; 1.5-, 1.8- and 2.1-fold, respectively, Figure 12 Left).

Table 17. Relative ADCY5 mRNA levels in CRISPR edited cells

Osteoblasts (ratio TT/CC)	**Fold change (±SE)**	**p-value**
D0 (AMSC)	1.6+0.4	0.0286
D14 (differentiated osteoblasts)	1.1+0.2	n.s.
Adipocytes (ratio CC/TT)	**Fold change (±SE)**	**p-value**
D0 (AMSC)	0.7+0.3	0.0286
D14 (differentiated osteoblasts)	1.03+0.3	n.s.

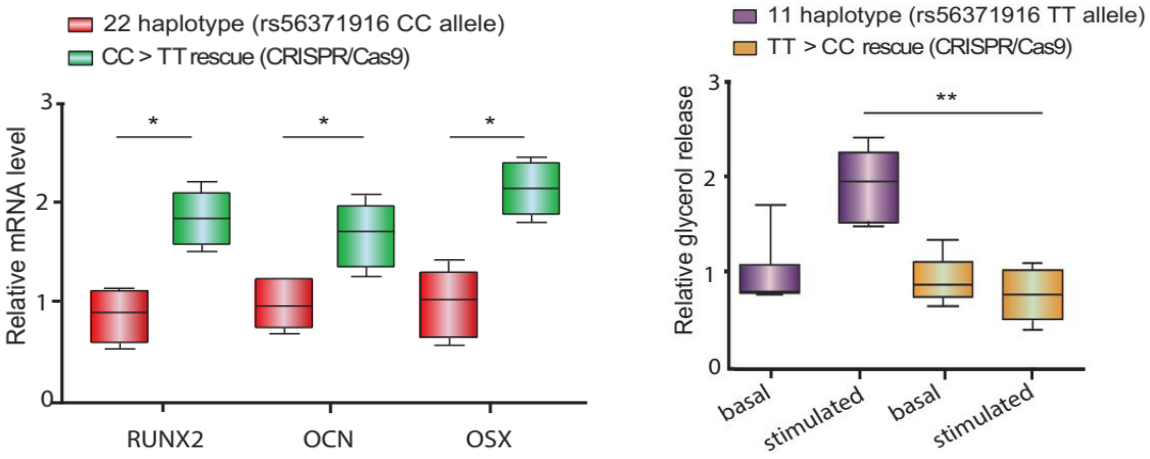

Figure 12. Left: Generation of isogenic AMSCs with genotype TT at rs56371916 starting from a CC homozygote. Isogenic lines were differentiated to osteoblasts after undergoing clonal expansion, and marker gene expression for osteoblast differentiation was measured by qPCR. Right: Generation of isogenic AMSCs with genotype CC at rs56371916 starting from a TT homozygote. Isogenic lines were differentiated to adipocytes after undergoing clonal expansion, and catecholamine-stimulated lipolysis was measured.

AMSCs from a homozygote for haplotype 1 (genotype TT at rs56371916) were also edited to create isogenic AMSCs with genotype CC. Following adipocyte induction, CC homozygous cells showed reduced expression of ADCY5 (1.6-fold, Table 17) and lipolysis marker genes (1.5- to 1.9-fold) measured by qPCR (Table 18), as well as a reduced rate of catecholamine-stimulated lipolysis (2.1-fold, Figure 12 Right). The genome-editing results in primary adipocytes and osteoblasts confirm that rs56371916 has a direct effect on *ADCY5* gene expression and cellular phenotypes relevant to FNBMD and glucose homeostasis.

Table 18. Relative mRNA levels in adipocytes (ratio TT/CC)

	Diff day 0		**Diff day 14**	
Gene	**Fold change**	**p-value**	**Fold change**	**p-value**
ATGL	1.3+0.4	0.02	1.5+0.9	0.07
HSL	1.8+0.63	0.09	1.8+0.4	0.03
PLIN2	1.9+0.42	0.05	1.9+1.2	0.05

4.2 Pleiotropy of AD and T2D

4.2.1 GWAS identifies bivariate loci for Alzheimer's disease and Type 2 Diabetes

A bivariate GWAS analysis was performed to uncover pleiotropy of AD and T2D. This analysis identified 15 bivariate loci at a suggestive significance level (bivariate p-value ≤ 5×10^{-6}), of which 10 were novel loci (Table S1).

The loci significantly associated with both traits were then annotated and mined to allow functional classification - such as determining if the locus is in a coding or non-coding region - and define its relevance for disease susceptibility. Afterwards, epigenomic profiling across 127 human cell types (Roadmap Epigenomics Consortium *et al.*, 2015) was performed to infer the regulatory states and cell types affected by the selected loci. The identified bivariate signals were enriched in blood and T cell related epigenomes, namely DND-41 leukemia T cell line, primary hematopoietic stem cells and thymus (Figure S2). The relevance of T cells in T2D-AD pleiotropy is also supported by the literature as discussed in the introduction. Taken together, these results pointed us to investigate the effects of candidate loci in T cells.

Prioritization of the 15 bivariate loci was done by computational analysis of linkage disequilibrium (LD) (R^2>0.8, 1000G Phase 1) and functional conservation scores based on the PMCA method (Claussnitzer *et al.*, 2014). From the top 5 loci, the *MAP2K5* locus contained several variants in high LD with the tagSNP rs16951304, localized in T cell precursor enhancers (Figure 13). Therefore, we focused on dissecting the effect of the *MAP2K5* locus in pleiotropy of T2D-AD.

Figure 13 (next page). Regional association plot of the AD-T2D associated SNPs resulting from bivariate genome-wide association analysis. Top: Genetic association with AD and T2D for MAP2K5 locus variants. Bivariate association (y-axis) and genomic coordinates (x-axis) for all common single nucleotide polymorphisms (SNPs; circles) in a 600 kb window of chromosome 15 centered on the MAP2K5 bivariate locus. The region of association contains several variants in high linkage disequilibrium (LD) in Europeans (1000 Genomes r^2, color). Bottom: Chromatin state annotations for the 600 kb bivariate locus. Genomic interval shows chromatin state across 12 human reference epigenomes related to blood and T cells profiled by the Roadmap Epigenomics projects, based on a 25-state chromatin state model (color code on the right) learned from 12 epigenomic marks using imputed signal tracks at 25-nucleotide resolution (Roadmap Epigenomics Consortium *et al.*, 2015).

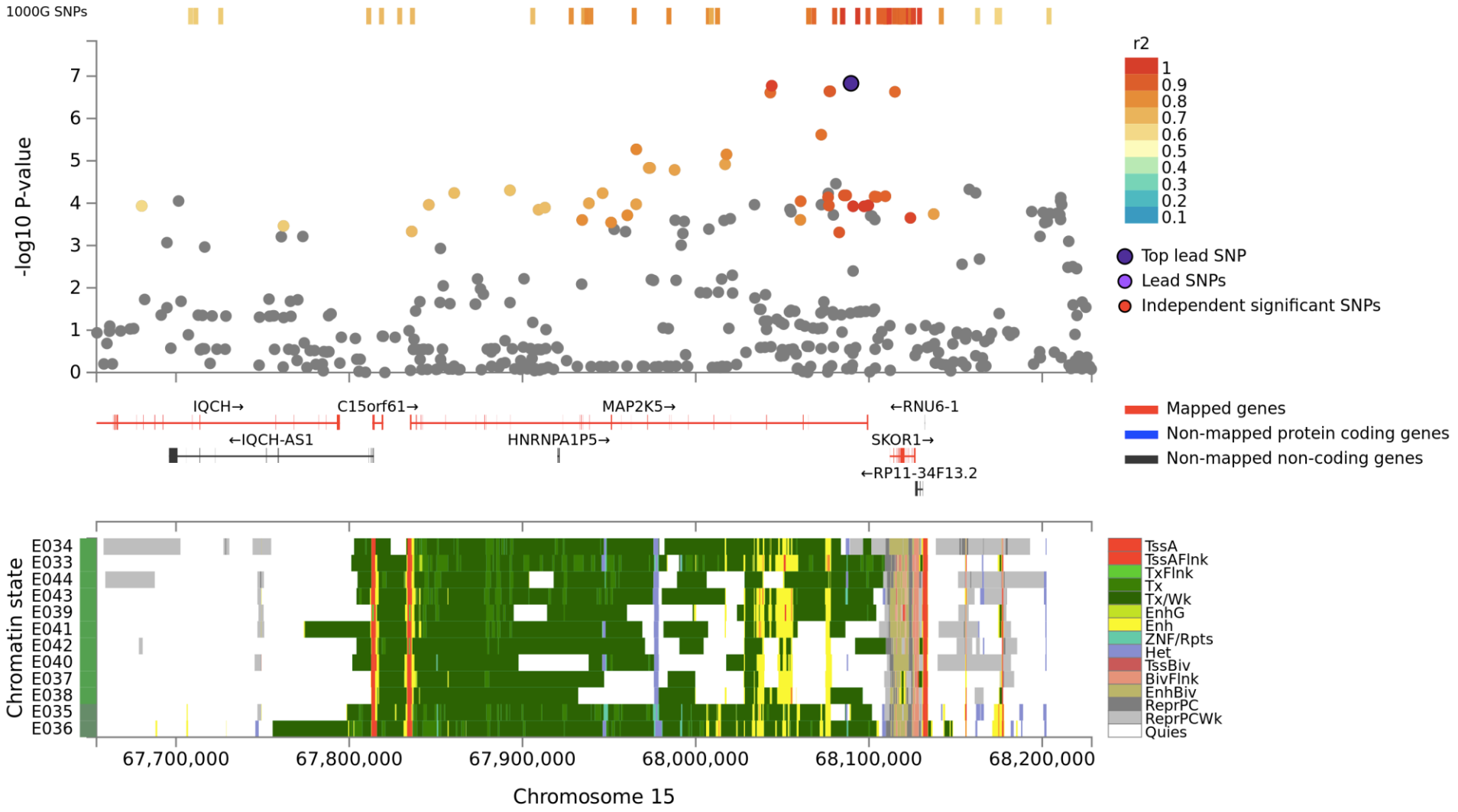
1000G SNPs
-log10 P-value
0
1
2
3
4
5
6
7
r2
1
0.9
0.8
0.7
0.6
0.5
0.4
0.3
0.2
0.1
Top lead SNP
Lead SNPs
Independent significant SNPs
IQCH→
C15orf61→
MAP2K5→
←RNU6-1
←IQCH-AS1
HNRNPA1P5→
SKOR1→
←RP11-34F13.2
Mapped genes
Non-mapped protein coding genes
Non-mapped non-coding genes
Chromatin state
E034
E033
E044
E043
E039
E041
E042
E040
E037
E038
E035
E036
TssA
TssAFlnk
TxFlnk
Tx
Tx/Wk
EnhG
Enh
ZNF/Rpts
Het
TssBiv
BivFlnk
EnhBiv
ReprPC
ReprPCWk
Quies
67,700,000
67,800,000
67,900,000
68,000,000
68,100,000
68,200,000
Chromosome 15

4.2.2 Establishment of a $CD4^+$ T cell differentiation model

$CD4^+$ T cells were isolated from healthy male volunteers as described in the methods. Selected $CD4^+$ T cells were stimulated to differentiate using different cocktails of specific stimulatory molecules to direct them towards regulatory T cells (Treg) and T helper 17 cells (Th17). Differentiation of $CD4^+$ T cells into Treg is promoted by TGF-β1 and IL-2 in addition to CD3 and CD28 stimulation. On the other hand, differentiation of Th17 is promoted by the presence of IL-6, IL-1β, IL-23 and TGF-β1. The presence of IL-4 and IFNy suppresses Th17 differentiation, therefore antibodies against these molecules were used to prevent its binding to their respective receptors.

Cells were kept in culture to differentiate for 7 days. Assessment of differentiation efficiency was done by measuring gene expression of markers specific for Treg and Th17 cells. Protocols 2 (Treg P2 and Th17 P2) produced the best stimulation of expression of differentiation markers for both Treg and Th17 phenotypes (Figure 14) and were therefore selected for subsequent experiments.

Table 19 Media tested for Treg differentiation

Treg	**Protocol 1**	**Protocol 2**	**Protocol 3**
	ng/ml	ng/ml	ng/ml
TGF-β1	1	2	5
IL-2	5	5	5
	µg/ml	µg/ml	µg/ml
anti-CD3	5	5	5
anti-CD28	1	1	1

Table 20 Media tested for Th17 differentiation

Th17	**Protocol 1**	**Protocol 2**	**Protocol 3**
	ng/ml	ng/ml	ng/ml
IL-6	10	30	10
IL-1β	10	20	10
IL-23	10	30	10
TGF-β1	5-10	2,25	5
	µg/ml	µg/ml	µg/ml
anti-IL4	10	2,5	2,5
anti-IFNy	10	1	1
anti-CD3	10	5	5
anti-CD28	1	1	1

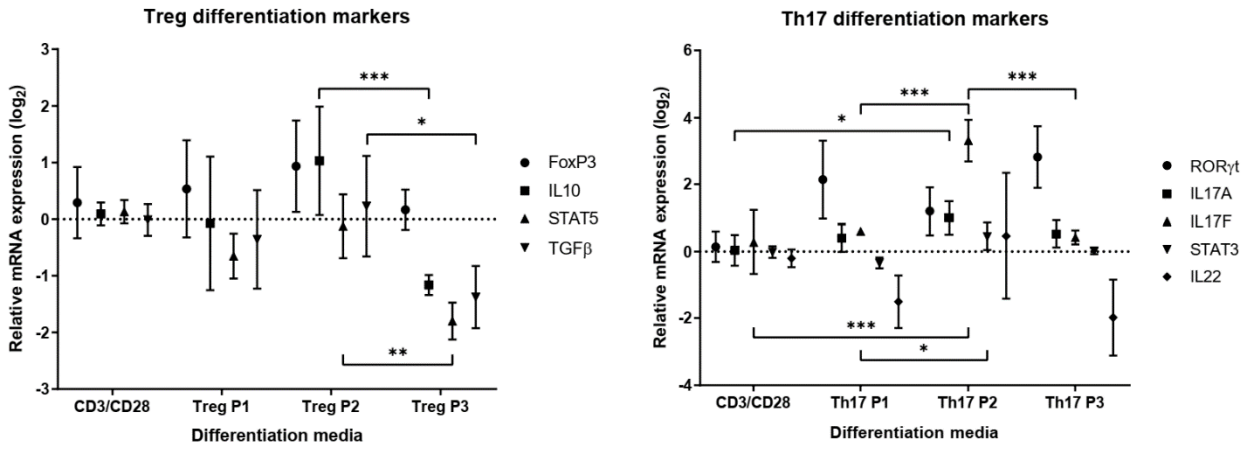

Figure 14. Gene expression of differentiation markers after 7 days of differentiation. CD3/CD28 - cells were stimulated only with anti-CD3 and anti-CD28 antibodies; P1, P2 and P3 refers to the corresponding differentiation protocols indicated in Table 19 and Table 20. n=3, mean (SD), two-way ANOVA, *p<0.05, **p<0.01, **p<0.001.

4.2.3 Establishment of *MAP2K5* KD

In order to choose the best time window for KD of *MAP2K5*, the expression pattern of T cell differentiation markers and *MAP2K5* was assessed in a differentiation time-curve (Figure 15). Gene expression of differentiation markers for both Treg and Th17 peaked within 6 hours of stimulation and *MAP2K5* increased up to 24 hours, therefore the KD was performed before differentiation induction and cells were harvested 6 hours after induction to determine the role of *MAP2K5* in the differentiation process from the very beginning.

The KD method selected was Accelll siRNA from Dharmacon, which is designed for difficult to transfect cells such as T cells. The transfection kit includes a siRNA targeting GAPD for positive control and a green (FAM labeled) non-targeting siRNA for visual assessment of transfection efficiency (Figure 16 Right). Both positive control and MAP2K5 siRNA produced a significant KD (90% KD GAPD and 87% KD MAP2K5, Figure 16 Left) without affecting cell viability (over 90% live cells after 72 hours KD). Considering the KD efficiency and low cytotoxicity, Accell siRNA transfection was selected for further KD experiments.

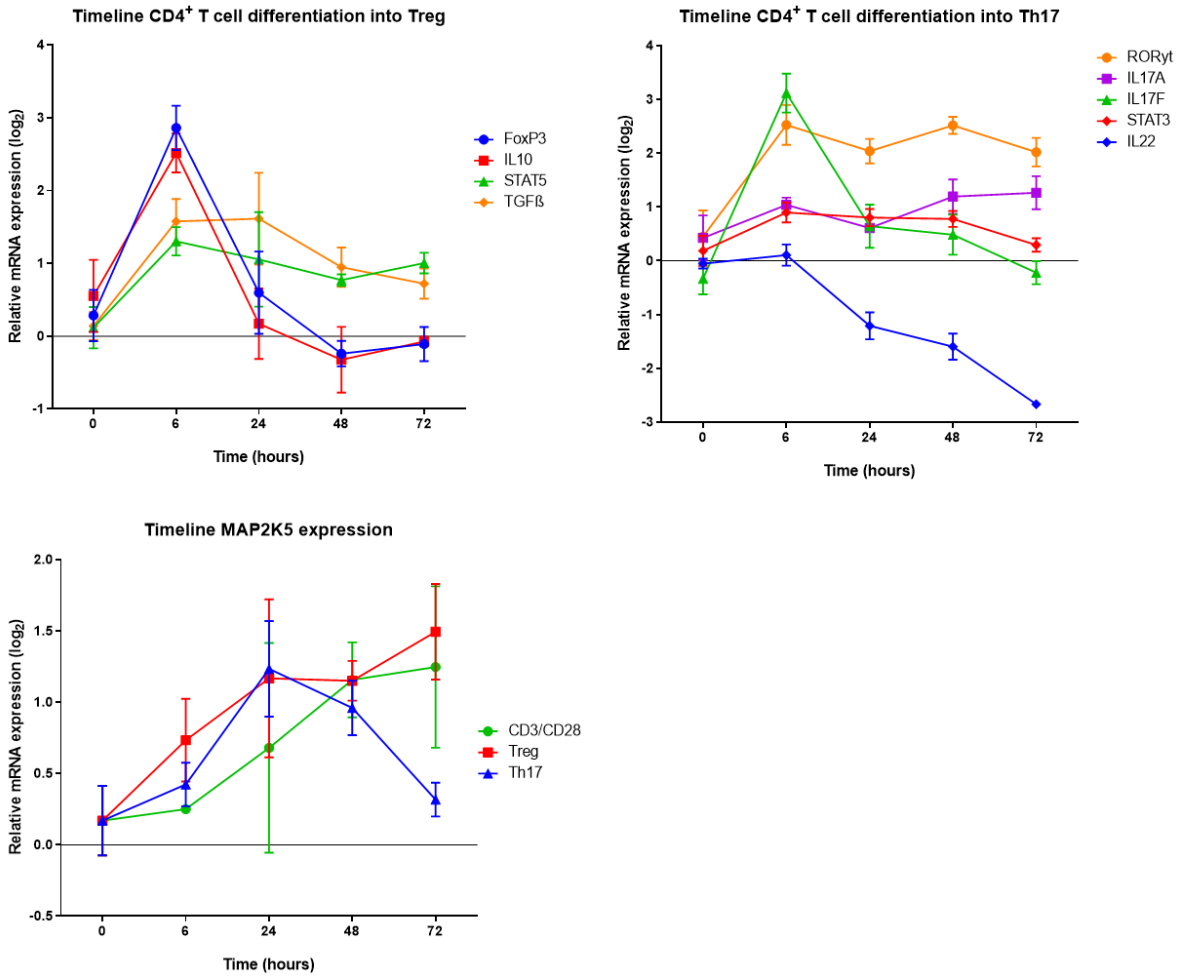

Figure 15. Gene expression time course of differentiation markers and *MAP2K5* in CD4⁺ T cells. Cells were stimulated with the differentiation cocktail previously determined and harvested at selected time points for RNA isolation and qPCR. n=3, mean (SD).

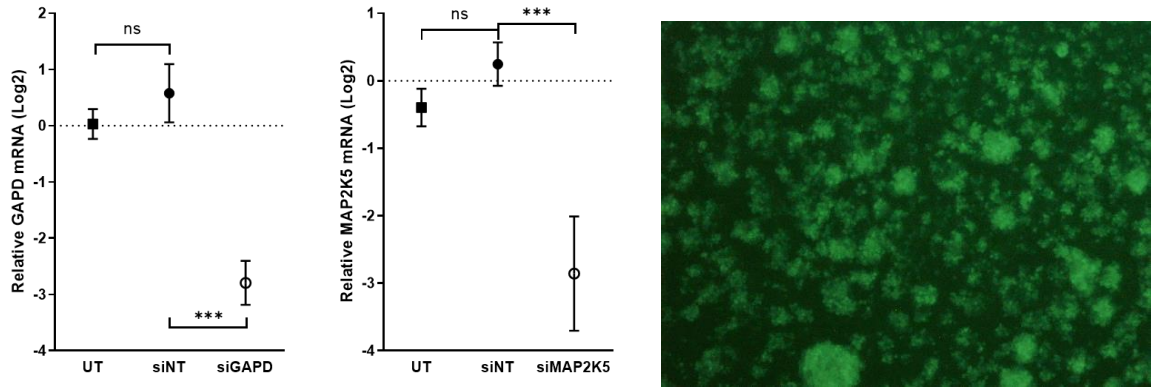

Figure 16. Left: Accell siRNA KD test. Transfection with 1 µM accell siRNA non-targeting (siNT), targeting *GAPD* (siGAPD) and SMART pool with 4 siRNAs targeting *MAP2K5* (siMAP2K5). n=3, one-way ANOVA with multiple comparisons, ns=non-significant, *** p<0.001. **Right:** Visual assessment of transfection efficiency of green non-targeting siRNA.

4.2.4 Effect of *MAP2K5* KD in CD4$^+$ T cell differentiation

Once an efficient KD method was established, the relevance of MAP2K5 during T cell differentiation was assessed. Cells were isolated from 17 healthy male volunteers (phenotyping in Table 21) and frozen once in liquid nitrogen before use. The experimental set up used to determine the effect of *MAP2K5* KD in CD4$^+$ T cell differentiation is depicted below in Figure 17.

Table 21. Characterization of the male study population

Parameter	Average	SD
Age (years)	26.2	3.9
BMI (kg/m^2)	22.6	2.2
Waist circumference (cm)	82.7	6.6
Fasting glucose (mg/dL)	94.1	6.3
% CD4$^+$ T cells	19.8	4.9

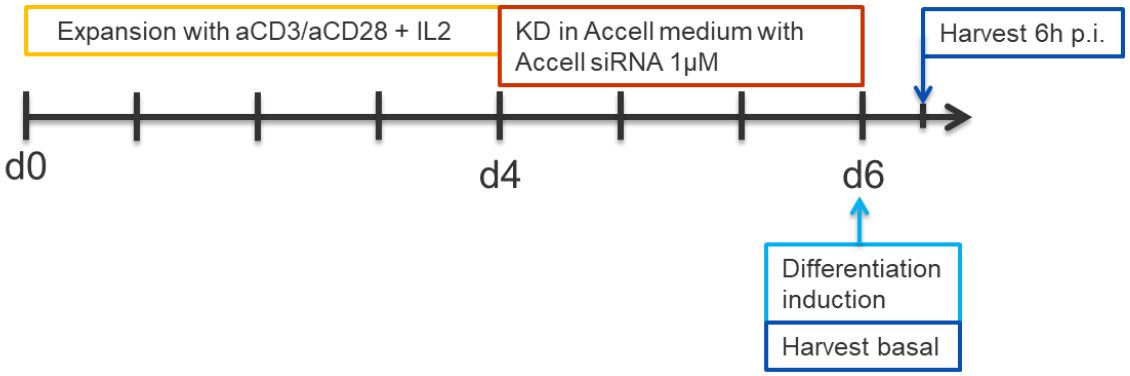

Figure 17. Diagram of the experimental timeline for accessing the effect of MAP2K5 KD in CD4$^+$ T cell differentiation.

Of the 17 individuals tested, a significant MAP2K5 KD was achieved at basal in 14 individuals, with only 4 showing a significant effect of *MAP2K5* KD in expression of T cell differentiation markers. One individual showed a significant increase in mRNA levels of Th17 cytokines IL17A, IL17F and IL22 (Figure 18). Both IL17A and IL17F are key cytokines for the recruitment, activation and migration of macrophages and neutrophils to the site of inflammation, and can also target non-immune cells such as fibroblast and endothelial cells to produce pro-inflammatory molecules (Maddur *et al.*, 2012).

Two individuals showed a significant reduction in Treg differentiation markers (Figure 19 and Figure 20). FoxP3 is the main transcription factor responsible for differentiation of naïve CD4$^+$ T cells into Tregs and essential for its function as modulators of inflammation and immune response, along with the secretion of immunosuppressive cytokines IL10 and TGFβ capable of suppressing proinflammatory responses in dendritic cells, macrophages, natural killer cells, among others. (Plitas and Rudensky, 2016).

These results emphasize the importance of the individual genetic background when assessing the phenotype effects of manipulating gene expression. The direction of effects observed supports our hypothesis that the causal locus would promote CD4$^+$ T cell differentiation into Th17 and reduce the differentiation into Treg.

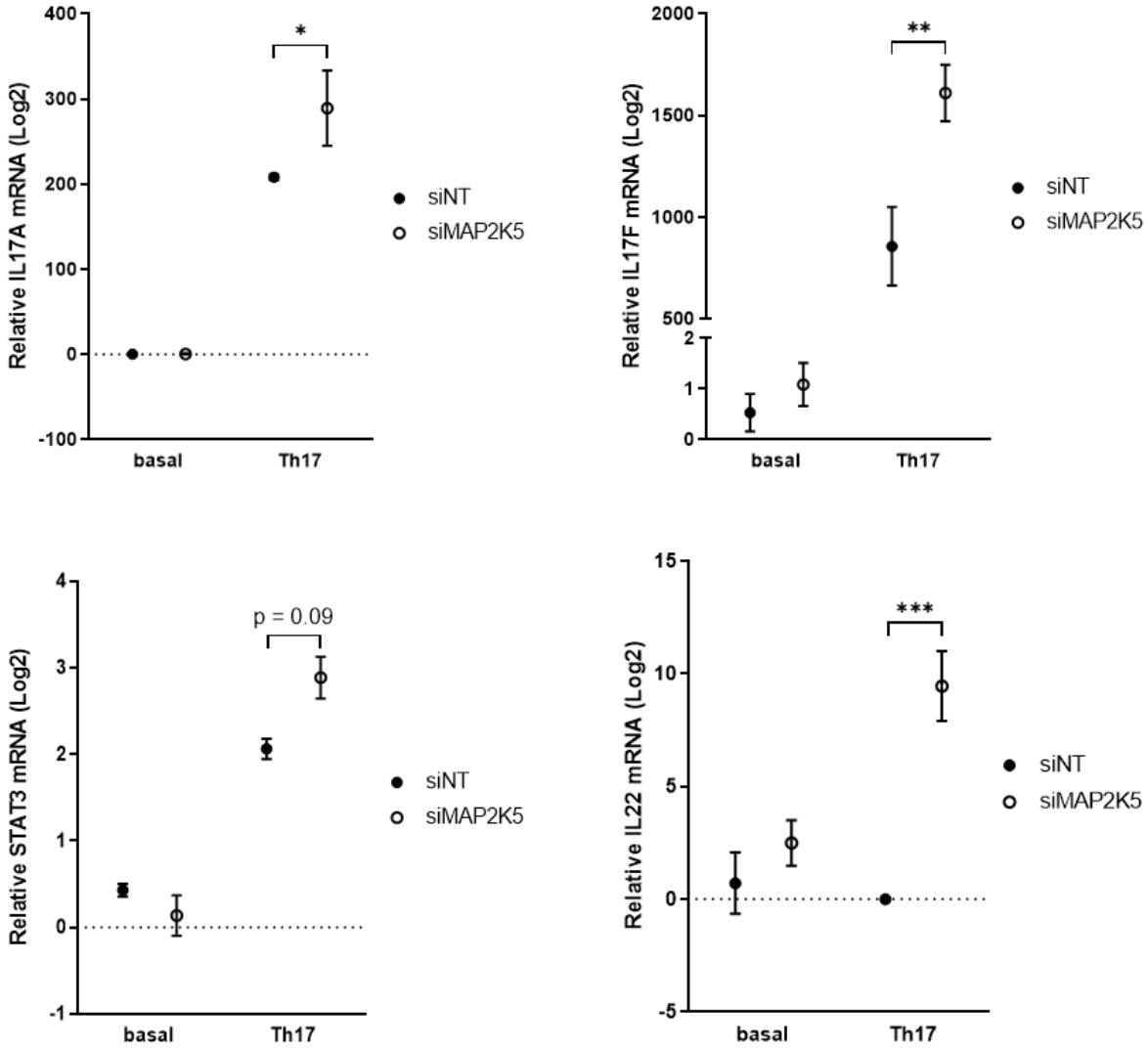

Figure 18. *MAP2K5* KD in CD4⁺ T cells from SH1 followed by 6 hour differentiation into Th17. mRNA expression of Th17 differentiation markers of one experiment with technical replicates. Symbols show mean ± SD (error bars smaller than the symbol not shown). Two-way ANOVA with multiple comparisons (Tukey), * $p<0.05$, ** $p<0.01$, *** $p<0.001$. siRNA silencing produced a significant KD (61%, $p<0.001$) of MAP2K5 at basal condition. In this individual, the KD of MAP2K5 at differentiation onset produced a significant increase in mRNA expression of Th17 main cytokines IL17A, IL17F and IL22.

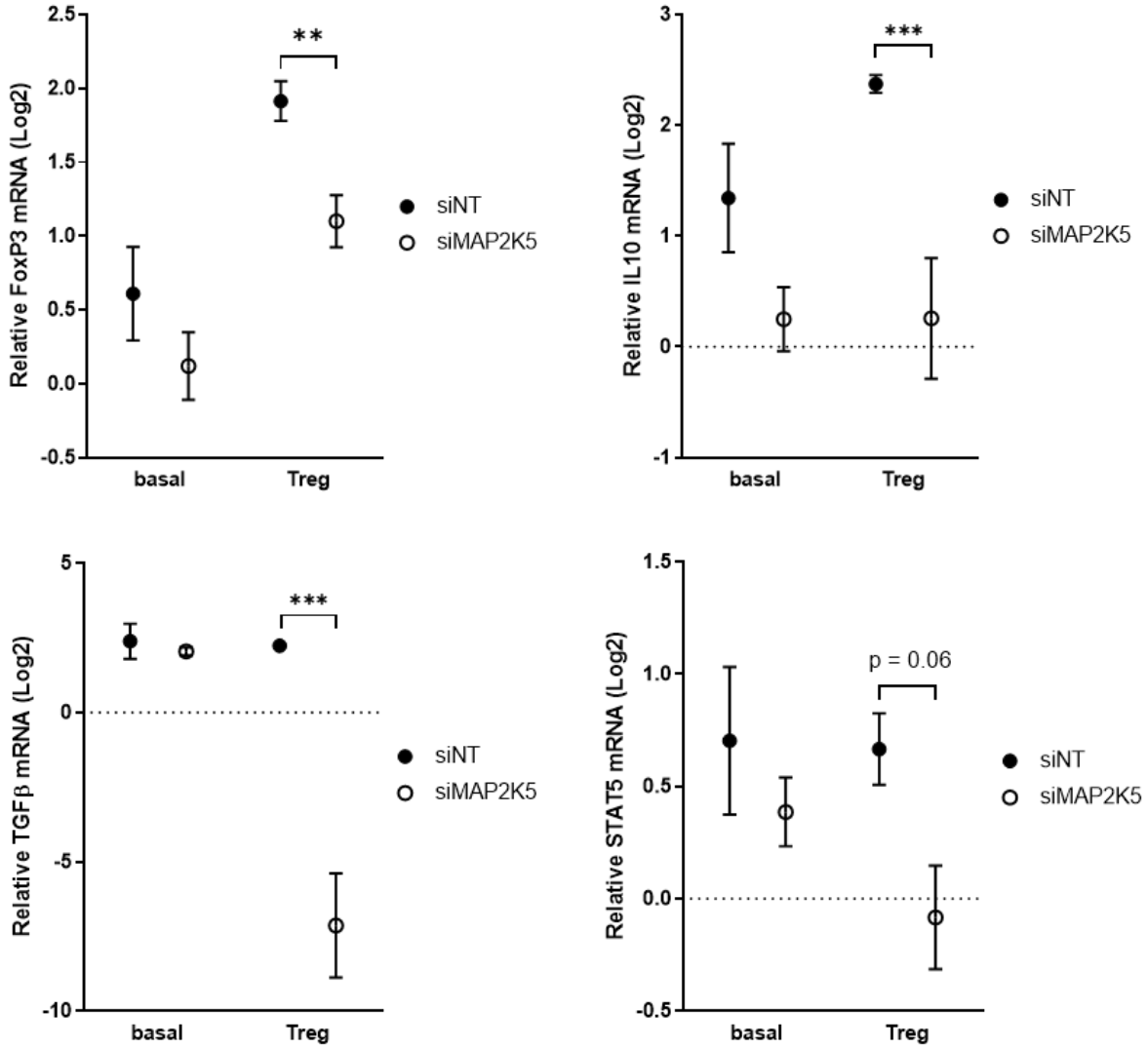

Figure 19. *MAP2K5* KD in CD4$^+$ T cells from JB1 followed by 6 hour differentiation into Treg. mRNA expression of Treg differentiation markers (*FoxP3*, *IL10*, *STAT5*, *TGFβ*) of one experiment with technical replicates. Symbols show mean ± SD (error bars smaller than the symbol not shown). Two-way ANOVA with multiple comparisons (Tukey), ns= non-significant, * p<0.05, ** p<0.01, *** p<0.001. siRNA silencing produced a significant KD (56%, p<0.001) of MAP2K5 at basal condition. In this individual, the KD of MAP2K5 at differentiation onset produced a significant reduction in mRNA expression of Treg transcription factor FoxP3 and cytokines IL10 and TGFβ.

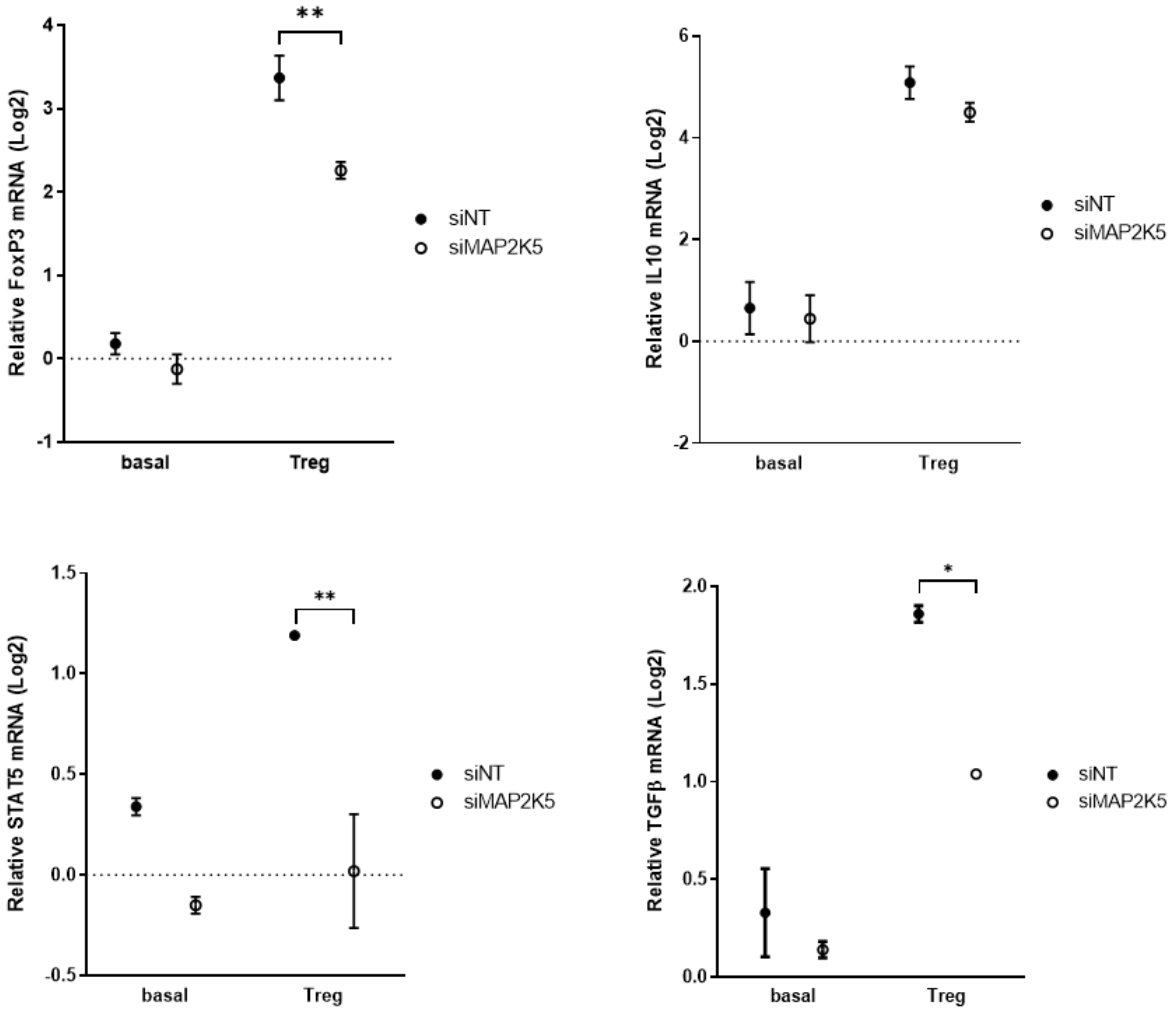

Figure 20. *MAP2K5* KD in CD4$^+$ T cells from FN1 followed by 6 hour differentiation into Treg. mRNA expression of Treg differentiation markers (*FoxP3*, *IL10*, *STAT5*, *TGFβ*) of one experiment with technical replicates. Symbols show mean ± SD (error bars smaller than the symbol not shown). Two-way ANOVA with multiple comparisons (Tukey), ns=non-significant, * p<0.05, ** p<0.01, *** p<0.001. siRNA silencing produced a significant KD (72%, p<0.001) of MAP2K5 at basal condition. In this individual, the KD of MAP2K5 at differentiation onset produced a significant reduction in mRNA expression of Treg transcription factors FoxP3 and STAT5, and the cytokine TGFβ.

4.2.5 Establishment of SH-SY5Y as a neuronal cell model

Differentiation of the SH-SY5Y cell line into neuronal like cells was accomplished with retinoic acid, which induces expression of cell neurites and a neuron-like phenotype, followed by maintenance in BDNF containing medium. During differentiation, SH-SY5Y cells form neurites to establish a neuronal network, as shown in Figure 21. The genes selected for characterization of SH-SY5Y cells are differentially expressed genes related to axonal guidance (NTRK2, NTF4, SLITRK6, PLNXD1) and neuronal markers (MAP2, SYN1) (Pezzini *et al.*, 2017).

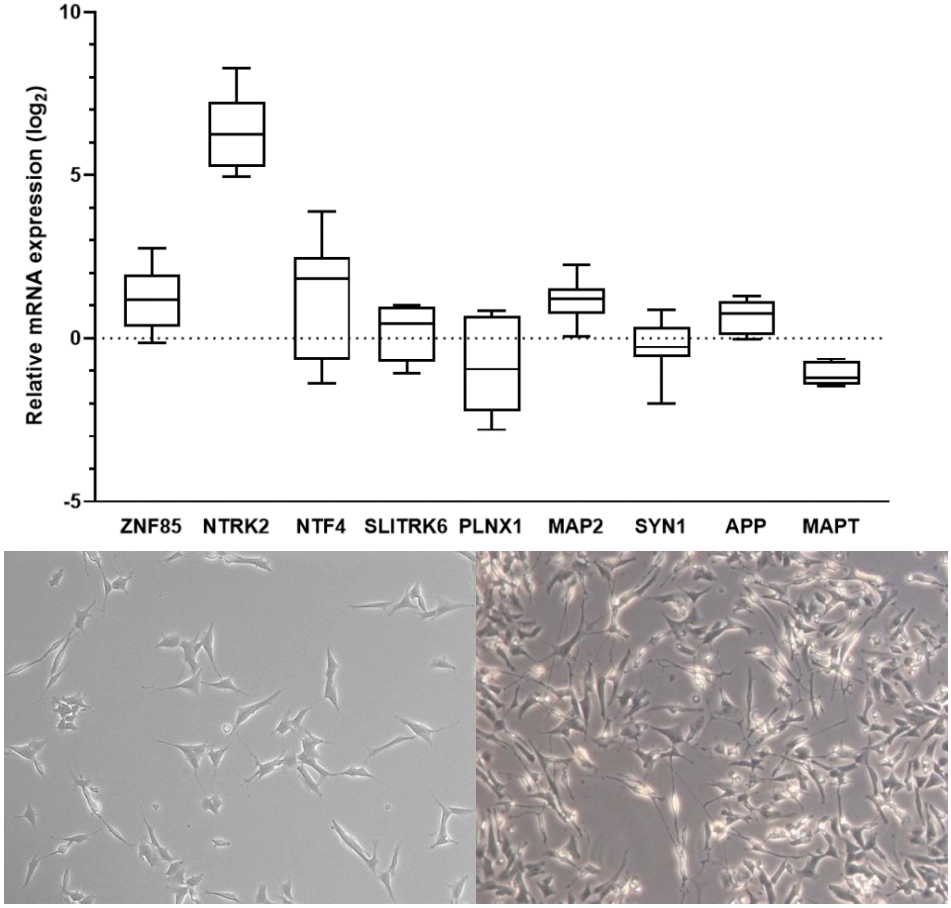

Figure 21. Characterization of SH-SY5Y differentiation into neuronal-like cells. **Top:** Gene expression of neuronal differentiation markers. **Bottom:** Live cell images of undifferentiated (left) and differentiated cells (right) with observed neurite formation. Micrograph taken at 10x magnification under an Inverted Laboratory Microscope LEICA DM IL LED.

4.2.6 Co-culture of *MAP2K5* KD CD4$^+$ T cells with human preadipocytes and human neuronal cell line SH-SY5Y

In order to establish pleiotropy of the *MAP2K5* locus, we analyzed the effect of CD4$^+$ T cells with *MAP2K5* KD in co-culture with human preadipocytes and the human neuronal cell line SH-SY5Y. The co-culture was set up by first plating PAC and SH-SY5Y, differentiating them and then adding CD4$^+$ T cells with *MAP2K5* KD directly into the wells. This approach was chosen instead of using co-culture inserts to determine the effects of direct contact between T cells and differentiated adipocytes/neuronal cells. The supernatant from T cell differentiation was also added to both PAC and SH-SY5Y to distinguish cytokine mediated from direct cell-cell contact effects.

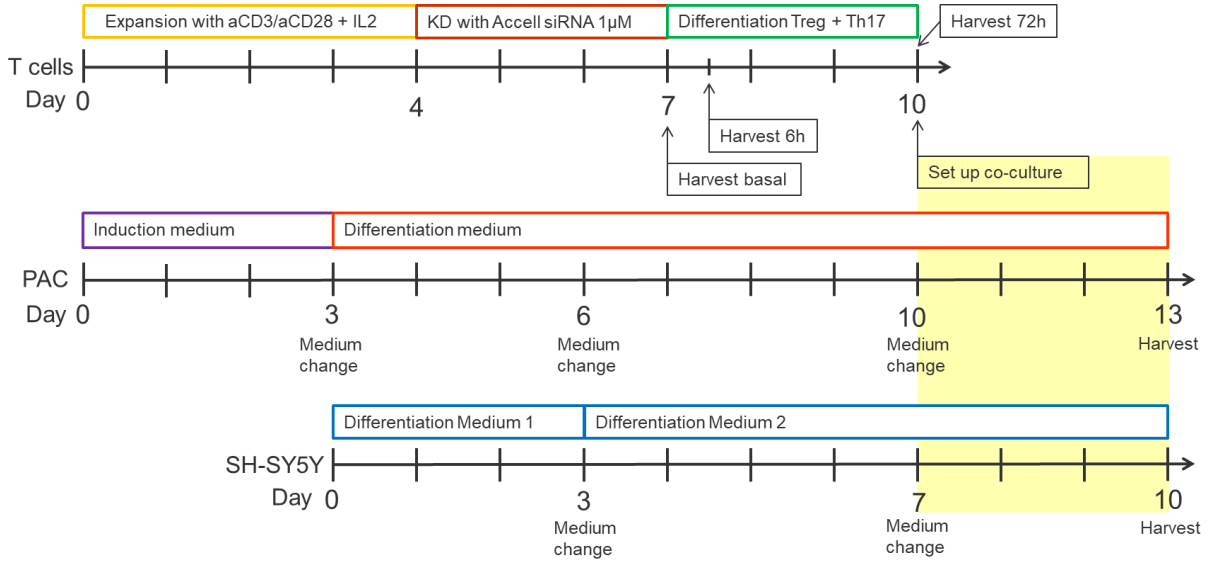

Figure 22. Diagram of experimental timeline for co-culture experiments. PAC and SH-SY5Y were expanded, plated and induced when confluent (expansion time not shown). T cells were expanded, KD for MAP2K5, and differentiated into Treg and Th17 for 72h. Afterwards, co-culture was set up by transferring both T cells and their supernatant into differentiated PAC and SH-SY5Y cultures. Readouts were performed after 3 days of co-culture.

4.2.6.1 MAP2K5 KD in T cells

T cells were first expanded followed by induction of *MAP2K5* KD and differentiation into Treg and Th17. *MAP2K5* KD was significant at basal level (56%, $p<0.001$). It is important to mention that the cells at basal are split into Treg and Th17 differentiation media, so that the KD conditions are the same at the start of differentiation. The differentiation protocol produced changes in gene expression of Treg and Th17 phenotypes as previously shown. Metabolic regulators of T cell differentiation also exhibited a significant variation in expression pattern with time, with *MAP2K5* KD significantly increasing *ACACA* and *SLC2A1* expression in Th17 differentiation at 72 hours (Figure 23).

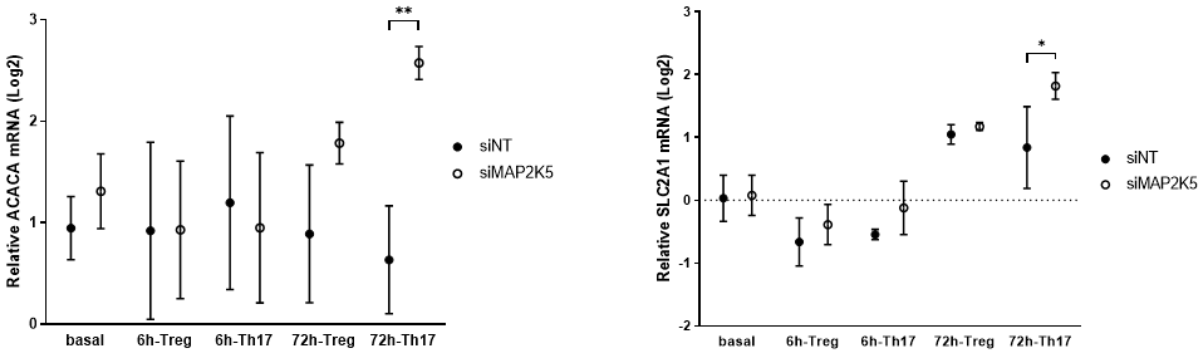

Figure 23. *MAP2K5* KD in CD4$^+$ T cells followed by differentiation into Treg and Th17. mRNA expression of metabolic regulators of T cell development. One experiment with technical replicates, symbols show mean ± SD. Two-way ANOVA with multiple comparisons (Tukey), * p<0.05, ** p<0.01.

4.2.6.2 Co-culture of T cells with differentiated PAC

Viability of differentiated PAC in the presence of T cells was assessed via reduction of tetrazolium salt WST-8 to formazan (Figure 24 left). Although not statistically significant, co-culture of T cells with *MAP2K5* KD and their supernatant showed a tendency to reduce preadipocyte viability. Regarding lipid storage, co-culture of differentiated PAC with T cell supernatant significantly reduced lipid accumulation, with *MAP2K5* KD showing a tendency for a stronger reduction (Figure 24 right).

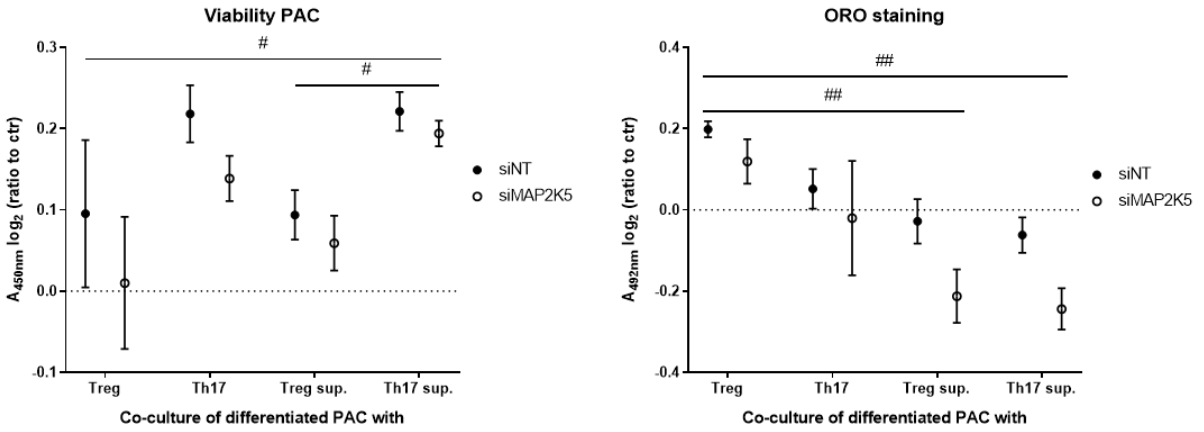

Figure 24. **Left:** Assessment of viability of differentiated PAC in co-culture with T cells and their supernatant. Absorbance of formazan at 450 nm shown as ratio to control (differentiated PAC without co-culture). **Right:** Quantification of lipid accumulation in differentiated PAC in co-culture with T cells and their supernatant. Absorbance of isopropanol at 492 nm shown as ratio to control (differentiated PAC without co-culture). One experiment with technical duplicates, symbols show mean ± SD. Two-way ANOVA with multiple comparisons (Tukey), # p<0.05 and ## p<0.01 indicate significant effect of differentiated T cells and their supernatant independent of KD.

The effect of T cells on the inflammatory status of differentiated PAC was assessed via gene expression of inflammation markers (Table 22).

Table 22. Inflammation markers measured in differentiated preadipocytes.

Pro-inflammatory markers	Anti-inflammatory markers
TNF-α	*Adiponectin*
MCP-1	*IL-10*
IL-6	
Leptin	

Treg cells with *MAP2K5* KD caused a decrease in *IL-6* and *MCP-1* expression compared to control siRNA, but their supernatant had the opposite effect, inducing a significant increase in *IL-6* and *MCP-1* expression (Figure 25 top). The supernatant of Th17 cells with *MAP2K5* KD caused a significant reduction in *Adiponectin* expression, and a significant increase in *Leptin* expression, indicating an increase in inflammation of the differentiated PAC.

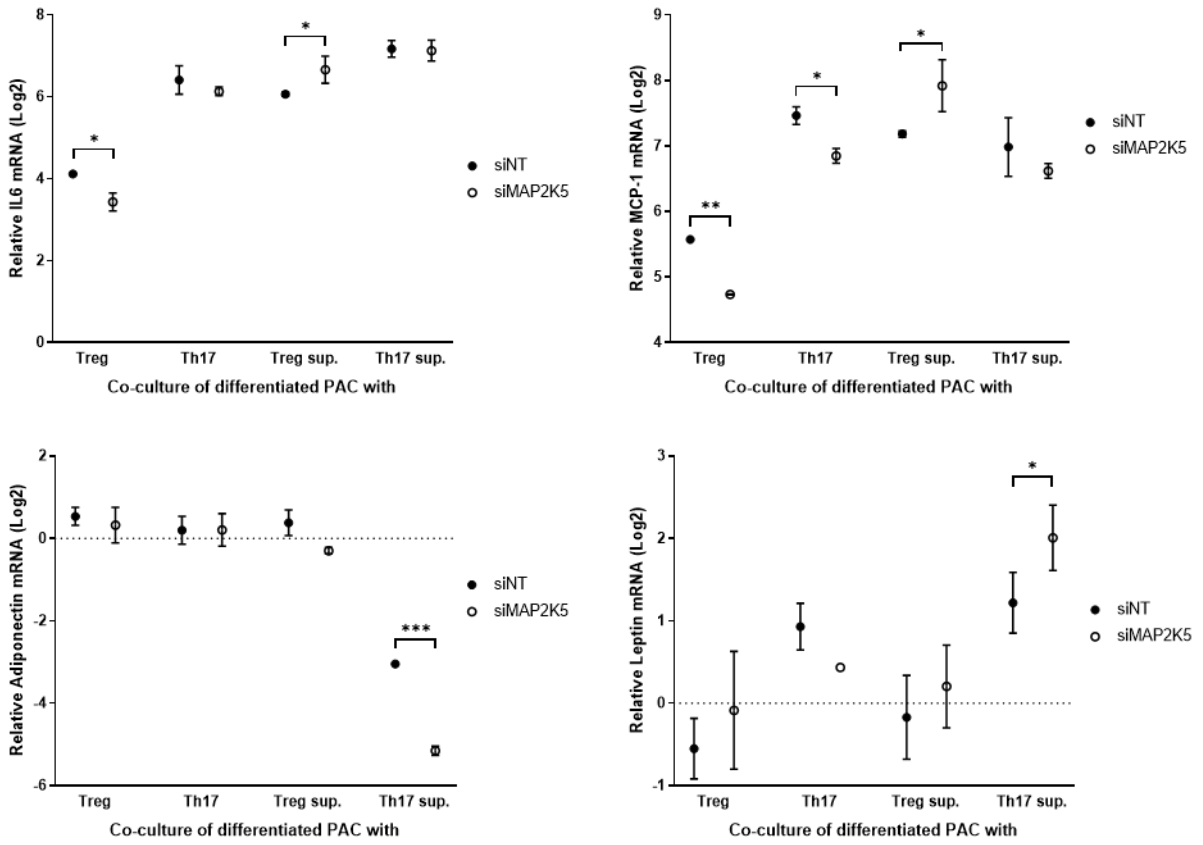

Figure 25. Co-culture of *MAP2K5* KD CD4$^+$ T cells with differentiated preadipocytes. mRNA expression of inflammation markers relative to preadipocytes without co-culture. Treg=co-culture with Treg differentiated cells, Th17=co-culture with Th17 differentiated cells, sup=co-culture with supernatant of differentiated cells. One experiment with technical replicates, symbols show mean ± SD (error bars smaller than the symbol not shown). Two-way ANOVA with multiple comparisons (Tukey), * p<0.05, ** p<0.01, *** p<0.001. # indicates a significant effect of differentiated T cells and supernatant independent of KD.

The effect of co-culture on lipolysis genes was very consistent, with the supernatant of Th17 cells with *MAP2K5* KD causing a significant reduction in mRNA expression (Figure 26). *PNPLA2* encodes adipose triglyceride lipase (ATGL), which converts triglycerides to diglycerides; *LIPE* encodes hormone-sensitive lipase (HSL), which converts diglycerides to monoglycerides; *PLIN1* encodes for perilipin-1, a central regulator of ATGL activity. Downregulation of PLIN1 and reduction in perilipin-1 activity leads to constitutive activation of ATGL, unrestrained lipolysis and hyperlipidemia (Grabner *et al.*, 2021), a common characteristic of T2D and a risk factor for AD (Feringa and van der Kant, 2021).

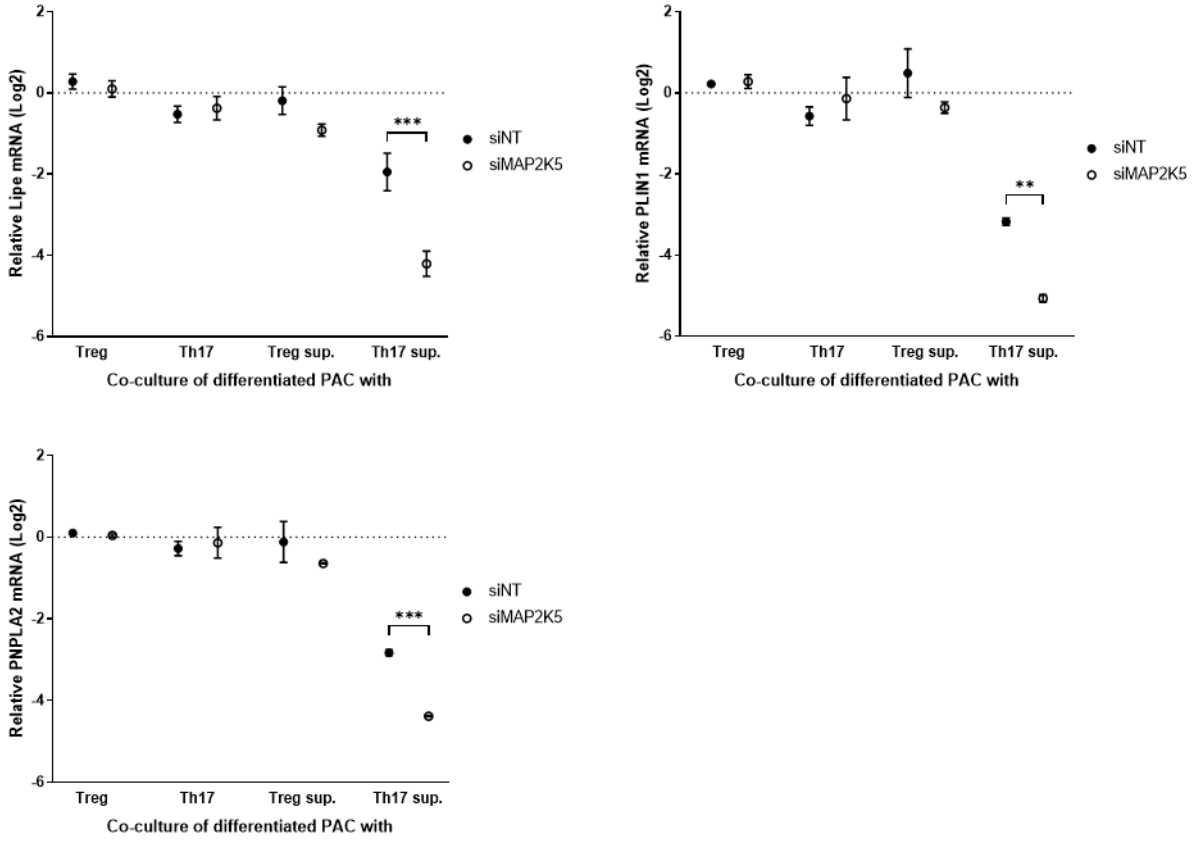

Figure 26. Co-culture of *MAP2K5* KD CD4$^+$ T cells with differentiated preadipocytes. mRNA expression of lipid storage and hydrolysis genes relative to preadipocytes without co-culture. Treg=co-culture with Treg differentiated cells, Th17=co-culture with Th17 differentiated cells, sup=co-culture with supernatant of differentiated cells. One experiment with technical replicates, symbols show mean ± SD (error bars smaller than the symbol not shown). Two-way ANOVA with multiple comparisons (Tukey), * $p<0.05$, ** $p<0.01$, *** $p<0.001$. # indicates significant effect of differentiated T cells and supernatant independent of KD.

4.2.6.3 Co-culture of T cells with differentiated SH-SY5Y

Viability of differentiated SH-SY5Y in the presence of T cells was also assessed via reduction of WST-8 to formazan. Overall, there was a negative effect of co-culture in viability of differentiated SH-SY5Y cells, with Treg cells with *MAP2K5* KD showing a stronger tendency to reduce SH-SY5Y viability (Figure 27).

The effect of T cell co-culture on SH-SY5Y differentiation was assessed by gene expression of several differentiation markers (Table 23).

Co-culture of SH-SY5Y cells with T cell supernatant reduced expression of differentiation markers independent of KD (Figure 28), suggesting a negative impact of the presence of T cell cytokines in neuronal differentiation.

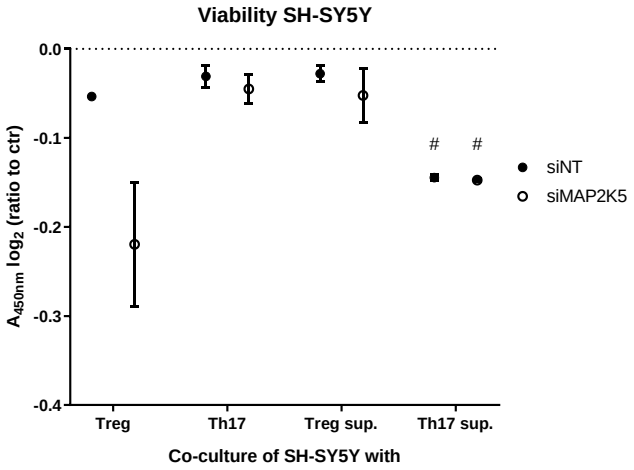

Figure 27. Assessment of viability of differentiated SH-SY5Y in co-culture with T cells and their supernatant. Absorbance of formazan at 450 nm shown as ratio to control (differentiated SH-SY5Y without co-culture). One experiment with technical duplicates, symbols show mean ± SD. Two-way ANOVA with multiple comparisons (Tukey), # $p<0.05$ indicates a significant effect compared to control.

Table 23. Neuronal marker genes tested in differentiated SH-SY5Y

Expressed highly in differentiated cells	**Neuronal markers**
NTRK2	*MAP2*
NTF4	*SYN1*
SLITRK6	
PLNX1	

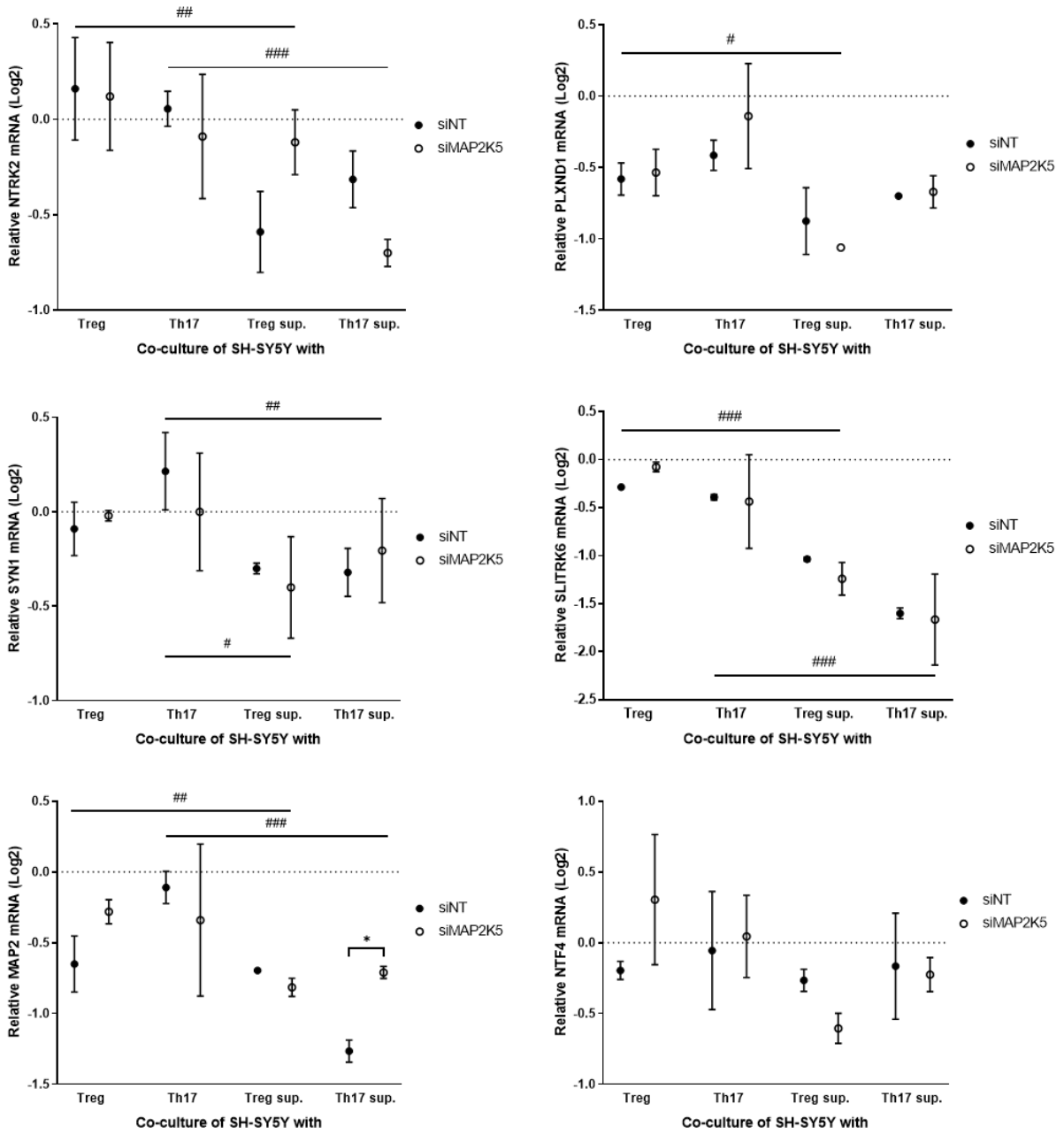

Figure 28. Co-culture of *MAP2K5* KD CD4⁺ T cells from SH1 with differentiated SH-SY5Y cells. mRNA expression of neuronal differentiation markers relative to SH-SY5Y cells without co-culture. Treg=co-culture with Treg differentiated cells, Th17=co-culture with Th17 differentiated cells, sup=co-culture with supernatant of differentiated cells. Technical replicates, symbols show mean ± SD (error bars smaller than the symbol not shown). Two-way ANOVA with multiple comparisons (Tukey), * p<0.05, ** p<0.01, *** p<0.001. # indicates significant effect of differentiated T cells and supernatant, regardless of KD.

Expression of Alzheimer's disease markers *APP* and *MAPT* was also influenced by T cell co-culture (Figure 29). There was an overall increase in gene expression with co-culture, particularly with Th17 cells, but there was no significant KD effect. This suggests a negative effect of direct Th17 cell contact with neurons in potentiating the development of AD.

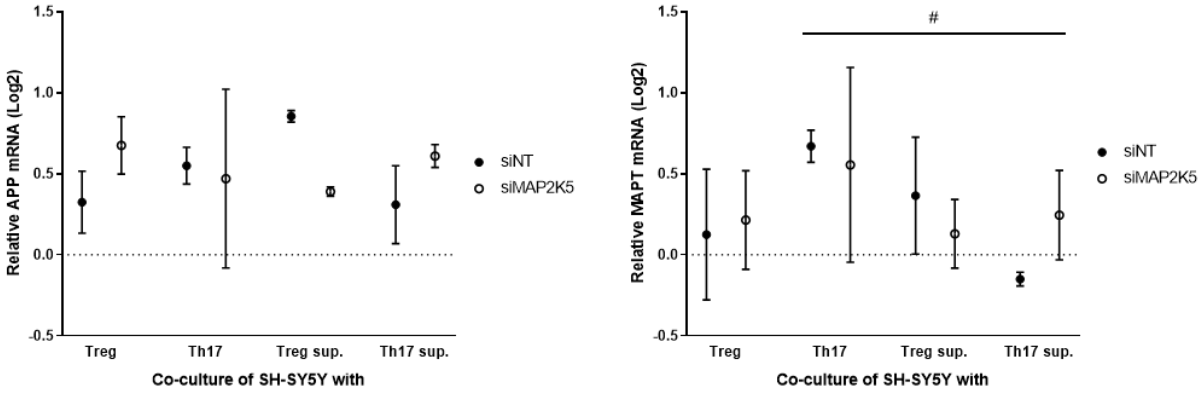

Figure 29. Co-culture of *MAP2K5* KD $CD4^+$ T cells from SH1 with differentiated SH-SY5Y cells. mRNA expression of amyloid precursor protein and microtubule associated protein tau relative to SH-SY5Y cells without co-culture. Treg=co-culture with Treg differentiated cells, Th17=co-culture with Th17 differentiated cells, sup=co-culture with supernatant of differentiated cells. One experiment with technical replicates, symbols show mean ± SD (error bars smaller than the symbol not shown). Two-way ANOVA with multiple comparisons (Tukey), # $p<0.05$ indicates significant effect of differentiated T cells and supernatant independent of KD.

5 Discussion

While GWAS have largely focused on individual phenotypes, there is growing evidence that many loci have pleiotropic effects and are associated with multiple traits (Bulik-Sullivan *et al.*, 2015; Pickrell *et al.*, 2016). Studying pleiotropic effects of loci across cell types and tissues is thus important and may be useful for discovering causal variants and their mechanism of action in many complex diseases.

5.1 Dissection of pleiotropy: a new framework

This work presented a framework to analyze pleiotropy by dissecting the regulatory circuitry of non-coding bivariate loci (Figure 30). The analysis starts with the selection of relevant GWAS datasets from large studies of complex traits or diseases and performing bivariate genome-wide association analysis using CP-ASSOC (Zhu *et al.*, 2015), MTAG (Turley *et al.*, 2017) and eLX (Chen and Hsu, 2017) to identify potential pleiotropic SNPs. Reference epigenomes from the Roadmap Epigenomics Project (Roadmap Epigenomics Consortium *et al.*, 2015) were then used to analyze cell type enrichment and identify the chromatin states of the bivariate loci in the relevant cell types. The next step is to examine whether there are differences in chromatin structure between the two haplotypes in study in the relevant cell types previously identified. The type of assays performed in this step depend on the chromatin states, e.g. H3K27me3 ChIP-seq for Polycomb repression, H3K27ac ChIP-seq for enhancer activity, ATAC-seq for chromatin accessibility. Regulatory activity can be assessed functionally using luciferase reporter assays to further support the identified cell types.

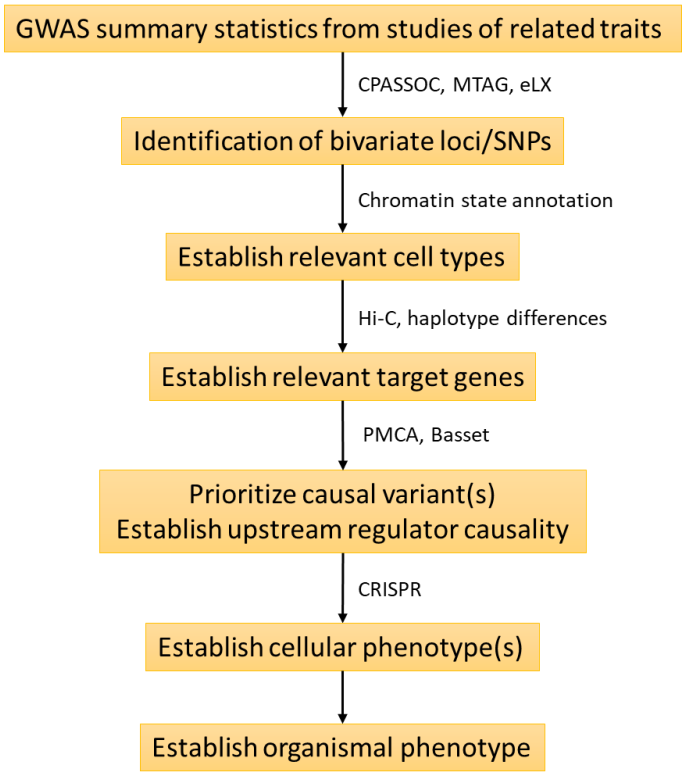

Figure 30. Scheme outlining our framework workflow to dissect pleiotropy of complex traits.

Afterwards, we examine the three-dimensional folding of the genome to map chromatin interactions using Hi-C assays (van Berkum *et al.*, 2010) in the relevant cell types. This identifies the contact domains of the loci of interest and their relevant target genes, which can be then confirmed by checking haplotype-specific differential gene expression. The potential causal variants within the identified target genes are then prioritized using two orthogonal computational approaches. Phylogenetic module complexity analysis (PMCA) (Claussnitzer *et al.*, 2014) groups at least three transcription-factor-binding motifs within a 120-bp-region that show good evolutionary conservation of sequence, order, and distance (in human and at least one other vertebrate species). The Basset method uses a sequence-based deep convolutional neural network (CNN) approach to learn the relevant sequence motifs and the regulatory logic with which they are combined to determine cell-specific DNA accessibility. The SNPs with highest difference in chromatin accessibility between haplotypes are the likely causal variant(s). The Basset model can also predict the effect of every mutation on the accessibility of the region, thus highlighting the individual nucleotides most critical to a sequence's activity and the associated regulatory element (e.g. a transcription factor binding site).

Once the causal variant and upstream regulator are identified, the cellular phenotype can be elucidated by manipulating the expression of the target gene, its regulator, and using CRISPR genome editing of the causal variant to produce the distinct genotypes. From there, animal models can be used to further elucidate the pleiotropic function of the causal variant at an organismal level.

To illustrate the potential use of this framework, the first part of this study focused on shared genetics between BMD and glycemic traits, attempting to explain the molecular underpinnings of a clinically recognized link between type 2 diabetes and bone health. The second part aimed to dissect the common genetic background between type 2 diabetes and Alzheimer's disease, two pathologies with many recognized similarities in pathology and molecular signaling (Pugazhenthi, Qin and Reddy, 2017).

5.2 Pleiotropy of BMD and metabolic traits

Using GWAS summary statistics, this study found the ADCY5 locus to be associated with FNBMD and fasting glucose levels. The variant rs56371916 was shown to play a causal role in processes related to these phenotypes by affecting the binding affinity of the transcription factor SREBP1 in mesenchymal cells, leading to altered *ADCY5* gene expression and differentiation capacity in both adipocytes and osteoblasts. These results from genetic association in human populations and experimental studies of adipocytes and osteoblasts *in vitro* provide strong evidence that the expression levels of ADCY5 play a significant role in T2D and BMD.

ADCY5 is among several adenylate cyclases expressed at high levels in mesenchymal cells (Mabbott *et al.*, 2013). Supporting a pleiotropic role of ADCY5, variants in this locus have been associated with 2-hour glucose challenge (Saxena *et al.*, 2010), fasting glucose and T2D (Dupuis *et al.*, 2010; Knigge *et al.*, 2015; Fuchsberger *et al.*, 2016). Variants in this locus have also been reported to affect ADCY5 expression in pancreatic islets (Thurner *et al.*, 2018), which is crucial for coupling glucose to insulin secretion (Hodson *et al.*, 2014). This locus has also been associated with high-density lipoprotein cholesterol (HDL) and total cholesterol (TC) plasma concentrations in a multi-ethnic GWAS (Hoffmann *et al.*, 2018).

These results suggest that ADCY5 may act in multiple tissues to increase the risk of T2D and metabolic disease. Therefore, it is possible that rs56371916 may affect additional cell types or that other variants at the *3q.21.1* locus may also play a role in bone and metabolic traits. The observation that within the same risk region, multiple variants might act in distinct tissues lends more complexity to the analysis of pleiotropy (Solovieff *et al.*, 2013).

The results of this study indicate a key role for ADCY5 in adipocyte and osteoblast differentiation. While the physiological impact of lipolysis in adipocytes has been investigated in earlier studies (Lafontan and Langin, 2009), the role of lipid metabolism in osteoblasts and its impact on differentiation is still underexplored (Rendina-Ruedy, Guntur and Rosen, 2017). Recent studies highlight the requirement for fatty acid oxidation for osteoblast differentiation in skeletal development and bone repair (Alekos, Moorer and Riddle, 2020). Further exploration of these results beyond osteoblast differentiation will help explain the apparent paradox of higher bone density in T2D being associated with greater bone fragility. However, future studies will be required to carefully study organismal physiology in both humans and genetically engineered animal models, with the prospect of developing treatment regimens for either trait without adverse effects on the other.

5.3 Pleiotropy of AD and T2D

The second part of this study aimed to elucidate the pleiotropy between T2D and AD. These pathologies overlap in several mechanistic alterations that suggest an underlying link between them (Salas and De Strooper, 2019).

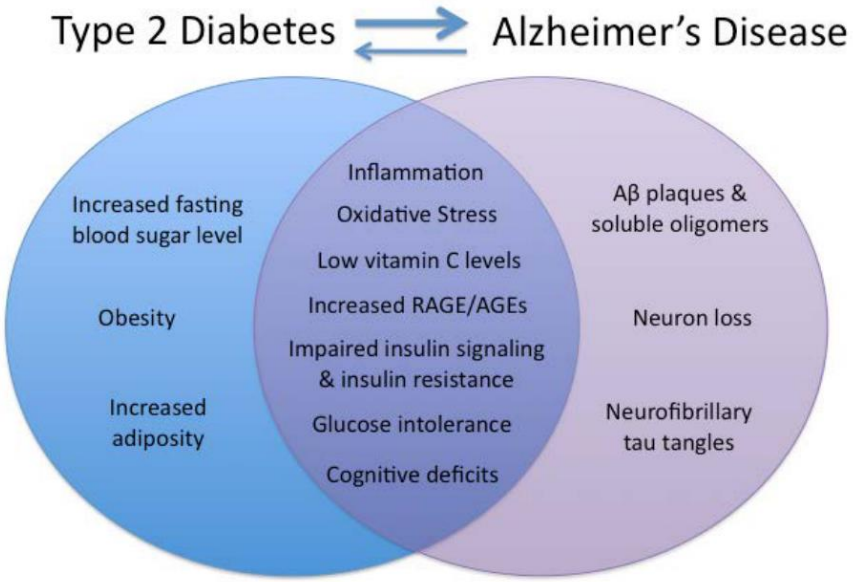

Figure 31. Hallmarks of T2D and AD and their overlap. From Walker and Harrison, 2015.

The identified bivariate signals were enriched in blood and T cell related epigenomes, which is in alignment with literature supporting the relevance of T cells in T2D-AD pleiotropy. Therefore we focused on candidate loci with higher expression in T cells. In particular, the MAPK2K5 locus stood out as impacting the differentiation of $CD4^+$ T cells by favoring them into pro-inflammatory Th17 cells in detriment of anti-inflammatory Tregs. This shift in

Treg/Th17 ratio promotes a pro-inflammatory environment favoring the development of both AD and T2D, as supported by the literature and highlighted in our hypothesis (Figure 32). We thus hypothesized that a causal SNP in the MAP2K5 locus promotes the differentiation of naïve $CD4^+$ T cell into Th17 cells and depletion of the naïve pool.

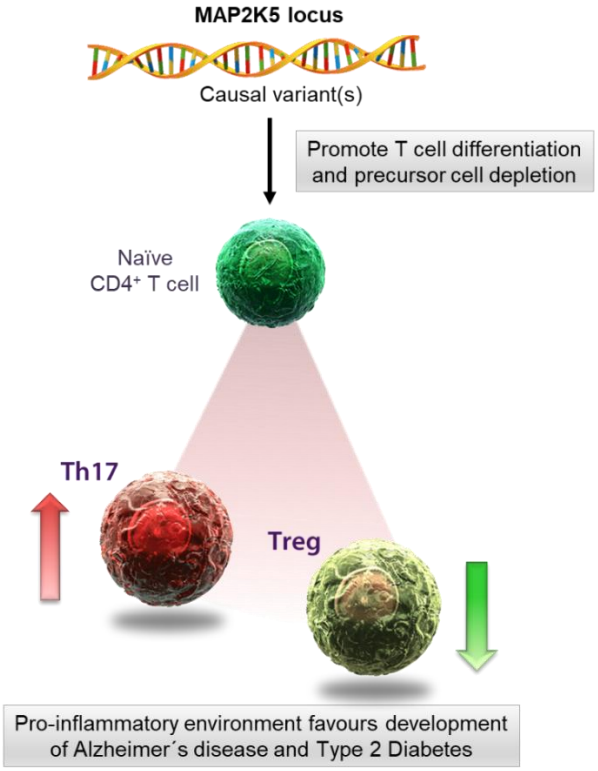

Figure 32. Working hypothesis on the pleiotropy of AD and T2D. We predict that (a) causal variant(s) in the MAP2K5 locus promotes an increase in $CD4^+$ T cell number and differentiation, favoring an increase in Th17 cell number and reduction in number/activity of Treg cells, contributing to a proinflammatory environment that favors both diseases.

T2D and AD are both considered inflammatory conditions, with studies demonstrating the association between elevated circulating levels of markers of inflammation and insulin resistance and the development of T2D and AD (Kamal *et al.*, 2014). Clinical studies have reported higher peripheral concentrations of inflammatory cytokines such as IL-6 and TNF-α, and higher CSF concentrations of TGF-β, supporting the role of inflammation in the pathophysiology of AD (Carranza-naval *et al.*, 2021).

Insulin resistance, a hallmark of T2D, has also been established as a key component of AD pathology, with impaired brain insulin signaling underpinning brain inflammation, neurodegeneration, and cognitive impairment (De Felice, Gonçalves and Ferreira, 2022). Dysregulation of insulin receptors and components of the insulin signaling pathway are reported in both diseases (Lynn *et al.*, 2021). In AD patients, the most consistent change observed in the insulin pathway is the reduction in insulin receptor substrate (IRS) levels, accompanied by an increase in IRS-1 serine phosphorylation, a marker of insulin resistance (Moloney *et al.*, 2010). Insulin resistance can lead to both Aβ plaque formation and tau hyperphosphorylation: insulin-degrading enzyme (IDE) is required for both insulin and Aβ degradation; during hyperinsulinemia in type 2 diabetes, insulin and Aβ compete for insulin-

degrading enzyme, leading to Aβ accumulation and plaque formation (Sims-Robinson *et al.*, 2010). A decrease in insulin receptor signaling leads to inhibition of Akt and dephosphorylation (activation) of GSK-3β, and results in tau hyperphosphorylation.

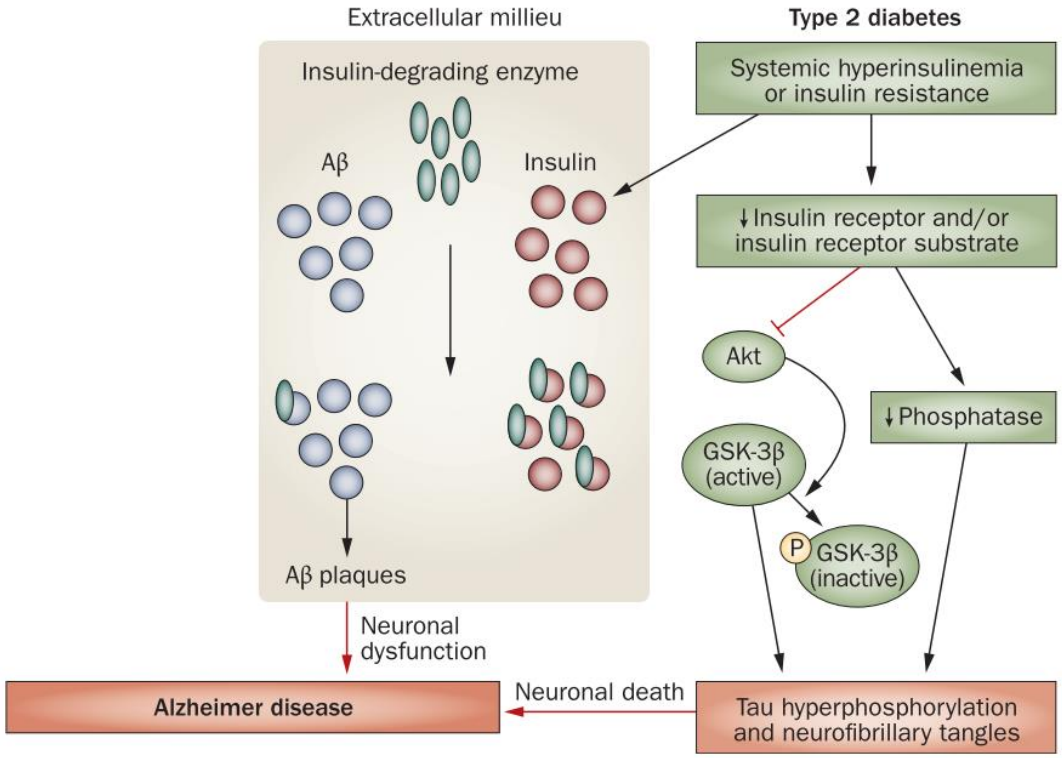

Figure 33. Altered insulin signaling in T2D contributes to AD pathophysiology. Adapted from Sims-Robinson *et al.*, 2010.

Although the brain is an immune-privileged organ, cross-talks between peripheral and central inflammation have been reported. Damage to the blood brain barrier (BBB) during aging can lead to infiltration of immune cells and inflammatory cytokines into the brain, promoting microglia activation and neuroinflammation observed in AD patients (Chaney, Williams and Boutin, 2019). Several studies support a role for T cells in AD: higher T cell numbers have been detected in AD brains compared to controls and other neurodegenerative diseases (Togo *et al.*, 2002), particularly in the hippocampus (Merlini *et al.*, 2018) and temporal cortex (Sardi *et al.*, 2011). Specifically, there is an increase in $CD4^+$ T cells resulting in lower proportions of naïve cells, more late-differentiated cells and higher percentages of activated $CD4^+CD25^+$T cells without a Treg phenotype in AD patients (Pellicanò *et al.*, 2012). Regulatory T cells have been shown to play a beneficial role in the pathophysiology of AD in a murine model (APPPS1 mice), by slowing disease progression and modulating microglial response to Aβ deposition (Dansokho *et al.*, 2016).

The downstream target of MAP2K5, ERK5, modulates the density of TCR/CD3 at the cell surface by promoting CD3 degradation and TCR/CD3 recovery after anti-CD3 stimulation (Rovira-Clave *et al.*, 2016). Our results suggest that inhibition of MAP2K5 in human $CD4^+$ T cells promotes their activation/differentiation following anti-CD3 stimulation likely due to impaired TCR/CD3 down-regulation. One could speculate that changes in ERK5 activation

resulting from SNP(s) altering the expression/activity of MAP2K5 could impair TCR/CD3 downregulation, consequently promoting T cell activation and impairing Treg development, leading to a Th17/Treg imbalance and depletion of the naive T cell pool.

It has also been shown that programmed downregulation of TCR expression is a negative feedback mechanism for inhibiting T cell activation in response to a pathogen, thus avoiding excess inflammation (Gallegos *et al.*, 2016). Expression profile of poorly controlled diabetics compared to well-controlled ones has demonstrated a systemic upregulation of genes related to immune response, including MAP2K5, and subsequent immune system overactivation and a hyperinflammatory state (Corbi *et al.*, 2017). This is relevant given that excess inflammation is associated with development of both AD (Parachikova *et al.*, 2007) and T2D (Cruz *et al.*, 2013).

The different responses produced by MAP2K5 KD in T cell differentiation emphasize the relevance of the individual genetic background when assessing the phenotypic effects of manipulating gene expression. The individual differences produced a similar imbalance in T cell differentiation, affecting either Treg or Th17 proliferation and leading to an identical shift in the Treg/Th17 ratio towards Th17 cells. This suggests a selection against the combined effect, which would be too deleterious given the central role of the Treg/Th17 balance in many autoimmune and inflammatory diseases (Noack and Miossec, 2014; Fasching *et al.*, 2017).

The reciprocal regulation between the Treg and Th17 differentiation pathways illustrates the immune-regulatory role of this axis (Yang *et al.*, 2008). The developmental pathways of Th17 and Treg cells overlap, with TGF-β inducing both FoxP3 and RORγt expression in naive $CD4^+$ T cells (Zhou *et al.*, 2008). In the presence of pro-inflammatory cytokines, such as IL-6 and IL-21, TGF-β induced-FoxP3 expression is down-regulated and RORγt expression is up-regulated. In the absence of significant inflammation TGF-β promotes Treg differentiation thus maintaining immune tolerance.

The metabolic environment plays a crucial role in controlling lymphocyte differentiation and function (Cohen, Danzaki and MacIver, 2017). In one individual, MAP2K5 KD impaired the induction of metabolic genes involved in Treg differentiation, indicating a possible mechanism by which MAP2K5 influences Treg differentiation. On the other hand, MAP2K5 KD maintained the upregulation of metabolism genes involved in Th17 differentiation, thus favoring Th17 differentiation. In mice, HFD drives Th17 differentiation via upregulation of FAS enzymes such as ACC1 (Endo *et al.*, 2015). Alterations in nutrient availability in obesity and T2D could therefore favor T cell differentiation towards pro-inflammatory Th17 cells at the expense of anti-inflammatory Tregs.

Lipid accumulation was reduced in adipocytes in both co-culture with T cells and their supernatant, as detected by ORO staining. This is in line with a previous study showing that co-culture of activated T cells significantly inhibits preadipocyte differentiation and triglyceride accumulation (Wu *et al.*, 2007). Additionally, T-cell co-culture induced an inflammatory response in differentiated PAC, significantly upregulating IL-6 and MCP-1, both proinflammatory markers. Previous studies have shown that T cells alter adipokine production and significantly increase the production of proinflammatory adipokines IL-6 and MCP-1, with a stronger effect observed with direct cell-cell contact versus T cell supernatant (Poggi *et al.*, 2009). Increase in adipocyte MCP-1 production due to direct T cell contact supports the observation that T cell infiltration precedes macrophage recruitment, suggesting

a major role for T cells in adipose tissue inflammation and development of insulin resistance (Kintscher *et al.*, 2008).

Adiponectin and leptin are the two adipokines most strongly linked to insulin resistance and T2D (Nikolajczyk *et al.*, 2011). In this study, adiponectin was reduced in PAC co-cultured with Th17 supernatant, and leptin was upregulated by Th17 cells and their supernatant. It has been previously shown that leptin levels in adipose tissue increase by exposure to inflammatory stimuli and that leptin itself exerts differential effects in T cells, promoting Th17 differentiation and inhibiting Treg expansion (La Cava, 2017). Adipocytes are sensitive targets of proinflammatory T-cell cytokines, expressing significant levels of IL-17 receptors and responding to IL-17 by secreting IL-6 (Shin, Shin and Noh, 2009). Overall this points to a pro-inflammatory feed-forward loop between adipose tissue and T cells, potentiating the transition from obese insulin-sensitive to insulin-resistant type 2 diabetic subjects (Nikolajczyk *et al.*, 2011).

Incubation of differentiated PAC with Th17 cell supernatant resulted in downregulation of lipolysis genes, with a stronger reduction with MAP2K5 KD. IL-17 has been previously implicated in the regulation of metabolic functions of mature differentiated adipocytes (Zuniga *et al.*, 2010). Specifically, incubation of preadipocytes with IL-17 during differentiation was shown to inhibit the expression of lipolysis-related genes (HSL, perilipin, ATGL), resulting in reduced lipid accumulation detected as reduced ORO staining, and impaired adipocyte function. Hyperlipidemia is often present in individuals with T2D, and this can damage the integrity of the BBB, increasing its permeability and allowing the infiltration of peripheral cholesterol, which can promote Aβ pathology in AD patients (Sun *et al.*, 2020).

Studies have shown that activated T cells cause neurotoxicity by direct cell-cell contact and do not target other CNS cell types (oligodendrocytes and astrocytes), indicating T cell selectivity towards neurons (Giuliani *et al.*, 2003). $CD4^+$ T cells cannot recognize antigens on neurons due to the lack of expression of MHC class II molecules, but they can induce apoptosis through the TNF-related apoptosis-inducing ligand (TRAIL) pathway (Aktas *et al.*, 2005). Among $CD4^+$ T cells, Th17 cells exhibit a preferential ability to engage sustained contacts with neurons and induce neuronal injury (Siffrin *et al.*, 2010). In this study, co-culture of SH-SY5Y neuronal cells with T cells showed a tendency to reduce viability, especially with Th17 cell supernatant, as well as reduce expression of differentiation marker genes, indicating a negative effect of Th17 cells and their cytokines on neuronal differentiation. IL17 has been shown to play a critical role in regulating brain inflammation by promoting recruitment of inflammatory cells (Stromnes *et al.*, 2008). In AD models, Aβ-reactive Th17 cells accelerate disease progression by downregulating anti-inflammatory and immunosuppressive Tregs, both within CNS and in the periphery (Machhi *et al.*, 2021).

The dysregulation of the Treg/Th17 balance towards a proinflammatory environment that promotes disease can be explored therapeutically with anti-inflammatory drugs targeting Th17 cells and related cytokines, as well as enhancing Treg differentiation (Drew, Burow and Beckman, 2012; Fasching *et al.*, 2017). Various candidate molecules that beneficially reshape the Th17/Treg imbalance have shown promising results in animal models (Huh *et al.*, 2011; Baek *et al.*, 2014; Skepner *et al.*, 2015; Takaishi *et al.*, 2017), but still need further study before being tested in humans. Current AD drugs vary in their influence on $CD4^+$ T cell subpopulations and none is specifically designed to target the dysregulation of the Th17/Treg ratio (Kubick *et al.*, 2020). Future drug design approaches should specifically consider inhibiting $CD4^+$ Th17 to improve AD prognosis.

5.3.1 Further exploration

The direction of effects observed supports our hypothesis that altering MAP2K5 expression/ function favors $CD4^+$ T cell differentiation into Th17 cells in detriment of the Treg phenotype, shifting the Treg/Th17 balance to a proinflammatory environment that is conducive to the development of T2D and AD.

The next step would be to narrow down the causal SNPs by using CRISPR-Cas9 gene editing technology in naive T cells to edit each candidate SNP in the MAP2K5 locus and identify the ones with an effect on T cell differentiation, comparing the Treg/Th17 ratio in the edited population via flow cytometry. The different populations would then be sorted for further investigation of the mechanisms of action of the causal SNPs at a cellular level, such as changes in gene and protein expression of the differentiation signaling pathways, as well as the cytokine profile produced by differentiated T cells. Following a cellular characterization, the edited cells would be used in co-culture experiments to elucidate their impact on differentiated adipocytes and neurons, particularly in promoting an inflammatory response in these cell types. The impact on disease susceptibility and development would need to be confirmed at an organismal level, with tissue targeted *MAP2K5* knockout animal models.

5.4 Limitations of this study

One of the challenges in this study was the induction of knock down in primary immune cells, which are notoriously difficult to transfect. We tested different chemical protocols, as well as electroporation, and selected the accell transfection method for providing the best knock down with lowest impact on cell viability. Due to the transient nature of siRNA KD, we also attempted to produce shRNA for lentiviral delivery and stable silencing of MAP2K5. Unfortunately we faced several issues during the cloning process and cell culture which excluded this option. The limited availability of primary T cells also made this technique difficult to implement, given the high amount of cells required for infection, selection and expansion.

6 Conclusion

This work employed a framework to uncover the biological mechanisms underlying pleiotropic traits by a systematic functional dissection of pleiotropic GWAS loci. To translate GWAS results into biological function, we combined public resources (epigenomic annotations, chromosome conformation, and regulatory motif conservation), targeted experiments for different haplotypes (gene expression, cellular profiling), and directed perturbations in human primary cells (targeted knockdown, CRISPR–Cas9 genome editing). This approach specifically aims to elucidate the function of noncoding variants, which constitute the majority of GWAS signals and over 90% of disease-associated variants (Gallagher and Chen-Plotkin, 2018). One of the ultimate objectives of genetic research is to drive translational advances that enable more effective prevention and/or treatment of disease, and GWAS studies have already successfully informed drug targets for type 2 diabetes, rheumatoid arthritis and psoriasis, for example (Visscher *et al.*, 2017). This work contributes to facilitate the understanding of pleiotropy and its role in complex human traits and diseases.

References

Ahmad, O. S. *et al.* (2017) 'A Mendelian Randomization Study of the Effect of Type-2 Diabetes and Glycemic Traits on Bone Mineral Density', *Journal of Bone and Mineral Research*, 32(5), pp. 1072–1081. doi: 10.1002/jbmr.3063.

Ahuja, M. *et al.* (2017) 'Immunological alteration & toxic molecular inductions leading to cognitive impairment & neurotoxicity in transgenic mouse model of Alzheimer's disease', *Life Sciences*, 177, pp. 49–59. doi: 10.1016/j.lfs.2017.03.004.

Akomolafe, A. *et al.* (2006) 'Diabetes mellitus and risk of developing Alzheimer disease', *Arch Neurol*, 63(11), pp. 1551–1555. doi: doi:10.1001/archneur.63.11.1551.

Aktas, O. *et al.* (2005) 'Neuronal damage in autoimmune neuroinflammation mediated by the death ligand TRAIL.', *Neuron*, 46(3), pp. 421–32. doi: 10.1016/j.neuron.2005.03.018.

Alekos, N. S., Moorer, M. C. and Riddle, R. C. (2020) 'Dual Effects of Lipid Metabolism on Osteoblast Function', *Frontiers in Endocrinology*, 11, p. 707. doi: 10.3389/FENDO.2020.578194/BIBTEX.

Angelo, F. *et al.* (2018) 'The obesity paradox and osteoporosis', *Eating and Weight Disorders - Studies on Anorexia, Bulimia and Obesity*, pp. 1–10. doi: 10.1007/s40519-018-0505-2.

Baek, S. *et al.* (2014) 'Ursolic acid ameliorates autoimmune arthritis via suppression of Th17 and B cell differentiation.', *Acta pharmacologica Sinica*, 35(9), pp. 1177–87. doi: 10.1038/aps.2014.58.

Bandea, C. I. (2013) 'Aβ, tau, α-synuclein, huntingtin, TDP-43, PrP and AA are members of the innate immune system : a unifying hypothesis on the etiology of AD, PD, HD, ALS, CJD and RSA as innate immunity disorders', (i), pp. 1–10.

Becher, B., Bechmann, I. and Greter, M. (2006) 'Antigen presentation in autoimmunity and CNS inflammation: How T lymphocytes recognize the brain', *Journal of Molecular Medicine*, 84(7), pp. 532–543. doi: 10.1007/s00109-006-0065-1.

Becker, K. G. (2004) 'The common variants/multiple disease hypothesis of common complex genetic disorders', *Medical Hypotheses*, 62(2), pp. 309–317. doi: 10.1016/S0306-9877(03)00332-3.

Van Beek, L. *et al.* (2014) 'Increased systemic and adipose tissue inflammation differentiates obese women with T2DM from obese women with normal glucose tolerance', *Metabolism: Clinical and Experimental*, 63(4), pp. 492–501. doi: 10.1016/j.metabol.2013.12.002.

van Berkum, N. L. *et al.* (2010) 'Hi-C: A Method to Study the Three-dimensional Architecture of Genomes', *J. Vis. Exp*, (39), p. 1869. doi: 10.3791/1869.

Billings, L. K. *et al.* (2012) 'Impact of common variation in bone-related genes on type 2 diabetes and related traits', *Diabetes*, 61(8), pp. 2176–2186. doi: 10.2337/db11-1515.

Bitter, A. *et al.* (2015) 'Human sterol regulatory element-binding protein 1a contributes significantly to hepatic lipogenic gene expression', *Cellular Physiology and Biochemistry*, 35(2), pp. 803–815. doi: 10.1159/000369739.

Blanchette, M. *et al.* (2004) 'Aligning multiple genomic sequences with the threaded blockset aligner', *Genome Research*, 14(4), pp. 708–715. doi: 10.1101/gr.1933104.

Bonds, D. E. *et al.* (2006) 'Risk of Fracture in Women with Type 2 Diabetes: the Women's Health Initiative Observational Study', *The Journal of Clinical Endocrinology & Metabolism*, 91(9), pp. 3404–3410. doi: 10.1210/jc.2006-0614.

Bulik-Sullivan, B. *et al.* (2015) 'An atlas of genetic correlations across human diseases and traits', *Nature Publishing Group*, 47(11), pp. 1236–1241. doi: 10.1038/ng.3406.

Carranza- naval, M. J. *et al.* (2021) 'Alzheimer's disease and diabetes: Role of diet, microbiota and inflammation in preclinical models', *Biomolecules*, 11(2), pp. 1–25. doi: 10.3390/biom11020262.

La Cava, A. (2017) 'Leptin in inflammation and autoimmunity', *Cytokine*, 98, pp. 51–58. doi: 10.1016/j.cyto.2016.10.011.

Chaney, A., Williams, S. R. and Boutin, H. (2019) 'In vivo molecular imaging of neuroinflammation in

Alzheimer's disease', *Journal of Neurochemistry*, 149(4), pp. 438–451. doi: 10.1111/JNC.14615.

Chen, Q. *et al.* (2016) 'Fate decision of mesenchymal stem cells: Adipocytes or osteoblasts?', *Cell Death and Differentiation*, 23(7), pp. 1128–1139. doi: 10.1038/cdd.2015.168.

Chen, X. and Hsu, Y.-H. (2017) 'Identifying Pleiotropic Effects: A Two-Stage Approach Using Genome-Wide Association Meta-Analysis Data', *bioRxiv*, p. 184895. doi: 10.1101/184895.

Clarke, J. R. *et al.* (2015) 'Alzheimer-associated A b oligomers impact the central nervous system to induce peripheral metabolic deregulation', 7(2), pp. 190–210.

Claussnitzer, M. *et al.* (2014) 'Leveraging cross-species transcription factor binding site patterns: From diabetes risk loci to disease mechanisms', *Cell*, 156(1–2), pp. 343–358. doi: 10.1016/j.cell.2013.10.058.

Cohen, S., Danzaki, K. and MacIver, N. J. (2017) 'Nutritional effects on T-cell immunometabolism', *European Journal of Immunology*, 47(2), pp. 225–235. doi: 10.1002/eji.201646423.

Corbi, S. C. T. *et al.* (2017) 'Expression Profile of Genes Potentially Associated with Adequate Glycemic Control in Patients with Type 2 Diabetes Mellitus', *Journal of Diabetes Research*, 2017, pp. 1–9. doi: 10.1155/2017/2180819.

Couper, K. N., Blount, D. G. and Riley, E. M. (2008) 'IL-10: The Master Regulator of Immunity to Infection', *The Journal of Immunology*, 180(9), pp. 5771–5777. doi: 10.4049/JIMMUNOL.180.9.5771.

Cruz, N. G. *et al.* (2013) 'The linkage between inflammation and Type 2 diabetes mellitus', *Diabetes Research and Clinical Practice*, 99(2), pp. 85–92. doi: 10.1016/J.DIABRES.2012.09.003.

Dansokho, C. *et al.* (2016) 'Regulatory T cells delay disease progression in Alzheimer-like pathology', *Brain*, 139(4), pp. 1237–1251. doi: 10.1093/brain/awv408.

Defer, N., Best-Belpomme, M. and Hanoune, J. (2000) 'Tissue specificity and physiological relevance of various isoforms of adenylyl cyclase', *American Journal of Physiology-Renal Physiology*, 279(3), pp. F400–F416. doi: 10.1152/ajprenal.2000.279.3.F400.

Deiuliis, J. *et al.* (2011) 'Visceral adipose inflammation in obesity is associated with critical alterations in tregulatory cell numbers', *PLoS ONE*, 6(1). doi: 10.1371/journal.pone.0016376.

Diller, M. L. *et al.* (2016) 'Balancing Inflammation: The Link between Th17 and Regulatory T Cells', *Mediators of Inflammation*, 2016, pp. 1–8. doi: 10.1155/2016/6309219.

DiSpirito, J. R. and Mathis, D. (2015) 'Immunological contributions to adipose tissue homeostasis', *Seminars in Immunology*, 27(5), pp. 315–321. doi: 10.1016/j.smim.2015.10.005.

Dixon, J. R. *et al.* (2015) 'Chromatin architecture reorganization during stem cell differentiation', *Nature*, 518(7539), pp. 331–336. doi: 10.1038/nature14222.

Drew, B. A., Burow, M. E. and Beckman, B. S. (2012) 'MEK5/ERK5 pathway: The first fifteen years', *Biochimica et Biophysica Acta - Reviews on Cancer*, 1825(1), pp. 37–48. doi: 10.1016/j.bbcan.2011.10.002.

Duncan, R. E. *et al.* (2007) 'Regulation of Lipolysis in Adipocytes', *Annual Review of Nutrition*, 27(1), pp. 79–101. doi: 10.1146/annurev.nutr.27.061406.093734.

Dupuis, J. *et al.* (2010) 'New genetic loci implicated in fasting glucose homeostasis and their impact on type 2 diabetes risk', *Nature Genetics*, 42(2), pp. 105–116. doi: 10.1038/ng.520.

Endo, Y. *et al.* (2015) 'Obesity Drives Th17 Cell Differentiation by Inducing the Lipid Metabolic Kinase, ACC1.', *Cell reports*, 12(6), pp. 1042–55. doi: 10.1016/j.celrep.2015.07.014.

Ernst, J. and Kellis, M. (2012) 'ChromHMM: Automating chromatin-state discovery and characterization', *Nature Methods*. Nature Publishing Group, pp. 215–216. doi: 10.1038/nmeth.1906.

Estrada, K. *et al.* (2012) 'Genome-wide meta-analysis identifies 56 bone mineral density loci and reveals 14 loci associated with risk of fracture.', *Nature genetics*, 44(5), pp. 491–501. doi: 10.1038/ng.2249.

Fabbrini, E. *et al.* (2013) 'Association between specific adipose tissue CD4+T-cell populations and insulin resistance in obese individuals', *Gastroenterology*, 145(2), pp. 366-374.e3. doi:

10.1053/j.gastro.2013.04.010.

Fasching, P. *et al.* (2017) 'Therapeutic potential of targeting the Th17/Treg axis in autoimmune disorders', *Molecules*, 22(1). doi: 10.3390/molecules22010134.

De Felice, F. G., Gonçalves, R. A. and Ferreira, S. T. (2022) 'Impaired insulin signalling and allostatic load in Alzheimer disease', *Nature Reviews Neuroscience*, 23(4), pp. 215–230. doi: 10.1038/s41583-022-00558-9.

Feringa, F. M. and van der Kant, R. (2021) 'Cholesterol and Alzheimer's Disease; From Risk Genes to Pathological Effects', *Frontiers in Aging Neuroscience*, 13, p. 333. doi: 10.3389/FNAGI.2021.690372/BIBTEX.

Ferron, M. *et al.* (2010) 'Insulin Signaling in Osteoblasts Integrates Bone Remodeling and Energy Metabolism', *Cell*, 142(2), pp. 296–308. doi: 10.1016/j.cell.2010.06.003.

Fuchsberger, C. *et al.* (2016) 'The genetic architecture of type 2 diabetes', *Nature*, 536(7614), pp. 41–47. doi: 10.1038/nature18642.

Gallagher, M. D. and Chen-Plotkin, A. S. (2018) 'The Post-GWAS Era: From Association to Function', *American Journal of Human Genetics*. Cell Press, pp. 717–730. doi: 10.1016/j.ajhg.2018.04.002.

Gallegos, A. M. *et al.* (2016) 'Control of T cell antigen reactivity via programmed TCR downregulation', *Nature Immunology*, 17(4), pp. 379–386. doi: 10.1038/ni.3386.

Garaude, J. *et al.* (2005) 'The role of ERK5 in T-cell signalling', *Scandinavian Journal of Immunology*, 62(6), pp. 515–520. doi: 10.1111/j.1365-3083.2005.01696.x.

Gejl, M. *et al.* (2016) 'In Alzheimer's Disease, 6-Month Treatment with GLP-1 Analog Prevents Decline of Brain Glucose Metabolism: Randomized, Placebo-Controlled, Double-Blind Clinical Trial', *Frontiers in Aging Neuroscience*, 8, p. 108. doi: 10.3389/fnagi.2016.00108.

Gibbs, R. A. *et al.* (2003) 'The international HapMap project', *Nature*, 426(6968), pp. 789–796. doi: 10.1038/nature02168.

Giuliani, F. *et al.* (2003) 'Vulnerability of Human Neurons to T Cell-Mediated Cytotoxicity', *The Journal of Immunology*, 171(1), pp. 368–379. doi: 10.4049/jimmunol.171.1.368.

Gjoneska, E. *et al.* (2015) 'Conserved epigenomic signals in mice and humans reveal immune basis of Alzheimer's disease.', *Nature*, 518(7539), pp. 365–9. doi: 10.1038/nature14252.

Grabner, G. F. *et al.* (2021) 'Lipolysis: cellular mechanisms for lipid mobilization from fat stores', *Nature Metabolism 2021 3:11*, 3(11), pp. 1445–1465. doi: 10.1038/s42255-021-00493-6.

Gyllenhammer, L. E. *et al.* (2016) 'Lower omental t-regulatory cell count is associated with higher fasting glucose and lower β-cell function in adults with obesity', *Obesity*, 24(6), pp. 1274–1282. doi: 10.1002/oby.21507.

Hackinger, S. and Zeggini, E. (2017) 'Statistical methods to detect pleiotropy in human complex traits', *Open Biology*, 7(11), p. 170125. doi: 10.1098/rsob.170125.

Hartwell, L. *et al.* (2002) 'From genes to genomes'.

Hodson, D. J. *et al.* (2014) 'ADCY5 couples glucose to insulin secretion in human islets', *Diabetes*, 63(9), pp. 3009–3021. doi: 10.2337/db13-1607.

Hoffmann, T. J. *et al.* (2018) 'A Large Multiethnic Genome-Wide Association Study of Adult Body Mass Index Identifies Novel Loci.', *Genetics*, 210(2), pp. 499–515. doi: 10.1534/genetics.118.301479.

Huh, J. R. *et al.* (2011) 'Digoxin and its derivatives suppress TH17 cell differentiation by antagonizing RORγt activity.', *Nature*, 472(7344), pp. 486–90. doi: 10.1038/nature09978.

Ip, B. *et al.* (2016) 'Th17 cytokines differentiate obesity from obesity-associated type 2 diabetes and promote TNFα production', *Obesity*, 24(1), pp. 102–112. doi: 10.1002/oby.21243.

Itzhaki, R. F. *et al.* (2016) 'Microbes and Alzheimer ' s Disease', 51, pp. 979–984. doi: 10.3233/JAD-160152.

Janghorbani, M. *et al.* (2007) 'Systematic review of type 1 and type 2 diabetes mellitus and risk of fracture', *American Journal of Epidemiology*, 166(5), pp. 495–505. doi: 10.1093/aje/kwm106.

Kagan, B. L. B. *et al.* (2012) 'Antimicrobial Properties of Amyloid Peptides', *Mol Pharm.*, 9(4), pp. 708–717. doi: 10.1111/j.1755-148X.2012.00970.x.Targeting.

Kamal, M. A. *et al.* (2014) 'Linking Alzheimer's Disease and Type 2 Diabetes Mellitus via Aberrant Insulin Signaling and Inflammation', *CNS & neurological disorders drug targets*, 13(2), p. 338. doi: 10.2174/18715273113126660137.

Kelley, D. R., Snoek, J. and Rinn, J. L. (2016) 'Basset: Learning the regulatory code of the accessible genome with deep convolutional neural networks', *Genome Research*, 26(7), pp. 990–999. doi: 10.1101/gr.200535.115.

Kintscher, U. *et al.* (2008) 'T-lymphocyte infiltration in visceral adipose tissue: A primary event in adipose tissue inflammation and the development of obesity-mediated insulin resistance', *Arteriosclerosis, Thrombosis, and Vascular Biology*, 28(7), pp. 1304–1310. doi: 10.1161/ATVBAHA.108.165100.

Kipnis, J. *et al.* (2004) 'T cell deficiency leads to cognitive dysfunction: implications for therapeutic vaccination for schizophrenia and other psychiatric conditions', *Proc Natl Acad Sci U S A*, 101(21), pp. 8180–8185. doi: 10.1073/pnas.0402268101.

Knigge, A. *et al.* (2015) 'ADCY5 Gene Expression in Adipose Tissue Is Related to Obesity in Men and Mice', *PLOS ONE*. Edited by J. Eckel, 10(3), p. e0120742. doi: 10.1371/journal.pone.0120742.

Korhonen, J. *et al.* (2009) 'MOODS: fast search for position weight matrix matches in DNA sequences', *Bioinformatics*, 25(23), pp. 3181–3182. doi: 10.1093/bioinformatics/btp554.

Kubick, N. *et al.* (2020) 'Drugs Modulating CD4+ T Cells Blood–Brain Barrier Interaction in Alzheimer's Disease', *Pharmaceutics 2020, Vol. 12, Page 880*, 12(9), p. 880. doi: 10.3390/PHARMACEUTICS12090880.

Kumar, D. *et al.* (2016) 'Amyloid- b peptide protects against microbial infection in mouse and worm models of Alzheimer ' s disease', *Science Translational Medicine*, 8(340), pp. 340ra72-340ra72. doi: 10.1126/scitranslmed.aaf1059.

Lafontan, M. and Langin, D. (2009) 'Lipolysis and lipid mobilization in human adipose tissue.', *Progress in Lipid Research*, 48(5), pp. 275–97. doi: 10.1016/j.plipres.2009.05.001.

Lambert, J. C. *et al.* (2010) 'Implication of the immune system in Alzheimer's disease: evidence from genome-wide pathway analysis', *Journal of Alzheimer's Disease*, 20(4), pp. 1107–1118. doi: 10.3233/JAD-2010-100018.

Lee, N. K. *et al.* (2007) 'Endocrine Regulation of Energy Metabolism by the Skeleton', *Cell*, 130(3), pp. 456–469. doi: 10.1016/j.cell.2007.05.047.

Li, L. and Hölscher, C. (2007) 'Common pathological processes in Alzheimer disease and type 2 diabetes: A review', *Brain Research Reviews*, 56(2), pp. 384–402. doi: 10.1016/j.brainresrev.2007.09.001.

Liblau, R. S. *et al.* (2013) 'Neurons as targets for T cells in the nervous system', *Trends in Neurosciences*, 36(6), pp. 315–324. doi: 10.1016/j.tins.2013.01.008.

Liu, J. *et al.* (2014) 'T cells promote the regeneration of neural precursor cells in the hippocampus of Alzheimer's disease mice.', *Neural regeneration research*, 9(16), pp. 1541–7. doi: 10.4103/1673-5374.139481.

Liu, Y. *et al.* (2011) 'Deficient brain insulin signalling pathway in Alzheimer's disease and diabetes.', *The Journal of pathology*, 225(1), pp. 54–62. doi: 10.1002/path.2912.

Livny, A. *et al.* (2016) 'Long-term variability in glycemic control is associated with white matter hyperintensities in APOE4 genotype carriers with type 2 diabetes', *Diabetes Care*, 39(6), pp. 1056–1059. doi: 10.2337/dc15-2331.

Lynn, J. *et al.* (2021) 'A Tale of Two Diseases: Exploring Mechanisms Linking Diabetes Mellitus with Alzheimer's Disease', *Journal of Alzheimer's Disease*, Preprint(Preprint), pp. 1–17. doi: 10.3233/JAD-210612.

Mabbott, N. A. *et al.* (2013) 'An expression atlas of human primary cells: inference of gene function from coexpression networks', *BMC Genomics*, 14(1), p. 632. doi: 10.1186/1471-2164-14-632.

Machhi, J. *et al.* (2021) 'CD4+ effector T cells accelerate Alzheimer's disease in mice', *Journal of Neuroinflammation*, 18(1), pp. 1–23. doi: 10.1186/S12974-021-02308-7/FIGURES/8.

Maddur, M. S. *et al.* (2012) 'Th17 cells: Biology, pathogenesis of autoimmune and inflammatory diseases, and therapeutic strategies', *American Journal of Pathology*, 181(1), pp. 8–18. doi: 10.1016/j.ajpath.2012.03.044.

Manning, Alisa K. *et al.* (2012) 'A genome-wide approach accounting for body mass index identifies genetic variants influencing fasting glycemic traits and insulin resistance', *Nature Genetics*, 44(6), pp. 659–669. doi: 10.1038/ng.2274.

Manning, Alisa K *et al.* (2012) 'A genome-wide approach accounting for body mass index identifies genetic variants influencing fasting glycemic traits and insulin resistance', *Nature Genetics*, 44(6), pp. 659–669. doi: 10.1038/ng.2274.

Marsh, S. E. *et al.* (2016) 'The adaptive immune system restrains Alzheimer ' s disease pathogenesis by modulating microglial function'. doi: 10.1073/pnas.1525466113.

Maurano, M. T. *et al.* (2015) 'Large-scale identification of sequence variants influencing human transcription factor occupancy in vivo', *Nature Genetics*, 47(12), pp. 1393–1401. doi: 10.1038/ng.3432.

McLaughlin, T. *et al.* (2014) 'T-cell profile in adipose tissue is associated with insulin resistance and systemic inflammation in humans', *Arteriosclerosis, Thrombosis, and Vascular Biology*, 34(12), pp. 2632–2636. doi: 10.1161/ATVBAHA.114.304636.

McManus, R. M. and Heneka, M. T. (2017) 'Role of neuroinflammation in neurodegeneration : new insights', *Alzheimer's Research & Therapy*, 9:14, pp. 1–7. doi: 10.1186/s13195-017-0241-2.

Merlini, M. *et al.* (2018) 'Extravascular CD3 + T Cells in Brains of Alzheimer Disease Patients Correlate with Tau but Not with Amyloid Pathology : An Immunohistochemical Study', pp. 49–56. doi: 10.1159/000486200.

Moloney, A. M. *et al.* (2010) 'Defects in IGF-1 receptor, insulin receptor and IRS-1/2 in Alzheimer's disease indicate possible resistance to IGF-1 and insulin signalling', *Neurobiology of Aging*, 31(2), pp. 224–243. doi: 10.1016/J.NEUROBIOLAGING.2008.04.002.

Monsonego, A. *et al.* (2003) 'Increased T cell reactivity to amyloid beta protein in older humans and patients with Alzheimer disease.', *The Journal of clinical investigation*, 112(3), pp. 415–22. doi: 10.1172/JCI18104.

Montagne, A. *et al.* (2015) 'Blood-Brain barrier breakdown in the aging human hippocampus', *Neuron*, 85(2), pp. 296–302. doi: 10.1016/j.neuron.2014.12.032.

Morris, J. A. *et al.* (2019) 'An atlas of genetic influences on osteoporosis in humans and mice.', *Nature genetics*, 51(2), pp. 258–266. doi: 10.1038/s41588-018-0302-x.

Moseley, T. A. *et al.* (2003) 'Interleukin-17 family and IL-17 receptors', *Cytokine and Growth Factor Reviews*, 14(2), pp. 155–174. doi: 10.1016/S1359-6101(03)00002-9.

Nikolajczyk, B. S. *et al.* (2011) 'State of the union between metabolism and the immune system in type 2 diabetes.', *Genes and immunity*, 12, pp. 239–250. doi: 10.1038/gene.2011.14.

Noack, M. and Miossec, P. (2014) 'Th17 and regulatory T cell balance in autoimmune and inflammatory diseases', *Autoimmunity Reviews*, 13(6), pp. 668–677. doi: 10.1016/j.autrev.2013.12.004.

Olsson, A. H. *et al.* (2014) 'Genome-Wide Associations between Genetic and Epigenetic Variation Influence mRNA Expression and Insulin Secretion in Human Pancreatic Islets', *PLoS Genetics*. Edited by J. M. Greally, 10(11), p. e1004735. doi: 10.1371/journal.pgen.1004735.

Parachikova, A. *et al.* (2007) 'Inflammatory changes parallel the early stages of Alzheimer disease', *Neurobiology of Aging*, 28(12), pp. 1821–1833. doi: 10.1016/j.neurobiolaging.2006.08.014.

Park, H. *et al.* (2016) 'Multivariate Analysis of Anthropometric Traits Using Summary Statistics of Genome-Wide Association Studies from GIANT Consortium', *PLOS ONE*. Edited by Q. Li, 11(10), p. e0163912. doi: 10.1371/journal.pone.0163912.

Pellicanò, M. *et al.* (2012) 'Immune profiling of Alzheimer patients.', *Journal of neuroimmunology*, 242(1–2), pp. 52–9. doi: 10.1016/j.jneuroim.2011.11.005.

Pezzini, F. *et al.* (2017) 'Transcriptomic Profiling Discloses Molecular and Cellular Events Related to Neuronal Differentiation in SH-SY5Y Neuroblastoma Cells', *Cellular and Molecular Neurobiology*, 37(4), pp. 665–682. doi: 10.1007/s10571-016-0403-y.

Pickrell, J. K. *et al.* (2016) 'Detection and interpretation of shared genetic influences on 42 human traits', *Nature Genetics*, 48(7), pp. 709–717. doi: 10.1038/ng.3570.

Plitas, G. and Rudensky, A. Y. (2016) 'Regulatory T cells: Differentiation and function', *Cancer Immunology Research*, 4(9), pp. 721–725. doi: 10.1158/2326-6066.CIR-16-0193.

Poggi, M. *et al.* (2009) 'The inflammatory receptor CD40 is expressed on human adipocytes: Contribution to crosstalk between lymphocytes and adipocytes', *Diabetologia*, 52(6), pp. 1152–1163. doi: 10.1007/s00125-009-1267-1.

Pugazhenthi, S., Qin, L. and Reddy, P. H. (2017) 'Common neurodegenerative pathways in obesity, diabetes, and Alzheimer's disease', *Biochimica et biophysica acta. Molecular basis of disease*, 1863(5), pp. 1037–1045. doi: 10.1016/J.BBADIS.2016.04.017.

Ravona-Springer, R. *et al.* (2014) 'The ApoE4 genotype modifies the relationship of long-term glycemic control with cognitive functioning in elderly with type 2 diabetes.', *European neuropsychopharmacology : the journal of the European College of Neuropsychopharmacology*, 24(8), pp. 1303–8. doi: 10.1016/j.euroneuro.2014.05.001.

Rendina-Ruedy, E., Guntur, A. R. and Rosen, C. J. (2017) 'Intracellular lipid droplets support osteoblast function', *Adipocyte*, 6(3), pp. 250–258. doi: 10.1080/21623945.2017.1356505.

Risch, N. and Merikangas, K. (1996) 'The future of genetic studies of complex human diseases.', *Science (New York, N.Y.)*, 273(5281), pp. 1516–1517. doi: doi: 10.1126/science.273.5281.1516.

Roadmap Epigenomics Consortium *et al.* (2015) 'Integrative analysis of 111 reference human epigenomes', *Nature*, 518(7539), pp. 317–329. doi: 10.1038/nature14248.

Roman, T. S. *et al.* (2017) 'A Type 2 Diabetes-Associated Functional Regulatory Variant in a Pancreatic Islet Enhancer at the ADCY5 Locus.', *Diabetes*, 66(9), pp. 2521–2530. doi: 10.2337/db17-0464.

Rosales-Corral, S. *et al.* (2015) 'Diabetes and alzheimer disease, two overlapping pathologies with the same background: Oxidative stress', *Oxidative Medicine and Cellular Longevity*, 2015. doi: 10.1155/2015/985845.

Rovira-Clave, X. *et al.* (2016) 'Dual role of ERK5 in the regulation of T cell receptor expression at the T cell surface', *Journal of Leukocyte Biology*, 99(1), pp. 143–152. doi: 10.1189/jlb.2A0115-034R.

Rutz, S., Eidenschenk, C. and Ouyang, W. (2013) 'IL-22, not simply a Th17 cytokine', *Immunological Reviews*, 252(1), pp. 116–132. doi: 10.1111/imr.12027.

Sakaguchi, S. *et al.* (2006) 'Foxp3+CD25+CD4+ natural regulatory T cells in dominant self-tolerance and autoimmune disease', *Immunological Reviews*, 212(1), pp. 8–27. doi: 10.1111/j.0105-2896.2006.00427.x.

Salas, I. H. and De Strooper, B. (2019) 'Diabetes and Alzheimer's Disease: A Link not as Simple as it Seems', *Neurochemical Research*, 44(6), pp. 1271–1278. doi: 10.1007/s11064-018-2690-9.

Samelson, E. J. *et al.* (2018) 'Diabetes and Deficits in Cortical Bone Density, Microarchitecture, and Bone Size: Framingham HR-pQCT Study', *Journal of Bone and Mineral Research*, 33(1), pp. 54–62. doi: 10.1002/jbmr.3240.

Sardi, F. *et al.* (2011) 'Alzheimer's disease, autoimmunity and inflammation. The good, the bad and the ugly', *Autoimmunity Reviews*, 11(2), pp. 149–153. doi: 10.1016/j.autrev.2011.09.005.

Saresella, M. *et al.* (2011) 'Brain , Behavior , and Immunity Increased activity of Th-17 and Th-9 lymphocytes and a skewing of the post-thymic differentiation pathway are seen in Alzheimer ' s disease', *Brain Behavior and Immunity*, 25(3), pp. 539–547. doi: 10.1016/j.bbi.2010.12.004.

Saxena, R. *et al.* (2010) 'Genetic variation in GIPR influences the glucose and insulin responses to an oral glucose challenge.', *Nature genetics*, 42(2), pp. 142–8. doi: 10.1038/ng.521.

Shin, J. H., Shin, D. W. and Noh, M. (2009) 'Interleukin-17A inhibits adipocyte differentiation in human mesenchymal stem cells and regulates pro-inflammatory responses in adipocytes', *Biochemical*

Pharmacology, 77(12), pp. 1835–1844. doi: 10.1016/J.BCP.2009.03.008.

Siffrin, V. *et al.* (2010) 'In vivo imaging of partially reversible th17 cell-induced neuronal dysfunction in the course of encephalomyelitis.', *Immunity*, 33(3), pp. 424–36. doi: 10.1016/j.immuni.2010.08.018.

Sims-Robinson, C. *et al.* (2010) 'How does diabetes accelerate Alzheimer disease pathology?', *Nature Reviews Neurology*, 6(10), pp. 551–559. doi: 10.1038/nrneurol.2010.130.

Sinnott-Armstrong, N. *et al.* (2021) 'A regulatory variant at 3q21.1 confers an increased pleiotropic risk for hyperglycemia and altered bone mineral density', *Cell Metabolism*, 33(3), pp. 615-628.e13. doi: 10.1016/j.cmet.2021.01.001.

Sivakumaran, S. *et al.* (2011) 'Abundant pleiotropy in human complex diseases and traits', *American Journal of Human Genetics*, 89(5), pp. 607–618. doi: 10.1016/j.ajhg.2011.10.004.

Skepner, J. *et al.* (2015) 'In vivo regulation of gene expression and T helper type 17 differentiation by RORγt inverse agonists.', *Immunology*, 145(3), pp. 347–56. doi: 10.1111/imm.12444.

Sochocka, M., Zwolińska, K. and Leszek, J. (2017) 'The Infectious Etiology of Alzheimer's Disease', *Current Neuropharmacology*, 15(7), pp. 996–1009. doi: 10.2174/1570159x15666170313122937.

Sohn, S. J. *et al.* (2005) 'Transcriptional Regulation of Tissue-Specific Genes by the ERK5 Mitogen-Activated Protein Kinase Transcriptional Regulation of Tissue-Specific Genes by the ERK5 Mitogen-Activated Protein Kinase', *Molecular and Cellular Biochemistry*, 25(19), pp. 8553–66. doi: 10.1128/MCB.25.19.8553.

Sohn, S. J., Lewis, G. M. and Winoto, A. (2008) 'Non-redundant function of the MEK5-ERK5 pathway in thymocyte apoptosis', *EMBO Journal*, 27(13), pp. 1896–1906. doi: 10.1038/emboj.2008.114.

Solovieff, N. *et al.* (2013) 'Pleiotropy in complex traits : challenges and strategies', *Nature Publishing Group*, 14(7), pp. 483–495. doi: 10.1038/nrg3461.

Soscia, S. J. *et al.* (2010) 'The Alzheimer ' s Disease-Associated Amyloid b -Protein Is an Antimicrobial Peptide', 5(3), pp. 1–10. doi: 10.1371/journal.pone.0009505.

Srikanthan, P. *et al.* (2014) 'Insulin Resistance and Bone Strength: Findings From the Study of Midlife in the United States', *Journal of Bone and Mineral Research*, 29(4), pp. 796–803. doi: 10.1002/jbmr.2083.

Stearns, F. W. (2010) 'One hundred years of pleiotropy: A retrospective', *Genetics*, 186(3), pp. 767–773. doi: 10.1534/genetics.110.122549.

Stromnes, I. M. *et al.* (2008) 'Differential regulation of central nervous system autoimmunity by TH1 and TH17 cells', *Nature medicine*, 14(3), p. 337. doi: 10.1038/NM1715.

Sun, Y. *et al.* (2020) 'Metabolism: A Novel Shared Link between Diabetes Mellitus and Alzheimer's Disease', *Journal of Diabetes Research*. J Diabetes Res. doi: 10.1155/2020/4981814.

Tabarkiewicz, J. *et al.* (2015) 'The Role of IL-17 and Th17 Lymphocytes in Autoimmune Diseases.', *Archivum immunologiae et therapiae experimentalis*, 63(6), pp. 435–49. doi: 10.1007/s00005-015-0344-z.

Takaishi, M. *et al.* (2017) 'Oral administration of a novel RORγt antagonist attenuates psoriasis-like skin lesion of two independent mouse models through neutralization of IL-17', *Journal of Dermatological Science*, 85(1), pp. 12–19. doi: 10.1016/j.jdermsci.2016.10.001.

Thurner, M. *et al.* (2018) 'Integration of human pancreatic islet genomic data refines regulatory mechanisms at Type 2 Diabetes susceptibility loci', *eLife*, 7, p. e31977. doi: 10.7554/eLife.31977.

Togo, T. *et al.* (2002) 'Occurrence of T cells in the brain of Alzheimer's disease and other neurological diseases', *J. Neuroimmunol.*, 124(1–2), pp. 83–92. Available at: http://dx.doi.org/10.1016/S0165-5728(01)00496-9 (Accessed: 14 April 2016).

Tramutola, A. *et al.* (2017) 'Modulation of GLP-1 signaling as a novel therapeutic approach in the treatment of Alzheimer's disease pathology', *Expert Review of Neurotherapeutics*, 17(1), pp. 59–75. doi: 10.1080/14737175.2017.1246183.

Turley, P. *et al.* (2017) 'MTAG: Multi-Trait Analysis of GWAS', *bioRxiv*, p. 118810. doi: 10.1101/118810.

Vasan, S. K. *et al.* (2011) 'Absence of birth-weight lowering effect of ADCY5 and near CCNL, but association of impaired Glucose-Insulin homeostasis with ADCY5 in Asian Indians', *PLoS ONE*, 6(6), pp. 1–6. doi: 10.1371/journal.pone.0021331.

Vestergaard, P. (2007) 'Discrepancies in bone mineral density and fracture risk in patients with type 1 and type 2 diabetes - A meta-analysis', *Osteoporosis International*, 18(4), pp. 427–444. doi: 10.1007/s00198-006-0253-4.

Visscher, P. M. *et al.* (2012) 'Five years of GWAS discovery', *American Journal of Human Genetics*, 90(1), pp. 7–24. doi: 10.1016/j.ajhg.2011.11.029.

Visscher, P. M. *et al.* (2017) '10 Years of GWAS Discovery: Biology, Function, and Translation', *American Journal of Human Genetics*, 101(1), pp. 5–22. doi: 10.1016/j.ajhg.2017.06.005.

Walker, J. M. and Harrison, F. E. (2015) 'Shared Neuropathological Characteristics of Obesity, Type 2 Diabetes and Alzheimer's Disease: Impacts on Cognitive Decline', *Nutrients 2015, Vol. 7, Pages 7332-7357*, 7(9), pp. 7332–7357. doi: 10.3390/NU7095341.

Wang, X. *et al.* (2002) 'Age-related changes in the collagen network and toughness of bone.', *Bone*, 31(1), pp. 1–7. doi: 10.1016/S8756-3282(01)00697-4.

Weirauch, M. T. *et al.* (2014) 'Determination and inference of eukaryotic transcription factor sequence specificity.', *Cell*, 158(6), pp. 1431–1443. doi: 10.1016/j.cell.2014.08.009.

Wolf, S. A. *et al.* (2009) 'CD4-Positive T Lymphocytes Provide a Neuroimmunological Link in the Control of Adult Hippocampal Neurogenesis', *The Journal of Immunology*, 182(7), pp. 3979–3984. doi: 10.4049/jimmunol.0801218.

Wu, H. *et al.* (2007) 'T-Cell Accumulation and Regulated on Activation, Normal T Cell Expressed and Secreted Upregulation in Adipose Tissue in Obesity', *Circulation*, 115(8), pp. 1029–1038. doi: 10.1161/CIRCULATIONAHA.106.638379.

Yang, X. O. *et al.* (2008) 'Molecular Antagonism and Plasticity of Regulatory and Inflammatory T Cell Programs', *Immunity*, 29(1), pp. 44–56. doi: 10.1016/j.immuni.2008.05.007.

Zhang, J. *et al.* (2013) 'Th17 cell-mediated neuroinflammation is involved in neurodegeneration of aβ1-42-induced Alzheimer's disease model rats.', *PloS one*, 8(10), p. e75786. doi: 10.1371/journal.pone.0075786.

Zhang, Y. *et al.* (2015) 'Matrine improves cognitive impairment and modulates the balance of Th17 / Treg cytokines in a rat model of A β 1-42 -induced Alzheimer ' s disease', 40(4), pp. 411–419. doi: 10.5114/ceji.2015.56961.

Zhou, L. *et al.* (2008) 'TGF-β-induced Foxp3 inhibits TH17 cell differentiation by antagonizing RORγt function', *Nature*, 453(7192), pp. 236–240. doi: 10.1038/nature06878.

Zhou, X. *et al.* (2011) 'The human epigenome browser at Washington University', *Nature Methods*. Nature Publishing Group, pp. 989–990. doi: 10.1038/nmeth.1772.

Zhu, X. *et al.* (2015) 'Meta-analysis of correlated traits via summary statistics from GWASs with an application in hypertension', *American Journal of Human Genetics*, 96(1), pp. 21–36. doi: 10.1016/j.ajhg.2014.11.011.

Zi, C. *et al.* (2022) 'Changes of Th17 cells, regulatory T cells, Treg/Th17, IL-17 and IL-10 in patients with type 2 diabetes mellitus: a systematic review and meta-analysis', *Endocrine*, 76(2), pp. 263–272. doi: 10.1007/s12020-022-03043-6.

Ziv, Y. *et al.* (2006) 'Immune cells contribute to the maintenance of neurogenesis and spatial learning abilities in adulthood.', *Nature neuroscience*, 9(2), pp. 268–75. doi: 10.1038/nn1629.

Zuniga, L. A. *et al.* (2010) 'IL-17 Regulates Adipogenesis, Glucose Homeostasis, and Obesity', *The Journal of Immunology*, 185(11), pp. 6947–6959. doi: 10.4049/jimmunol.1001269.

Appendix

1 Study documents

1.1 Study design

Interpretation von nicht-kodierenden Varianten, die der gemeinsamen Genetik (Pleiotropie) von Typ-2-Diabetes und Morbus Alzheimer zugrunde liegen

1. Verantwortlichkeiten

a. Studienleiter
Prof. Dr. med. Hans Hauner
Klinikum rechts der Isar der
Technischen Universität München
Institut für Ernährungsmedizin
Uptown München, Campus D
Georg-Brauchle-Ring 62
80992 München

b. beteiligte Wissenschaftler/innen

Asst. Prof. Dr. rer. nat. Melina Claussnitzer
Technische Universität München
Lehrstuhl für Ernährungsmedizin
derzeit Broad Institute of MIT and Harvard
75 Ames St.
Lab 10075
Cambridge, MA 02142, USA

PD Dr.med. Thomas Skurk
Technische Universität München
Lehrstuhl für Ernährungsmedizin
ZIEL – Institute for Food & Health
Core Facility Humanstudien
Gregor-Mendel-Str.2
85354 Freising-Weihenstephan

Isabel Sousa
Technische Universität München
Lehrstuhl für Ernährungsmedizin
ZIEL – Institute for Food & Health
Gregor-Mendel-Str.2
85350 Freising

4. Studienziele

a. primäre/sekundäre Ziele und/oder Hypothesen

Welcher Lokus (Kausalvariante) ist für die Pleiotropie zwischen AD und T2D verantwortlich?

b. konfirmatorisch/explorativ
Es handelt sich um eine explorative Studie.

5. Zielgrößen

a. primäre/sekundäre Zielgrößen
Die primären erwarteten Ergebnisse sind Veränderungen in der Aktivierungs- und Differenzierungskapazität von T-Zellen nach Gen-Knock-Down und Genom-Editing. Die sekundären Ergebnisse sind die Wirkungen der manipulierten T-Zellen im Fettgewebe und Hirngewebe, um die Pleiotropie zu bestätigen.

6. Studiendesign

a. monozentrisch/multizentrisch
Es handelt sich um eine monozentrische Studie mit gesunden Probanden.

b. Studienarme: Intervention/Kontrolle
Die Teilstudien sind einarmig.

c. Randomisierung
Entfällt

d. **Verblindung**
Entfällt

7. Studienpopulation

a. Ein- und Ausschlusskriterien
Einschlusskriterien:

- Gesunde Männer im Alter zwischen 18 und 40 Jahren
- BMI zwischen 18,5 und 30 kg/m²
- Schriftliche Einverständniserklärung

Ausschlusskriterien:

- Typ 1 und 2 Diabetes
- Raucher
- Kardiovaskuläre Erkrankungen
- sonstige schwere Erkrankung (wie z.B. Krebs)
- Antibiotikabehandlung in den letzten 6 Monaten

Ausschlusskriterien während der Studie:

- Probanden, bei denen unvertretbare, unerwünschte Ereignisse auftreten
- Probanden mit akuten Erkrankungen im Versuchszeitraum
- Probanden, die ihre Zustimmung zur Teilnahme an der Studie widerrufen
- Probanden, welche die Versuchsbedingungen nicht einhalten

b. Anzahl der Studienteilnehmer
In der Studie sollen 20 männliche Probanden getestet werden.

c. Rekrutierungsmaßnahmen (wo und wie werden die Teilnehmer rekrutiert?)
Die Teilnehmer werden am Campus Weihenstephan über Aushänge rekrutiert.

8. Studienablauf

a. Aufklärung der Probanden und Einholung der Einwilligung
Die Probanden werden vor Studienbeginn schriftlich und mündlich über Ziele und Art der geplanten Studie aufgeklärt. Die Teilnahme an der Studie ist freiwillig; die Zustimmung kann jederzeit ohne Angabe von Gründen und ohne Nachteile zurückgezogen werden. Die Zustimmung der Probanden wird durch ihre Unterschrift auf der Einverständniserklärung dokumentiert. Die Einverständniserklärung bleibt aus

datenschutzrechtlichen Gründen beim Studienleiter. Bei Rücktritt von der Studie wird bereits gewonnenes (Daten-)Material vernichtet. Der Proband wird jedoch darauf hingewiesen, dass bis zum Zeitpunkt des Rücktritts gesammelte Daten in anonymisierter Form weiterhin verwendet werden dürfen.

b. Erfassung der Zielgrößen (Untersuchungen, Messungen, Datenerhebungen)
   24 Std. vor der Untersuchung sollen die Probanden Koffein und sportliche Aktivitäten vermeiden. Die Probanden erhalten hierzu entsprechende Empfehlungen. 12 Std. vor der Blutabnahme darf bis auf Wasser keine Nahrung zugeführt werden.
   Der Ablauf der Untersuchung ist wie folgt vorgesehen:
   Die Probanden erscheinen morgens nüchtern im Studienzentrum. Dort wird ca. 50 ml Blut abgenommen. Außerdem werden Größe und Gewicht nach SOPs bestimmt.

c. Gesamtdauer der Studie
   Beginn der Studie ist unmittelbar nach Vorliegen eines positiven Votums der Ethikkommission der Fakultät für Medizin der TU München. Voraussichtliches Ende der Studie ist März 2018.

9. Nutzen-Risiko-Abwägung

a. mit der Studienteilnahme verbundene Belastungen und Risiken:
   Risiken bestehen in geringem Maße bei der Blutabnahme. Die Blutabnahme selbst erfolgt durch einen Studienarzt. In seltenen Fällen kann es zu stärkeren Nachblutung an der Einstichstelle kommen und in sehr seltenen Fällen zu einer Schädigung von Nerven bzw. Blutgefäßen.

b. Abbruchkriterien:
   Die Studie wird insgesamt abgebrochen bei:
   - Auftreten relevanter medizinischer oder ethischer Probleme
   - Auftreten von unerwünschten Ereignissen, deren Schwere und Dauer unbekannt sind

c. Statement zur ärztlichen Vertretbarkeit
   Von ärztlicher Seite bestehen auf Grund des geringen Risikos keine Bedenken.

10. Biometrie

a. konfirmatorische Studie:
   nicht zutreffend

b. explorative Studie: Erläuterung zur statistischen Methodik
   Es handelt sich um eine Studie zur Aufklärung der Dysregulation von Th17- und Treg-Populationen.

11. Datenmanagement und Datenschutz

a. Erfassung, Speicherung (Art, Ort, Dauer) und Weitergabe von Daten, Gewährleistung der Datensicherheit:
   Die Namen der Probanden und alle anderen vertraulichen Informationen unterliegen der ärztlichen Schweigepflicht und den Bestimmungen des Bundesdatenschutzgesetzes (BDSG). Die Probanden werden unmittelbar nach Einschluss in die Studie mit einem dreistelligen Zahlen- und Buchstabencode pseudonymisiert (ABx). Alle erhobenen Studiendaten werden in elektronischer Form am Lehrstuhl für Ernährungsmedizin erfasst und gespeichert.
   Alle erhobenen Daten und Originaldokumente werden nach Studienende oder -abbruch für 10 Jahre aufbewahrt. Dazu werden die Dokumente im Archiv des Lehrstuhls für Ernährungsmedizin gelagert. Falls der Proband mit einer Lagerung ausgewählter in der Biobank einverstanden ist, werden diese dort für einen langfristigen Zeitraum gelagert.

b. anonymisiert/pseudonymisiert:

siehe a

c. Widerruf, Datenlöschung:
Bei Rücktritt von der Studie wird bereits gewonnenes (Daten-)Material vernichtet oder beim Probanden angefragt, ob er mit der Auswertung des Materials einverstanden ist.

12. Umgang mit Biomaterialien

Die Biomaterialien (Blut) werden lediglich für das vorgestellte Projekt verwendet und auf Wunsch des Probanden nach Ende der Studie vernichtet.

13. Probandenversicherung (sofern zutreffend)

Es wird eine übliche Probandenversicherung abgeschlossen

14. Unterschriften: Studienleiter/in (Antragsteller/in)

Freising, 23. Juni 2017

Ort, Datum Prof. H. Hauner

1.2. Recruitment advertisement

ZIEL - Institute for Food & Health
Technische Universität München

Lehrstuhl für Ernährungsmedizin
Technische Universität München
Prof. Dr. med. Hans Hauner

2018.02.08

Teilnehmer gesucht

für

Studie:
Rolle von T-Zellen in Typ 2 Diabetes und Alzheimer-Krankheiten

Im Rahmen einer laufenden Studie, in welcher die Rolle von T-Zellen bei der Entstehung von Typ 2 Diabetes und Alzheimer-Krankheiten untersucht wird, suchen wir **gesunde, normalgewichtige Männer (Nichtraucher) zwischen 18 und 40 Jahren**.

Die Studie beinhaltet:

- Ein Termin am Studienzentrum (ca. 30min)
  - Aufklärung und Nüchtern-Blutabnahme
  - Erhebung von Daten zu Größe und Gewicht

Die Studie findet in Weihenstephan im Human Study Center (Gregor-Mendel-Str. 2) statt. Sie erhalten die gemessenen Daten zu Ihrer Körperzusammensetzung.

Zur Terminvereinbarung bzw. bei Fragen wenden Sie sich bitte an:
Frau Isabel Sousa
E-Mail: isabel.sousa@tum.de
Tel.: 08161-712011

Else Kröner-Fresenius-Zentrum für Ernährungsmedizin, Lehrstuhl für Ernährungsmedizin, Gregor-Mendel-Str. 2, 85354 Freising - Weihenstephan

1.3. Screening questionnaire including inclusion and exclusion criteria

Screening:
Interpretation von nicht-kodierenden Varianten, die der gemeinsamen Genetik (Pleiotropie) zwischen Typ-2-Diabetes und Alzheimer-Krankheit zugrunde liegen

Datum: __ __ / __ __ / __ __ __ __ Uhrzeit: |__||__|:|__||__| Uhr

❍ Telefonisch

❍ Persönlich im Studienzentrum

❍ Sonstiges _____

Nachname:		
Vorname:		
Telefonnummer:		
Email:		
Geburtsdatum:		
Größe:	Gewicht aktuell:	Gewicht vor 3 Monaten:
BMI:		

Einschlusskriterien

❍ Alter 18 – 40 Jahre
❍ männlich
❍ BMI zwischen 18,5 und 30 kg/m²
Einverständniserklärung unterschrieben

Ausschlusskriterien:

➔ *bei >= 1 Ja-Antwort Ausschluss des Probanden*

Ein- und Ausschlusskriterium	JA	NEIN	Kommentar
Aktuelle Teilnahme an Interventionsstudien			
Raucher			
Chronische Erkrankungen (ärztliche Diagnose):			
• Chronische Infektionen (z.B. HIV)			
• Diagnostizierte Lebererkrankungen (z.B. HCV, HBV)			
• Diagnostizierter Diabetes mellitus			
• Unbehandelte endokrinologische Erkrankungen (z.B. Schilddrüsenüber oder -unterfunktion)			
• Diagnostizierte Autoimmunerkrankung (z.B. Rheuma, Colitis Ulcerosa, Morbus Crohn)			
• Diagnostizierter Herzinfarkt innerhalb der letzten 3 Jahre			
• Diagnostizierter Schlaganfall innerhalb der letzten 3 Jahre			
• Herzschrittmacher			
• Unbehandelter Bluthochdruck (>160/95 mmHg)			
• Herzkrankheit, die innerhalb der letzten 3 Jahre ärztlich behandelt werden musste			
• Krebserkrankung, die innerhalb der letzten 3 Jahre ärztlich behandelt werden musste			
• Diagnostizierte psychische oder neurologische Erkrankungen in den letzten 3 Jahren (z.B. Schizophrenie, Epilepsie, Depression, Multiple Sklerose)			
Bluttransfusion in den letzten 3 Monaten			
Antibiotikabehandlung in den letzten 6 Monaten			
Immobilität (z.B. an den Rollstuhl gebunden)			
Kein stabiles Körpergewicht in den letzten drei Monaten (+-3kg)			

Sonstige Informationen:

Medikamente (Hinweis Medikamentenliste soll bei der Visite mitgebracht werden)

_____
_____

Erkrankungen / Akute Erkrankungen (z.B. Erkältung, Fieber, Durchfall, Bronchitis, Blasenentzündung)
(Hinweis: Befunde des letzten halben Jahres sollen zur Visite mitgebracht werden)

_____
_____

1.4. Participant information

Teilnehmerinformation

Interpretation von nicht-kodierenden Varianten, die der gemeinsamen Genetik (Pleiotropie) zwischen Typ-2-Diabetes und Alzheimer-Krankheit zugrunde liegen

Sehr geehrter Teilnehmer!

Sie sind eingeladen, an der oben genannten Studie teilzunehmen. Nachfolgend sind die wichtigsten Informationen zum Hintergrund, der Zielsetzung und dem Ablauf der Studie dargestellt. Bitte lesen Sie sich die Teilnehmerinformation sorgfältig und in Ruhe durch, bevor Sie Ihre Entscheidung zur Teilnahme treffen.

Hintergrund und Ziele der Studie

Neuste Forschungsergebnisse haben gezeigt, dass T-zellen bei der Entstehung von Typ 2 Diabetes und Alzheimer-Krankheiten eine wichtige Rolle spielen. In Anbetracht der aktuellen Literatur gehen wir davon aus, dass die Fehlregulation in spezifischen T-Zellen Populationen sowohl in Typ 2 Diabetes als auch in Alzheimerkrankheit durch einen genetische Variation erklärt werden kann, der die T-Zellen zu mehr pro-inflammatorischen und weniger entzündungshemmenden Zellpopulationen fördert. Um die Rolle von T-Zellen in beiden Krankheiten zu klären, wird im Rahmen dieser Studie Blut abgenommen zur Isolierung von T-Zellen.

Studienablauf

Im Rahmen der Studie möchten wir Sie bitten, zu einem Untersuchungstermin in das Studienzentrum in Freising-Weihenstephan zu kommen.
Zum jeweiligen Untersuchungstermin müssen Sie nüchtern erscheinen, d.h. die letzte Mahlzeit sollte 12 Stunden zurückliegen. Medikamente dürfen nach Absprache eingenommen werden. 24 h vor der Untersuchung und am Untersuchungstag sollen keine körperlich anstrengenden Tätigkeiten verrichtet werden (z.B. **nicht** mit dem Rad zu den Untersuchungen kommen). Zudem dürfen Sie 12 Stunden keinen Kaffee oder Schwarztee trinken.

Untersuchungsablauf

<u>Bioimpedanzanalyse (Körperfettmessung)</u>
Die Bioimpedanzanalyse (BIA) dient der Messung der Körperzusammensetzung (Muskel-, Fett-, Wasseranteil) mittels einer speziellen Körperanalysewaage.

<u>Blutabnahme</u>
Die Blutabnahme dient zur Isolierung der Primärblutzellen. Für die Abnahme benötigen wir etwa 50 ml Blut, das entspricht ungefähr 5 Esslöffeln. Das ist für den Körper vollkommen ungefährlich. Zum Vergleich: bei einer durchschnittlichen Blutspende werden 500 ml Blut entnommen.

Wer darf teilnehmen?

An der Studie teilnehmen dürfen:

- Gesunde Männer im Alter zwischen 18 und 40 Jahren
- BMI zwischen 18,5 und 30 kg/m^2

- Schriftliche Einverständniserklärung

Ausschlusskriterien sind:

- Typ 1 und Typ 2 Diabetes
- Raucher
- Kardiovaskuläre Erkrankungen (z.B. Herzinfarkt, Arteriosklerose)
- Andere schwere Krankheiten
- Antibiotikaeinnahme in den letzten 6 Monaten

Risiken

Bei der Blutentnahme kann es in seltenen Fällen zu einer Infektion an der Einstichstelle (allerdings ist die Wahrscheinlichkeit aufgrund der Hygienemaßnahmen sehr gering), einer Blutung oder einer Nervenverletzung kommen.
Bei jeder Datenerhebung, -speicherung und -übermittlung bestehen Vertraulichkeitsrisiken. Der Lehrstuhl für Ernährungsmedizin der Technischen Universität (TU) München versichert Ihnen, nach Möglichkeit alles zum Schutz Ihrer Privatsphäre zu tun (siehe „Wie werden Ihre Biomaterialien und Daten geschützt?“).

Nutzen

Persönlich können Sie für Ihre Gesundheit keinen unmittelbaren Vorteil oder Nutzen aus der Spende Ihrer Proben und Daten erwarten. Die Ergebnisse sind ausschließlich zu Forschungszwecken bestimmt.
Eine Rückmeldung von Ergebnissen aus der Untersuchung der Biomaterialien ist nicht vorgesehen.

Erhalten Sie eine Aufwandsentschädigung?

Eine Aufwandsentschädigung ist nicht vorgesehen. Sie erhalten die gemessenen Daten zu Ihrer Körperzusammensetzung.

Spende, Einlagerung und Nutzung von Biomaterialien sowie zur Erhebung, Verarbeitung und Nutzung von Daten in Biobanken

Der Lehrstuhl für Ernährungsmedizin der Technischen Universität München betreibt eine Biobank. Es handelt sich dabei um eine Sammlung von menschlichen Biomaterialien wie Speichel, Blut, Urin, Stuhl oder Gewebe, verknüpft mit ausgewählten medizinischen Daten. Die Untersuchung von menschlichen Biomaterialien und die Analyse der daraus gewonnenen oder zu gewinnenden Daten sind zu einem wichtigen Instrument medizinischer Forschung geworden. Deshalb fragen wir unsere Probanden, ob sie bereit sind, uns bestimmte Körpermaterialien und Daten für die Forschung zur Verfügung zu stellen. Die Teilnahme der Probanden ist völlig freiwillig. Soweit der Proband/die Probandin sich nicht beteiligen möchten oder Ihre Zustimmung später widerrufen möchten, entstehen den Probanden daraus keine Nachteile.

Um welche Art von Biomaterialien und Daten handelt es sich?

Bei dem Biomaterial handelt es sich in diesem Fall um Blut, die den Probanden anlässlich Ihrer Studienteilnahme entnommen werden sollen. Die erhobenen Daten umfassen Informationen zur Person, die verschlüsselt („pseudonymisiert“) werden.

Wie werden die Biomaterialien und Daten verwendet?

Die vom Probanden zur Verfügung gestellten Biomaterialien und Daten werden ausschließlich für die medizinische Forschung bereitgestellt. Sie sollen im Sinne eines breiten Nutzens für die Allgemeinheit

für viele verschiedene medizinische Forschungszwecke verwendet werden können. Zum derzeitigen Zeitpunkt können noch nicht alle zukünftigen medizinischen Forschungsziele beschrieben werden. Diese können sich sowohl auf bestimmte Krankheitsgebiete (z.B. Herz-Kreislauf-Erkrankungen) als auch auf heute zum Teil noch unbekannte Krankheiten und genetische Defekte beziehen. Es kann also sein, dass die Proben und Daten des Probanden auch für medizinische Forschungsfragen verwendet werden, die wir heute noch nicht absehen können. Deshalb werden an die Biomaterialien des Probanden möglicherweise auch genetische Untersuchungen, also Untersuchungen der Erbsubstanz, durchgeführt, und zwar unter Umständen auch eine Untersuchung des gesamten Genoms.

Die Biomaterialien und Daten sollen für unbestimmte Zeit aufbewahrt und für die medizinische Forschung bereitgestellt werden. Aus logistischen Gründen ist es der Biobank nicht möglich, individuelle Eingrenzungen (z.B. Ausschluss bestimmter Forschung, Ausschluss der Weitergabe der Materialien an Dritte) vorzunehmen. Wenn der Proband/die Probandin mit der beschriebenen Art und Dauer der Nutzung nicht in vollem Umfang einverstanden ist, werden die Biomaterialien und Daten des Probanden nicht für die Biobank verwendet.

Datenschutz

Ihre schriftliche Einwilligung ist Voraussetzung für die Gewinnung und Nutzung Ihrer Blutprobe samt den zugehörigen personenbezogenen Daten zu Forschungszwecken. Ihre Einwilligung ist freiwillig und kann jederzeit widerrufen werden (siehe auch Punkt „Widerrufs- und Informationsrecht“).

Ihre Biomaterialien und Daten werden am Lehrstuhl für Ernährungsmedizin der TU München unter standardisierten Qualitäts- und Sicherheitsbedingungen unbefristet aufbewahrt und auf Antrag für Forschungszwecke herausgegeben.

Alle unmittelbar Ihre Person identifizierenden Daten (Name, Geburtsdatum, Anschrift etc.) werden durch einen Code ersetzt (pseudonymisiert, verschlüsselt). Erst in dieser Form erhält die am Lehrstuhl für Ernährungsmedizin vorhandene Biobank die Verfügungsmacht über Ihre Biomaterialien und Daten. Danach wird der Datensatz nochmals neu kodiert und gespeichert. Bei einer derartigen doppelten Kodierung sind Rückschlüsse auf Ihre Person allein auf Grund der Bezeichnung von Biomaterialien/Daten ausgeschlossen.

Voraussetzung für die Verwendung der verschlüsselten Biomaterialien und Daten für medizinische Forschungsprojekte ist, dass das Forschungsvorhaben durch eine Ethikkommission zustimmend bewertet wurde.

Eine Entschlüsselung, d.h. eine Zuordnung der Biomaterialien / Daten zu Ihrer Person (Name, Geburtsdatum, Anschrift etc.), darf nur aus zwingenden wissenschaftlichen Gründen, oder aufgrund Ihres Verlangens erfolgen. Alle Entschlüsselungsvorgänge werden dokumentiert.

Wer hat Zugang zu Ihren Biomaterialien und Daten?

Die verschlüsselten Biomaterialien und Daten können auf Antrag an Dritte für medizinische Forschungsprojekte weitergegeben werden.

Biomaterialien und Daten, die an Dritte weitergegeben wurden, dürfen nur für den beantragten Forschungszweck verwendet und nicht nochmals weitergegeben werden. Nicht verbrauchtes Material wird an die Biobank zurückgegeben oder vernichtet.

Biomaterial und unmittelbar identifizierende Daten (Name, Geburtsdatum, Anschrift etc.) sowie medizinische Daten (z. B. Diagnose, Symptome, Laborwerte etc.) werden an jeweils unterschiedlichen Stellen gelagert und gespeichert. Die Verantwortung für die Einhaltung der Schutzmaßnahmen liegt beim Lehrstuhl für Ernährungsmedizin der TU München. Dort wird sichergestellt, dass kein unbefugter Dritter Zugang zu den Biomaterialien/Daten hat.

Wissenschaftliche Veröffentlichungen von Ergebnissen erfolgen in einer Form, die keine Rückschlüsse auf Ihre Person zulässt.

Für die Überlassung Ihrer Biomaterialien / Daten erhalten Sie kein Entgelt. Sollte aus der Forschung ein kommerzieller Nutzen erzielt werden, werden Sie daran nicht beteiligt.

Mit der Überlassung der Biomaterialien an den Lehrstuhl für Ernährungsmedizin der TU München werden diese Eigentum dieser Einrichtung. Ferner ermächtigen Sie den Lehrstuhl für Ernährungsmedizin der TU München, Ihre Daten zu nutzen.

Ihre Biomaterialien und Daten werden nicht an Dritte verkauft; für die Nutzung der Biobank kann jedoch eine angemessene Aufwandsentschädigung erhoben werden.

Erfolgt eine erneute Kontaktaufnahme mit Ihnen?

Zur Erhebung von Daten zum weiteren Verlauf kann es notwendig werden, dass der Lehrstuhl für Ernährungsmedizin der TU München zu einem späteren Zeitpunkt erneut Kontakt mit Ihnen aufnimmt, um ergänzende Informationen und/oder Biomaterialien von Ihnen zu erbitten. Zudem kann die erneute Kontaktaufnahme genutzt werden, um z. B. Ihre Einwilligung zum Abgleich mit anderen Datenbanken einzuholen oder um Ihnen eine Rückmeldung über bestimmte Forschungsergebnisse zu geben. Falls Sie eine erneute Kontaktaufnahme nicht wünschen, streichen Sie bitte den entsprechenden Passus in der Einwilligungserklärung.

Haftung

Hinsichtlich der Haftung gelten die gesetzlichen Bestimmungen

Welche Widerrufs- und Informationsrechte haben Sie?

Sie können Ihre Einwilligung zur Verwendung Ihrer Biomaterialien und Daten jederzeit ohne Angabe von Gründen und ohne nachteilige Folgen für Sie widerrufen. Im Falle eines Widerrufs wird die verschlüsselte Verknüpfung der Biomaterialien und Daten mit Ihren unmittelbar identifizierenden Daten (Name, Geburtsdatum, Anschrift etc.) gelöscht. Ihre Daten und Biomaterialien stehen dann auch für zukünftige Projekte nur noch anonymisiert zur Verfügung. Darüber hinaus haben Sie das Recht, die Löschung Ihrer Daten und die Vernichtung Ihrer Biomaterialien zu verlangen. Sollten Sie jedoch vorher bereits die Anonymisierung beantragt haben ist dies jedoch nicht mehr möglich. Zudem können Daten aus bereits durchgeführten Analysen nicht mehr entfernt werden.

Wenden Sie sich für einen Widerruf bitte an: Lehrstuhl für Ernährungsmedizin der TU München, Klinikum rechts der Isar, Georg-Brauchle-Ring 62, 80992 München, Tel.: 089-289-24021 oder EKFZ@mri.tum.de

An wen wenden Sie sich bei weiteren Fragen?

Sollten während des Verlaufs der Studie Fragen auftauchen, können Sie einen Ansprechpartner wie folgt erreichen:

M.Sc. Isabel Sousa, Tel: 08161/71 2011, Email: isabel.sousa@tum.de

1.5. Participant written informed consent

Einwilligungserklärung

Interpretation von nicht-kodierenden Varianten, die der gemeinsamen Genetik (Pleiotropie) zwischen Typ-2-Diabetes und Alzheimer-Krankheit zugrunde liegen

Teilnehmer: _____

(Name, Vorname)

Adresse : _____

Geb.-Datum: _____

Ich bin damit einverstanden, dass meine Blutprobe und Daten, wie in der Teilnehmerinformation beschrieben, an den Lehrstuhl für Ernährungsmedizin der Technischen Universität (TU) München gegeben und unbefristet für medizinische Forschungszwecke verwendet werden.

Durch meine Unterschrift bestätige ich, dass ich den Inhalt der Informationsschrift gelesen und verstanden habe. Ich hatte die Gelegenheit, Fragen zu stellen. Meine Fragen wurden mir zufriedenstellend beantwortet.

Ich weiß, dass meine Teilnahme freiwillig ist und ich meine Einwilligung jederzeit ohne Angabe von Gründen widerrufen kann, ohne dass mir daraus irgendwelche Nachteile entstehen.

Ich bin damit einverstanden, dass ich evtl. zu einem späteren Zeitpunkt erneut kontaktiert werde (ggf. streichen).

Datenschutzerklärung:

Ich erkläre mich damit einverstanden, dass der Lehrstuhl für Ernährungsmedizin der TU München Biomaterialien von mir unbefristet lagert und pseudonymisiert (verschlüsselt) für medizinische Forschungsvorhaben nutzt. Ferner stimme ich zu, dass personenbezogene Daten, insbesondere Angaben über meine Gesundheit, über mich erhoben oder aus meinen Krankenunterlagen entnommen und beim Lehrstuhl für Ernährungsmedizin der TU München aufgezeichnet und pseudonymisiert (verschlüsselt) für medizinische Forschungsvorhaben genutzt werden. Die Biomaterialien und Daten dürfen für medizinische Forschungsvorhaben unbefristet verwendet werden und pseudonymisiert (verschlüsselt) an Universitäten, Forschungsinstitute und forschende Unternehmen, ggf. auch ins Ausland, weitergegeben werden.

Ich bin darüber aufgeklärt worden, dass ich jederzeit die Teilnahme ohne Begründung beenden kann. Beim Widerruf meiner Einwilligung gegenüber dem Lehrstuhl für Ernährungsmedizin der TU München habe ich das Recht, die Löschung der Verknüpfung zu den mich unmittelbar identifizierenden Daten (Name, Geburtsdatum, Anschrift etc.) bzw. falls möglich auch die Löschung/Sperrung aller meiner bis dahin gespeicherten personenbezogenen Daten bzw. die Vernichtung der Biomaterialien für die Zukunft zu verlangen.

Der Lehrstuhl für Ernährungsmedizin der TU München versichert mir, meine Daten entsprechend den datenschutzrechtlichen Bestimmungen vertraulich zu behandeln.

Eine Kopie der Teilnehmerinformation und Einwilligungserklärung habe ich erhalten. Das Original verbleibt am Lehrstuhl für Ernährungsmedizin der TU München.

Name des Teilnehmers in Druckbuchstaben

Ort, Datum (vom Teilnehmer einzutragen) Unterschrift Teilnehmer/in

Ich habe das Aufklärungsgespräch geführt und die Einwilligung des Teilnehmers eingeholt.

_____
_

Name des Arztes in Druckbuchstaben

Ort, Datum Unterschrift des Arztes

1.6. Case Report Form (CRF)

CASE REPORT FORM

Teilstudie 1

Interpretation von nicht-kodierenden Varianten, die der gemeinsamen Genetik (Pleiotropie) zwischen Typ-2-Diabetes und Alzheimer-Krankheit zugrunde liegen

Teilnehmer Code |__||__||__||__||__||__|

Visite 1	Datum: __ __/__ __ __/__ __ __ __ Tag Monat Jahr

Allgemeine Angaben

Geburtsdatum: |__||__|.|__||__|.|__||__||__||__| Alter: |__||__| Jahre

Geschlecht: ❒ männlich ❒ weiblich

Nationalität: ❒ Europäisch_____ ❒ Asiatisch, Orientalisch

❒ Afrikanisch ❒ Andere: _____

Untersuchungsvorbereitung

Teilnehmer nüchtern? ❒ ja ❒ nein*

Wann haben Sie gestern zum letzten Mal etwas gegessen? |__||__|:|__||__| Uhr

Haben Sie am Vorabend bzw. am Morgen Sport gemacht? ❒ ja* ❒ nein

Haben Sie in den letzten 24 h Koffein zu sich genommen? ❒ ja* ❒ nein

Anthropometrie-/ BIA- Messung

Raumtemperatur: |__||__|,|__| °C

Körpergröße |__||__||__|, |__| cm

<u>Körperzusammensetzung (SECA)</u>

Körpergewicht: |__||__|,|__||__| kg

BMI: |__||__|,|__||__| kg/m²

Gesamtkörperwasser: |__||__|,|__||__| L

Gesamtkörperwasser: |__||__|,|__||__| %

Extrazelluläres Wasser: |__||__|,|__||__| L

Extrazelluläres Wasser: |__||__|,|__||__| %

Hydratation: |__||__|,|__||__| %

Fettfreie Masse: |__||__|,|__||__| kg

Fettfreie Masse: |__||__|,|__||__| %

Fettfreie-Masse-Index: |__||__|,|__||__| kg/m²

Fettmasse: |__||__|,|__|__| kg

Fettmasse: |__||__|,|__|__| %

Fettmasse-Index: |__||__|,|__|__| kg/m²

Skelettmuskelmasse (gesamt): |__||__|,|__||__| kg

Skelettmuskelmasse (gesamt): |__||__|,|__||__| %

Rechter Arm Skelettmuskelmasse: |__|,|__||__| kg

Linker Arm Skelettmuskelmasse: |__|,|__||__| kg

Rechtes Bein Skelettmuskelmasse: |__|,|__||__| kg

Linkes Bein Skelettmuskelmasse: |__|,|__||__| kg

Torso Skelettmuskelmasse: |__|,|__||__| kg

Viszerales Fett: |__||__|,|__||__| l

Ruheenergieverbrauch: |__||__||__||__|,|__||__| kcal/d

Gesamtenergieverbrauch (PAL 1,6): |__||__||__||__|,|__||__| kcal/d

Im Körper gespeicherte Energie: |__||__||__||__||__||__| kcal

Resistanz (R): |__||__||__|,|__||__| Ω

Reaktanz (Xc): |__||__|,|__||__| Ω

Phasenwinkel (φ): |__||__|,|__|°

Ausdruck (SECA) nachfolgend angefügt? ❒ ja ❒ nein

Blutabnahme

Heparin-monovettes (9 ml) ❒ k.A. ❒ 6x

*k.A. bedeutet keine Abnahme

Anamnesebogen

- Gesundheit -

1) Raucherstatus

❒ Nichtraucher ❒ Ex-Raucher

2) Nehmen Sie regelmäßig Medikamente? ja ❒ nein ❒

Wenn ja, bitte genaue Angaben!

Medikament/ Hersteller	**Tägl. Dosis**	**Verabreichungs-form**	**Beginn**	**Ende**	**Krankheitsbild**
Bsp: Ramipril Hexal (1,25 mg)	1 – 0 – 0	*Tablette*	*01.01.12*	-	*Bluthochdruck*

2. Supplementary tables

Table S1. Independent loci implicated by CP-ASSOC for association with both bone mineral density and glycaemic traits.

Locus	SNP rs#	Chr	Pos (GRCh37)	Ancestral	Derived	Derived Allele Frequency	Singleton Density Score	Variant Classes	Bivariate	Bone Traits (GEFOS)			Glycemic Traits (MAGIC)		
									P-value	Trait	P-value	Effect	Trait	P-value	Effect
GCKR	rs780110	2	27685388	A	G	0,56	-1,08	3'UTR, synonymous, intronic, intergenic	2,54E-15	LSBMD	4,49E-05	4,08	FG	2,84E-12	6,99
	rs1260326	2	27730940	C	T	0,40	-0,97	missense, intronic, intergenic	1,44E-10	LSBMD	3,64E-03	2,91	FI	1,18E-08	5,70
IGF1	rs2607988	12	102929883	G	A	0,84	-0,69	intergenic	4,71E-11	LSBMD	7,15E-03	-2,69	FI	1,96E-09	-6,00
ADRA2A	rs11595612	10	112972505	C	T	0,09	1,67	intergenic	1,03E-10	LSBMD	5,29E-03	2,79	FG	1,07E-09	6,10
	rs11195496	10	113021531	G	T	0,09	1,40	intergenic	6,22E-09	FNBMD	6,78E-03	2,71	HOMAB	2,47E-07	5,16
TCF7L2	rs17747324	10	114752503	T	C	0,22	-1,34	intronic	9,14E-09	FNBMD	9,57E-03	-2,59	HOMAB	2,33E-07	-5,17
CYP19A1	rs1062033	15	51547938	C	G	0,46	1,12	intronic	1,11E-07	FNBMD	1,61E-05	-4,31	HOMAIR	1,32E-04	-3,82
								intronic	4,20E-07	FNBMD	1,61E-05	-4,31	HOMAB	1,45E-03	-3,19
ADCY5	rs2124500	3	123093530	C	T	0,27	1,94	intronic	1,83E-07	FNBMD	2,96E-03	2,97	FG	2,26E-06	4,73
	rs11717195	3	123082398	T	C	0,25	1,79	intronic	9,25E-07	FNBMD	3,99E-03	2,88	HOMAB	5,39E-05	4,04
POM121C	rs6944634	7	75061769	C	G	0,19	N/A	intronic	2,46E-07	LSBMD	3,22E-03	-2,95	FI	1,23E-05	-4,37
SUSD4	rs17161988	1	223444263	A	G	0,57	-0,43	intronic	2,82E-07	FNBMD	6,54E-05	3,99	HOMAB	4,71E-04	3,50

LSBMD, lumbar spine BMD; FNBMD, femur neck BMD; FG, fasting glucose; FI, fasting insulin

Table S2. Associations discovered using the eLX and MTAG bivariate association tools.

Method	Locus	SNP rs#	Chr	Pos (GRCh37)	Ancestral	Derived	Derived Allele Frequency	Bivariate P-value	Bone Traits (GEFOS)			Glycemic Traits (MAGIC)		
									Trait	P-value	Effect	Trait	P-value	Effect
eLX	*ADCY5*	rs11717195	3	123082398	T	C	0,18	5,73E-09	FNBMD	1,99E-03	3,091	FG	6,93E-08	0,02
MTAG	*ADCY5*	rs11717195	3	123082398	T	C	0,174	3,22E-09	FNBMD	1,99E-03	3,091	FG	6,93E-08	0,02

Table S3. Prioritization of the variants at the 3q21.1 locus using PMCA and Basset. Motif conservation and accessibility predictions were used.

SNP	r^2 with rs2124500	PMCA conservation score		Basset accessibility score (trained on ATAC-seq data in AMSC (day 24)		
		number of jointly conserved motif occurrences	estimated p-value	p(accessible | haplotype 1 allele)	p(accessible | haplotype 2 allele)	p(accessible | haplotype 1 allele) - p(accessible | haplotype 2 allele)
rs6794202	0,98	0	1	0,22201	0,2181	0,00391
rs9883204	0,97	67	0,0536	0,2132	0,21558	-0,00238
rs2124500	1	2	0,0013	0,2131	0,21543	0,00233
rs11720108	0,84	40	0,0002	0,18567	0,19503	-0,00936
rs11719201	0,84	10	0,001	0,21545	0,2121	0,00334
rs35841686	0,96	24	0,0016	0,22071	0,22016	-0,00056
rs11717195	0,87	12	0,0002	0,20349	0,19531	0,00818
rs7614016	0,86	44	<0.0001	0,21623	0,22565	-0,00942
rs34970607	0,96	52	<0.0001	0,20129	0,21054	-0,00925
rs7613951	0,86	54	<0.0001	0,19648	0,18315	0,01333
rs2877716	0,98	67	<0.0001	0,217	0,22147	0,00447
rs6798189	0,98	72	<0.0001	0,19747	0,20886	-0,01139
rs56371916	**0,98**	**189**	**<0.0001**	**0,19873**	**0,16755**	**0,03118**

3. Supplementary figures

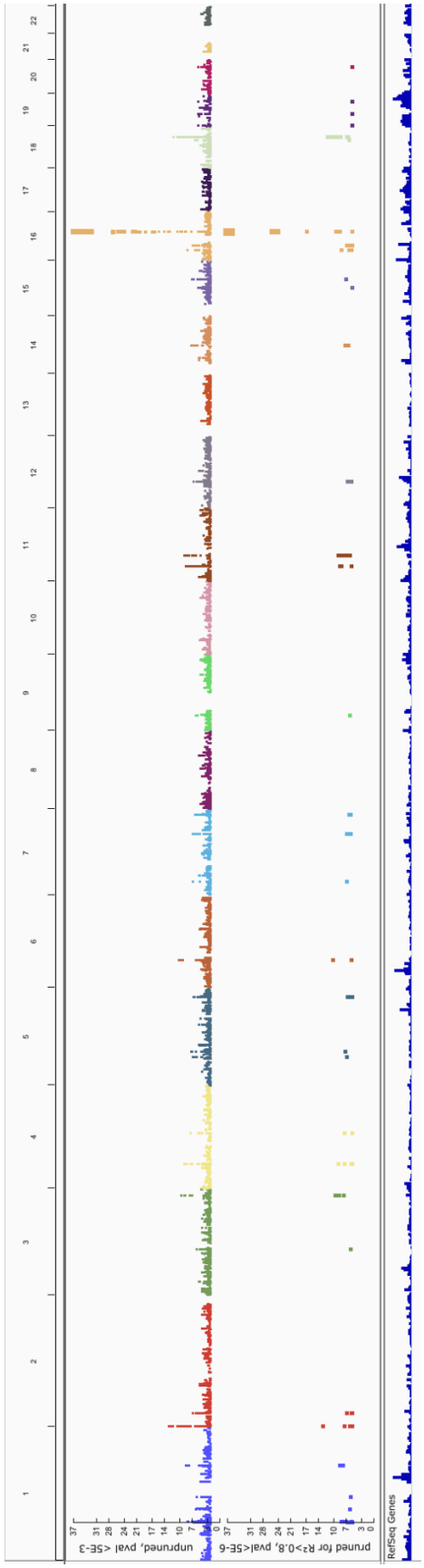

Figure S1 manhattan plot of bivariate genome-wide association analysis AD-T2D associated SNPs.

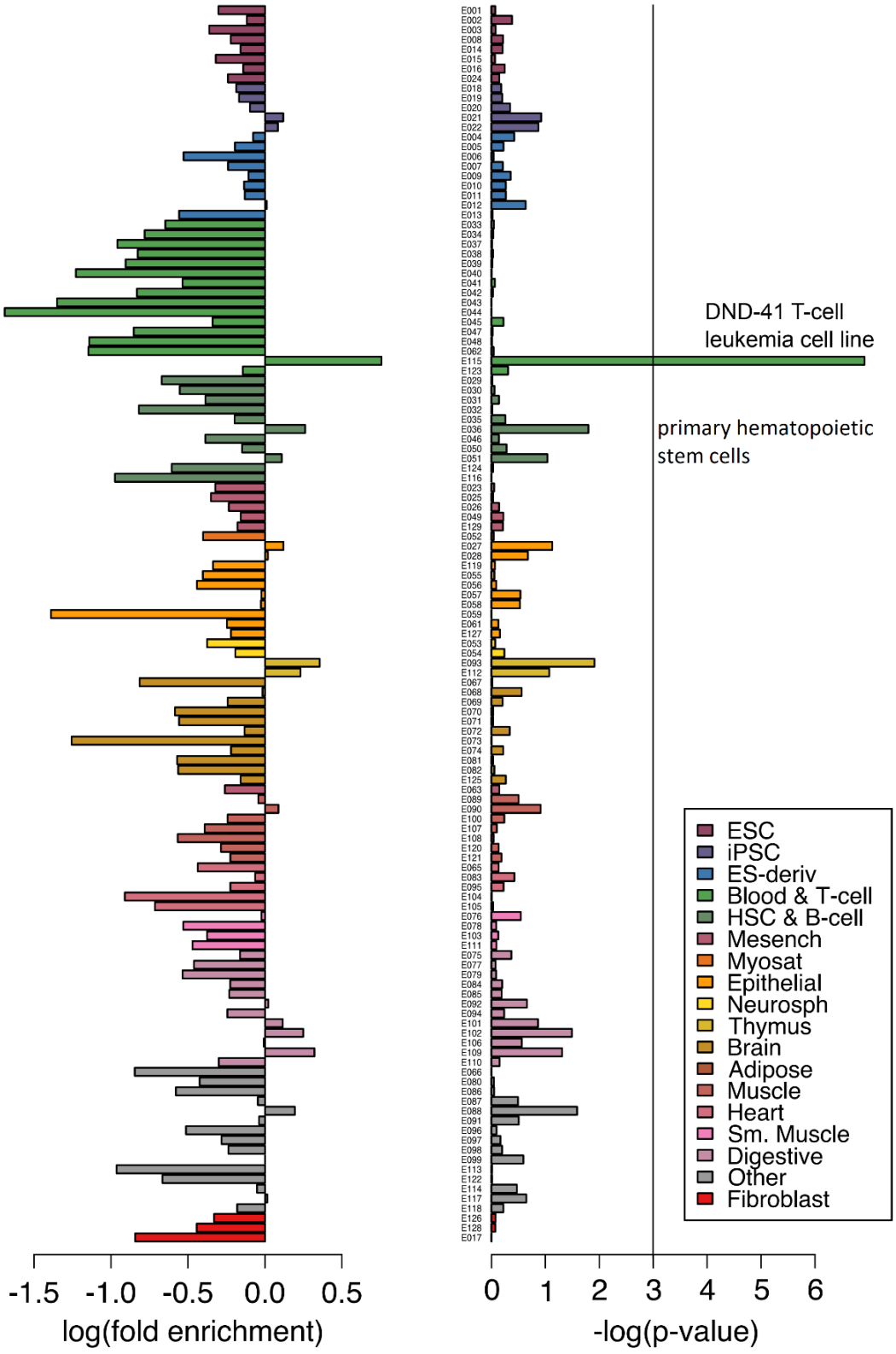

Figure S2. Cell type enrichment across 127 reference epigenomes (Roadmap) for the AD-T2D bivariate loci. The identified bivariate signals were enriched in blood and T cell related epigenomes, namely DND-41 leukemia T cell line, primary hematopoietic stem cells and thymus.

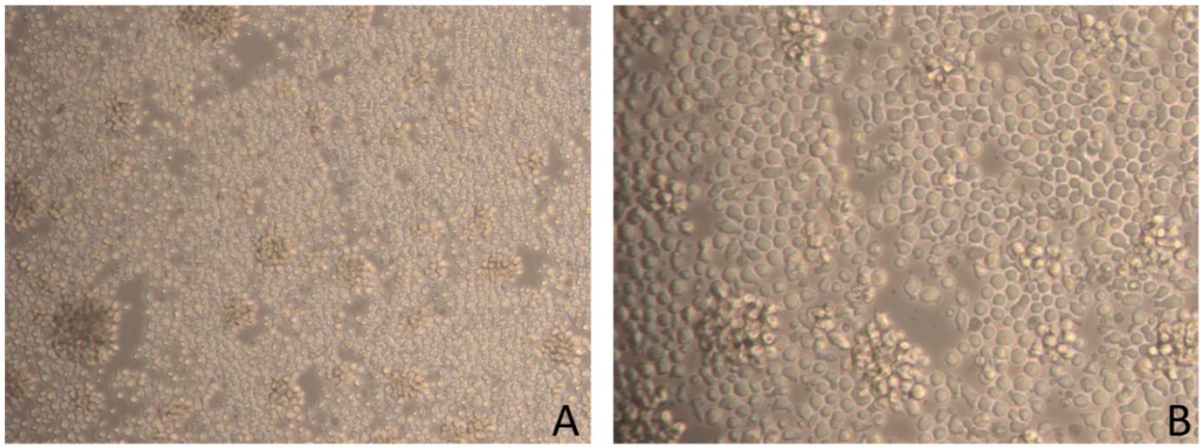

Figure S3. Micrographs from $CD4^+$ T cells in culture. A. Magnification 10x; B. Magnification 20x.

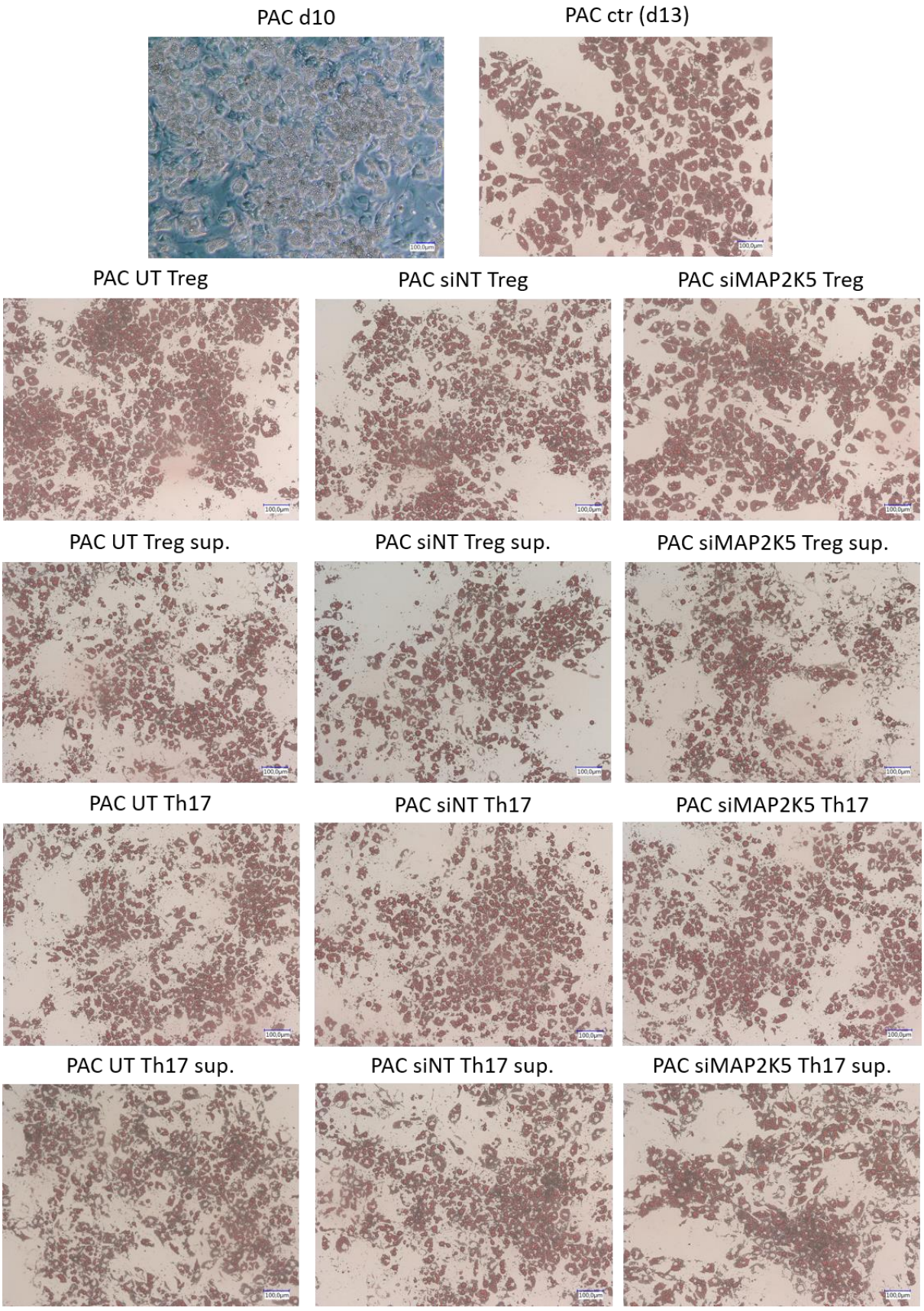

Figure S4. Micrographs from co-culture experiment of differentiated PAC with SH1 $CD4^+$ T cells. Magnification 10x.

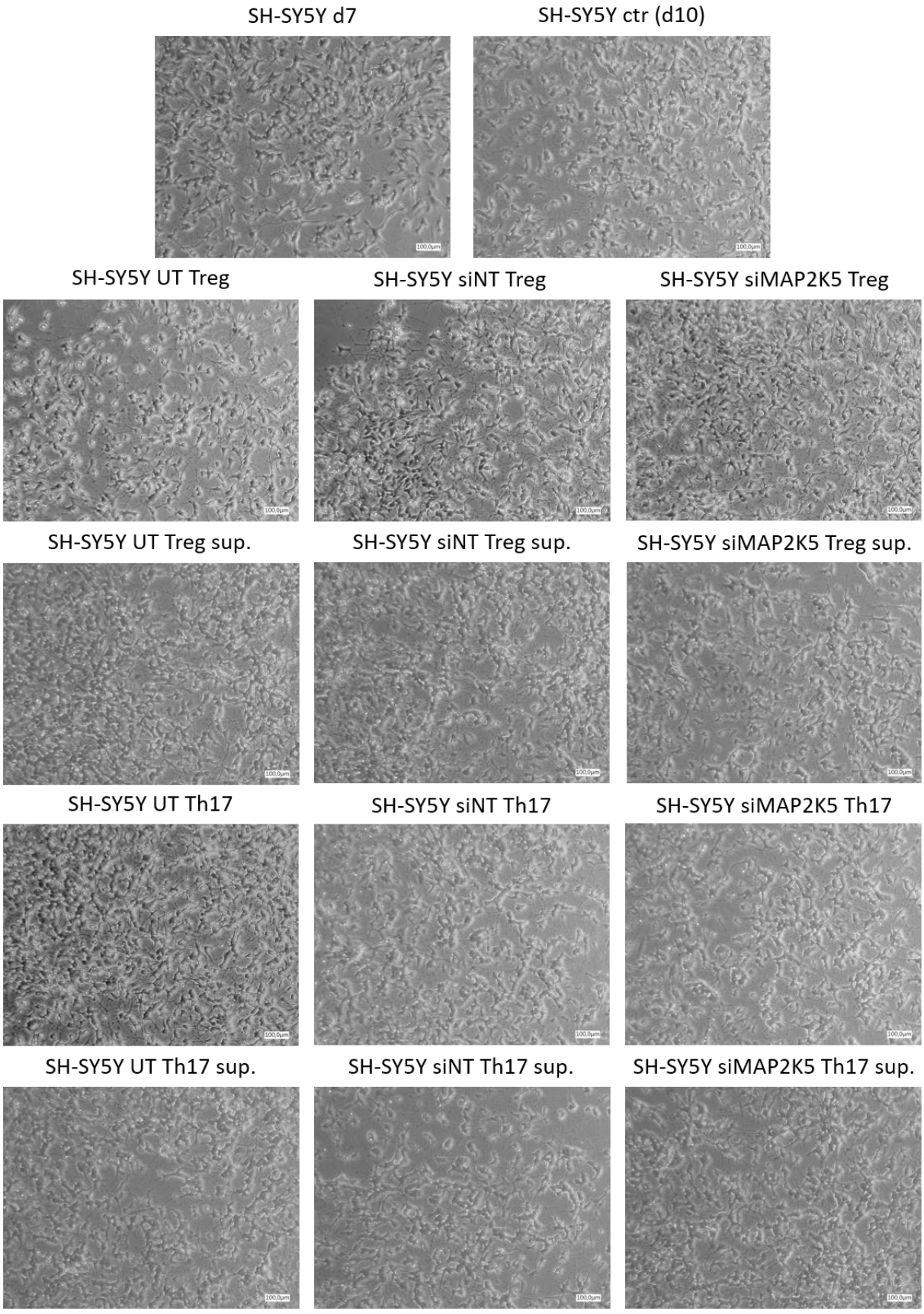

Figure S5. Micrographs from co-culture experiment of differentiated SH-SY5Y cells with SH1 $CD4^+$ T cells. Magnification 10x.

List of Tables

List of Figures

Page